DEVELOPMENT OF POLYMER-COATED NANOPARTICLE IMAGING AGENTS FOR DIAGNOSTIC APPLICATIONS

A Dissertation
Presented to
The Academic Faculty

by

Brad A. Kairdolf
B.S., Louisiana State University, 2003

In Partial Fulfillment
Of the Requirements for the Degree
Doctor of Philosophy in the
Wallace H. Coulter Department of Biomedical Engineering

Georgia Institute of Technology
Emory University
December 2009

DEVELOPMENT OF POLYMER-COATED NANOPARTICLE IMAGING AGENTS FOR DIAGNOSTIC APPLICATIONS

Approved by:

Dr. Shuming Nie, Advisor
School of Biomedical Engineering
Georgia Institute of Technology

Dr. Gang Bao
School of Biomedical Engineering
Georgia Institute of Technology

Dr. Zhong L. Wang
School of Material Science and Engineering
Georgia Institute of Technology

Dr. Niren Murthy
School of Biomedical Engineering
Georgia Institute of Technology

Dr. Vijay Varma
School of Medicine
Emory University

Date Approved: September 9th, 2009

To my family: Alyssa, Shane, Mom and Dad.

ACKNOWLEDGEMENTS

There have been a number of family, mentors and friends who were vital in the successful completion of this PhD dissertation. I am extremely blessed to have these people in my life and am forever grateful for the support they have given me.

Mentors

I would like to first thank all of the many professional mentors that have advised and encouraged me during my career at Georgia Tech and Emory. In particular, this work would not have been possible without the support of my mentor and advisor, Dr. Shuming Nie. Shuming has given me considerable guidance and the tools and intellectual freedom to purse my academic and career interests. His advice and support has been invaluable during my graduate work and during the pursuit of my professional career goals. During my time in his lab, I have learned an incredible amount about nanotechnology and more broadly, about science and scientific discovery. The discussions have challenged and pushed me to be the best scientist I can be and I believe I am a better thinker for it. While I will be ending this chapter of my life, I hope to stay in close contact with him and remain colleagues and friends as I begin the next chapter.

Next, I would like to thank Dr. Marie Thursby, Dr. Carolyn Davis, Ms. Anne Rector, Ms. Kathleen Kurre and Ms. Margi Berbari of the TI:GER program at Georgia Tech and Emory University. The amazing opportunities that I was awarded in the TI:GER program are truly unparalleled and my career path will be forever altered because of the experiences. Their encouragement and support of DiagNano, both inside the classroom and outside, has opened doors for me that I would never have had

without their help. I am forever grateful to their practical experience, hard work and advice in taking DiagNano from the classroom to the real world.

I would also like to thank Dr. Lee Herron: his encouragement and strong support of DiagNano has been incredible and I can't thank him enough for all of the help and counsel that he provided our team. His advice has made the DiagNano venture immeasurably better and I hope I have the opportunity to work further with him in the future.

Labmates

Next, I would like to thank all of the graduate students, postdoctoral fellows and lab personnel that I have had the pleasure of working with during my time in the Nie lab. I would like to thank the former graduate students who have helped me, in particular, Dr. Amit Agrawal, Dr. Matthew Rhyner, Dr. Tushar Sathe and Dr. Andrew Smith. Their experience in the lab and willingness to help and mentor me is greatly appreciated and I hope to stay in touch with them and perhaps have the opportunity to work together again in the future. I am also lucky to have the opportunity to work closely with a number of newer group members, particularly Michael Mancini, Anthony Nicolini, Kate Lee and Mary Wen. I would like to thank them for their support, collaborations and friendship. They have made the lab a constructive yet entertaining place to work and I give them at least partial credit for me enjoying my time everyday in the lab. Thanks also to the postdocs, Dr. Aaron Mohs, Dr. Ximei Qian, Dr. Jian Liu, Dr. Hongwei Duan and Dr. Min Kuang for the help, discussions and advice about my research. I would also like to thank the administrators, especially Michelle Denney and Ryan Jowers. Their tireless effort allows the lab to function and I appreciate all of their hard work and friendship.

Family

Above all, I want to thank my family for all of the love, support, patience and understanding that they have given me. Without them, I definitely would not have been able to accomplish this. My incredible wife, Alyssa, has been amazingly supportive of me, even when it was difficult to do. Without her love and support, I would not be who I am today. I can't wait to move on to the next chapter of our lives together. My mom and dad have always pushed me to be the best that I could be. I can't thank them enough for all of the love and support they've shown to me and Alyssa and the sacrifices they made to make sure my brother Shane and I had the best opportunities. I'd also like to thank everyone else who has support helped me get here today, including my grandparents, Shane and Mr. Jimmy and Mrs. Judy.

TABLE OF CONTENTS

	PAGE
ACKNOWLEDGEMENTS	IV
LIST OF TABLES	XII
LIST OF FIGURES	XIII
LIST OF SYMBOLS AND ABBREVIATIONS	XVI
SUMMARY	XX
CHAPTER	
1. CANCER AND THE PROMISE OF NANOTECHNOLOGY	1
1.1 ABSTRACT	1
1.2 INTRODUCTION	1
1.3 THE MOLECULAR COMPLEXITY OF CANCER	4
Acquired Traits of Cancer Cells	4
Independence from External Growth Signals	5
Avoiding Programmed Cell Death	6
Finding New Nutrient Sources	7
Cancer Heterogeneity	7
1.4 NANOTECHNOLOGY AND IMPLICATIONS FOR THERAPEUTICS AND DIAGNOSTICS	9
Nano-Diagnostics	10
Nano-Therapeutics	11
1.5 DISSERTATION STRUCTURE	12
1.6 CONCLUSIONS	13
2. QUANTUM DOTS FOR USE IN BIOLOGICAL ENVIRONMENTS	14
2.1 ABSTRACT	14

2.2 INTRODUCTION 14
2.3 SEMICONDUCTOR NANOCRYSTALS 15
2.4 COATING STRATEGIES AND TRASFER TO WATER 18
Ligand Exchange with Small Molecules 19
Polymer Coatings 21
2.5 QUANTUM DOT-BASED ASSAYS FOR CLINCAL APPLICATIONS 22
Solutions Assays 22
Cell and Tissue Staining 23
In vivo Imaging 26
2.6 CHALLENGES AND OPORTUNITIES 27
2.7 CONCLUSIONS 28
3. SYNTHESIS AND CHARACTERIZATION OF AMPHIPHILIC POLYMERS FOR QUANTUM DOT COATING 30
3.1 ABSTRACT 30
3.2 INTRODUCTION 31
3.3 METHODS 35
3.4 RESULTS AND DISCUSSION 42
Polymer Development and Selection 43
Polymer Synthesis and Purification 44
Polymer Characterization and Analysis 46
Phase Transfer of Quantum Dots using Amphiphilic Polymers 50
Analysis of Quantum Dot Optical and Colloidal Properties 55
Effects of Polymer Chain Length on Quanutm Dot Properties 60
3.5 CONCLUSIONS 61
4. AMPHIPHILIC MULTIDENTATE POLYMERS FOR ONE-POT

SYNTHESIS, ENCAPSULATION AND SOLUBILIZATION OF QUANTUM DOTS 63
4.1 ABSTRACT 63
4.2 INTRODUCTION 64
4.3 METHODS 67
4.4 RESULTS AND DISCUSSION 70
Multidentate Precursor Preparation 70
Quantum Dot Synthesis and Reaction Kinetics 71
One-pot Synthesis 75
In-Situ Capping with an Inorganic Passivating Shell 79
4.5 CONCLUSIONS 81
5. AMPHIPHILIC MULTIDENTATE POLYMERS FOR ONE-POT SYNTHESIS OF SERS ACTIVE GOLD NANOPARTICLES 82
5.1 ABSTRACT 82
5.2 INTRODUCTION 83
5.3 METHODS 86
5.4 RESULTS AND DISCUSSION 89
Gold Nanoparticle Synthesis using Multidentate Polymers 89
Polymer Procedure Reaction Kinetics 92
Gold Nanoparticle Characterization 96
Large Gold Nanoparticles and Synthesis of SERS-Active Particles 99
5.5 CONCLUSIONS 103
6. NEW NANOPARTICLE SURFACE CHEMISTRIES TO ELIMINATE NONSPECIFIC BINDING 104
6.1 ABSTRACT 104
6.2 INTRODUCTION 104

6.3 METHODS 107

6.4 RESULTS AND DISCUSSION 112

Surface Coating Chemistry 113

Hydroxylation Kinetics 115

Quantum Dot Size, Charge and Optical Properties 117

Nonspecific Cellular Binding 121

Surface Charge Variations 123

Nonspecific Binding in Biological Fluids 125

6.5 CONCLUSIONS 127

7. LOW BINDING, HYDROXYL QUANTUM DOTS FOR TISSUE STAINING APPLICATIONS 129

7.1 ABSTRACT 129

7.2 INTRODUCTION 129

7.3 METHODS 134

7.4 RESULTS AND DISCUSSION 137

Bioconjugation Strategies 137

Quantum Dot Stability in Coupling Buffer 138

Reactivity of Quantum Dots with Cyanogen Bromide 140

Targeted Cell Staining Using Quantum Dots 142

7.5 CONCLUSIONS 144

8. FUTURE DIRECTIONS 145

8.1 ABSTRACT 145

8.2 SUMMARY 145

8.3 FUTURE DIRECTIONS FOR DISSERTATION TECHNOLOGY 148

Optimization of SERS-active Gold Nanoparticles for Biological studies 148

Multiplexed Tissue Staining using Nonstick Quantum Dots 149

Ultrasensitive Detection of Rare Cells in Fluid Samples 149

8.4 CONCLUSIONS 150

REFERENCES 151

CURRICULUM VITAE 167

LIST OF TABLES

PAGE

Table 3.1: Amphiphilic polymer variants used in this dissertation 45

LIST OF FIGURES

PAGE

Figure 1.1: Decrease in death rates for 4 major causes of mortality in the United States 2

Figure 1.2: Death rates for cancer and heart disease, 1975—2004 3

Figure 1.3: The complexity of cancer biology 8

Figure 1.4: The nano scale 10

Figure 2.1: Unique optical properties of quantum dots 17

Figure 2.2: Schematic structure of a hydrophobic, core-shell quantum dot 19

Figure 2.3: Quantum dot coatings and colloidal properties 20

Figure 2.4: Biomedical applications of quantum dots 25

Figure 3.1: Self-assembly of block copolymer melts 32

Figure 3.2: Illustration of a graft copolymer structure 33

Figure 3.3: Reaction scheme for an amphiphilic polymer to be used for synthesis and coating of nanoparticles for biological applications 36

Figure 3.4: Quantum dot coating and water purification schematic 39

Figure 3.5: Polymer critical micelle concentration (CMC) 49

Figure 3.6: Hydrodynamic size of polymer aggregates in water, as measured by dynamic light scattering (DLS) 50

Figure 3.7: Removal of excess polymer from water solubilized quantum dots 54

Figure 3.8: Characterization of quantum dot optical properties 55

Figure 3.9: Confirmation of polymer thickness and particle size 56

Figure 3.10: Analysis of excess polymer removal and quantum dot hydrodynamic size using Fast Protein Liquid Chromatography (FPLC) 58

Figure 3.11: pH stability analysis of quantum dots 59

Figure 3.12: Quantum dot fluorescence intensity as a function of polymer concentration and carbon chain length 61

Figure 4.1: Illustration of cadmium oleate, a common cadmium precursor for

quantum dot synthesis 65

Figure 4.2: Schematic structures of amphiphilic multidentate ligand and polymer coated quantum dots 71

Figure 4.3: Unique growth properties of polymer synthesis procedure for quantum dots 72

Figure 4.4: Comparison of reaction kinetics CdTe quantum dot synthesis using standard and polymer based procedures 74

Figure 4.5: Phase transfer of polymer synthesized quantum dots to water using octadecene and polyethylene glycol 76

Figure 4.6: Fluorescence emission and electron microscopy structural properties of CdTe core quantum dots prepared using multidentate polymer ligands in a one-pot procedure 79

Figure 4.7: Size histogram of CdTe core quantum dots 80

Figure 4.8: Type-II core-shell CdTe/CdSe quantum dots synthesized in a one-pot method 82

Figure 5.1: Gold nanoparticle synthesis using citrate reduction 86

Figure 5.2: Gold nanoparticle synthesis using amphiphilic polymers for reduction and surface stabilization 93

Figure 5.3: Gold nanoparticle synthesis reaction kinetics using citrate reduction 95

Figure 5.4: Gold nanoparticle synthesis reaction kinetics using polymer methods 97

Figure 5.5: Gold nanoparticle size characterization 99

Figure 5.6: Stability of polymer coated gold nanoparticles 100

Figure 5.7: Synthesis of large gold nanoparticles 102

Figure 5.8: Polymer-coated SERS active gold nanoparticles for imaging applications 104

Figure 6.1: Quenching hydroxylation procedure using hydroxylamine 111

Figure 6.2: Surface coating chemistry and structure of polymer-encapsulated quantum dots (CdSe/CdS/ZnS) 117

Figure 6.3: Quantum dot hydroxylation reaction kinetics 118

Figure 6.4: Comparison of the absorption and emission properties of quantum dots before and after surface hydroxylation 121

Figure 6.5: Size and charge comparison of quantum dots with varying surface coatings 123

Figure 6.6: Fluorescence microscopy images of hydroxylated and carboxylated quantum dots nonspecifically bound to fixed human cells 125

Figure 6.7: Quantitative evaluation and comparison of nonspecific cellular binding for various quantum dot surface coatings 126

Figure 6.8: Effect of hydroxylation degree on the cellular nonspecific binding of quantum dots 128

Figure 6.9: Nonspecific binding of quantum dots in staining buffers 129

Figure 6.10: Nonspecific binding of quantum dots in biological fluids 130

Figure 7.1: Standard tissue staining procedures, shown on liver cancer tissue sections 134

Figure 7.2: Multicolor staining of cells using quantum dots 137

Figure 7.3: Reaction scheme for coupling targeting molecules, such as antibodies, to hydroxyl-coated quantum dots using cyanogens bromide 141

Figure 7.4: Behavior of polymer-coated quantum dots in the presence of acetonitrile 142

Figure 7.5: Reactivity of cyanogens bromide with hydroxyl-coated quantum dots 144

Figure 7.6: Labeling of MDA MB 231 breast cancer cells using antibody-conjugated, hydroxyl quantum dots 146

LIST OF SYMBOLS AND ABBREVIATIONS

eV	Electron Volts
g	Gravity
K_d	Dissociation Constant
k_{off}	off rate
k_{on}	on rate
°C	Degree Celsius
T	Temperature
χN	Flory-Huggins Parameter
ACN	Acetonitrile
APD	3-Amino-1,2-Propanediol
Au	Gold
AuNP	Gold Nanoparticle
BSA	Bovine Serum Albumin
Cd	Cadmium
CdO	Cadmium Oxide
CdS	Cadmium Sulfide
CdSe	Cadmium Selenide
CdTe	Cadmium Telluride
$CHCl_3$	Chloroform
CMC	Critical Micellar Concentration
CNBr	Cyanogen Bromide
COOH	Carboxylic Acid
CT	Computed Tomography
CTC	Circulating Tumor Cells

DA	Decylamine
Da	Dalton
DAP	1,3-Amino-2-Propanol
DAPI	4’,6-Diamidino-2-Phenylindole Dihydrochloride
DCC	Dicyclohexylcarbodiimide
DCU	Dicyclohexylurea
DDA	Dodecylamine
DHLA	Dihydrolipoic acid
DI	deionized
DLS	Dynamic Light Scattering
DMF	Dimethylformamide
DNA	Deoxynucleic Acid
EDTA	Ethylenediaminetetraacetic Acid
EDAC	1-Ethyl-3-(3-Dimethylaminopropyl) Carbodiimide
EPR	Enhanced Permeability and Retention
EtOH	Ethanol
FBS	Fetal Bovine Serum
FDA	Food and Drug Administration
FFPE	Formalin-Fixed Paraffin-Embedded
FGF	Fibroblast Growth Factor
FNA	Fine Needle Aspiration
FPLC	Fast Protein Liquid Chromatography
FWHM	Full Width Half Max
HA	Hexylamine
HCl	Hydrochloric Acid
HDA	Hexadecylamine

H&E	Hematoxylin & Eosin
HRP	Horseradish Peroxidase
HWHM	Half Width Half Max
IHC	Immunohistochemistry
InAs	Indium Arsenide
LED	Light Emitting Diode
MAA	Mercaptoacetic Acid
MCG	Malachite Green
MeOH	Methanol
MRI	Magnetic Resonance Imaging
MWCO	Molecular Weight Cutoff
MW	Molecular Weight
Na2HPO4	Sodium Phosphate Dibasic
NaCl	Sodium Chloride
NaOH	Sodium Hydroxide
NHS	N-Hydroxysuccinimide
OA	Octylamine
ODA	Octadecylamine
ODE	Octadecene
OH	Hydroxyl
PAA	Poly(Acrylic Acid)
PAA-DA	Poly(Acrylic Acid) Decylamine
PAA-DDA	Poly(Acrylic Acid) Dodecylamine
PAA-HDA	Poly(Acrylic Acid) Hexadecylamine
PAA-OA	Poly(Acrylic Acid) Octylamine
PAA-ODA	Poly(Acrylic Acid) Octadecylamine

PAA-TDA	Poly(Acrylic Acid) Tetradecylamine
PBS	Phosphate Buffered Saline
PEG	Poly(Ethylene Glycol)
PEI	Polyethyleneimine
PET	Positron Emission Tomography
pRb	Retinoblastoma Protein
PTA	Phosphotungstic Acid
QD	Quantum Dot
QY	Quantum Yield
Se	Sellenium
SERS	Surface Enhanced Raman Scattering
TAE	Tris-Acetate-EDTA
TDA	Tetradecylamine
Te	Tellurium
TEM	Transmission Electron Microscopy
TGFβ	Transforming Growth Factor Beta
TOP	Trioctylphosphine
Uv-Vis	Ultraviolet-Visible
VEGF	Vascular Endothelial Growth Factor
ZnS	Zinc Sulfide
ZnSe	Zinc Selenide

SUMMARY

Cancer is the second most common cause of death in the United States, with over 500,000 deaths expected this year. While significant progress has been made in the treatment and management of cancer, challenges remain because of the complexity and the heterogeneous nature of the disease. The improvement that has been seen in survival rates reflects advancements not only in treatment, but also in early stage detection and diagnostics for certain cancers. In particular, early stage detection and treatment of cancer before it has metastasized to other organs has resulted in a dramatic improvement in patient survival rates. One area of research that has shown considerable promise in further advancing diagnostics and early cancer detection is nanotechnology. Specifically, semiconductor and metal nanoparticles have great potential to provide advanced technology platforms for ultrasensitive and multiplexed detection of disease markers and probe disease on the molecular level. Because they are in the same size regime as biological molecules, these nanoparticles exhibit unique interactions with proteins, nucleic acids and other biomarkers of interest for detecting and diagnosing disease. However, high-quality nanoparticles are often unsuited for use in complex biological environments because of their coatings and surface chemistry.

In this dissertation, we describe the design and development of polymer-coated nanoparticle imaging agents for use in blood, cell and tissue diagnostic applications. First, low-molecular weight, amphiphilic polymers, with hydrocarbon chains capable of noncovalent interactions with nanoparticle surface ligands and a hydrophilic backbone to render the nanoparticle water soluble, were synthesized and characterized for use in nanoparticle coating applications. We demonstrate that the hydrophobic and hydrophilic interactions between the nanoparticle surface, the amphiphilic polymer and the aqueous

solvent were able to drive the coating and water solubilization of quantum dots. Second, synthesis techniques were developed using amphiphilic polymers in a one-pot method to make high quality nanoparticles and stabilize and encapsulate the particles for transfer into water. Using the polymer functional groups as multidentate ligands, nanoparticles were synthesized with a high degree of size control and increased stability. In addition, by performing the synthesis in a noncoordinating amphiphilic solvent such as polyethylene glycol, nanoparticles were immediately transferred to water with the excess polymer forming a water soluble coating.

Next, nanoparticle surface charge and how it relates to the nonspecific binding of nanoparticles in cells, tissues and other complex biological samples was studied. We have found that highly charged (negative and positive) particles exhibit significant nonspecific binding to biomolecules and other cellular components in biological environments. By reducing the surface charge through the incorporation of hydroxyl functional groups, we have nearly eliminated the nonspecific binding of quantum dots in blood, cells and tissues. Moreover, through crosslinking and altering the surface chemistry of the polymer-coated quantum dots, we have increased the stability of the nanoparticles while maintaining a small hydrodynamic size. Finally, we have investigated the use of the low-binding, hydroxyl quantum dots in tissue staining applications, where nonspecific binding presents a considerable challenge to detection sensitivity and specificity. A number of biomolecule conjugation techniques were examined for the coupling of quantum dots to antibody targeting molecules and preliminary staining experiments were performed.

In summary, this dissertation makes significant contributions to the fields of nanotechnology and cancer diagnostics, particularly with new polymer coatings for quantum dots and other nanoparticles. Novel synthesis techniques were developed using multidentate amphiphilic polymers to produce water soluble nanoparticle imaging

agents in a one-pot method. Nanoparticle surface chemistry was also explored as a means to improve the functionality of these imaging agents in biological environments, leading to a novel, non-stick hydroxyl surface chemistry for nanoparticles with utility in clinical applications, particularly blood, cell and tissue assays. These advancements further elucidate the properties of polymer coatings and nanoparticle surfaces and enhance our understanding of nanoparticle interactions in clinically relevant environments. The technologies developed in this work will have a significant impact on nanoparticle use in ultrasensitive biomarker detection in complex biological samples and provide further advancements in early stage disease diagnostics.

CHAPTER 1

CANCER AND THE PROMISE OF NANOTECHNOLOGY

1.1 ABSTRACT

Nanotechnology is the field of study dealing with the control of matter on the "nanoscale", where at least one dimension is between 1 and 100 nm. Surprisingly, while the initial focus of this technology has been in applications ranging from energy to materials science, medicine is likely to be impacted most in the near future. Indeed, a number of applications in diagnostics as well as therapeutics have been developed from these technologies, with a few now being adopted in the clinic. Applications in cancer are of particular interest due to the complexity of the disease and the unique properties nanoparticles offer. The ability to perform highly sensitive, multiplexed diagnostic assays as well as targeted drug delivery has intensified research in cancer nanotechnology. Here, we explore the needs present in cancer diagnostics and treatment and present the potential nanotechnology offers.

1.2 INTRODUCTION

Approximately 1.4 million new cancer cases were diagnosed in 2008 in the United States alone with over 12 million diagnosed worldwide [1]. Cancer is the second most common cause of death in the US, surpassed only by cardiovascular disease, with over 500,000 deaths expected this year. Although new research in this field has vastly expanded our knowledge of cancer and cancer biology, particularly with new insights into the molecular workings of the disease [2, 3], the death rate for cancer has seen only a moderate decrease in the past 50 years. In contrast, other leading causes of death have seen dramatic reductions in their mortality rate. In particular, the mortality rate for

heart disease has been reduced by over 60% compared to its value in 1950, as seen in Figure 1.1. The cancer rate has decreased by approximately 10%, with a mortality rate at around 93% of the 1950 value in 2006.

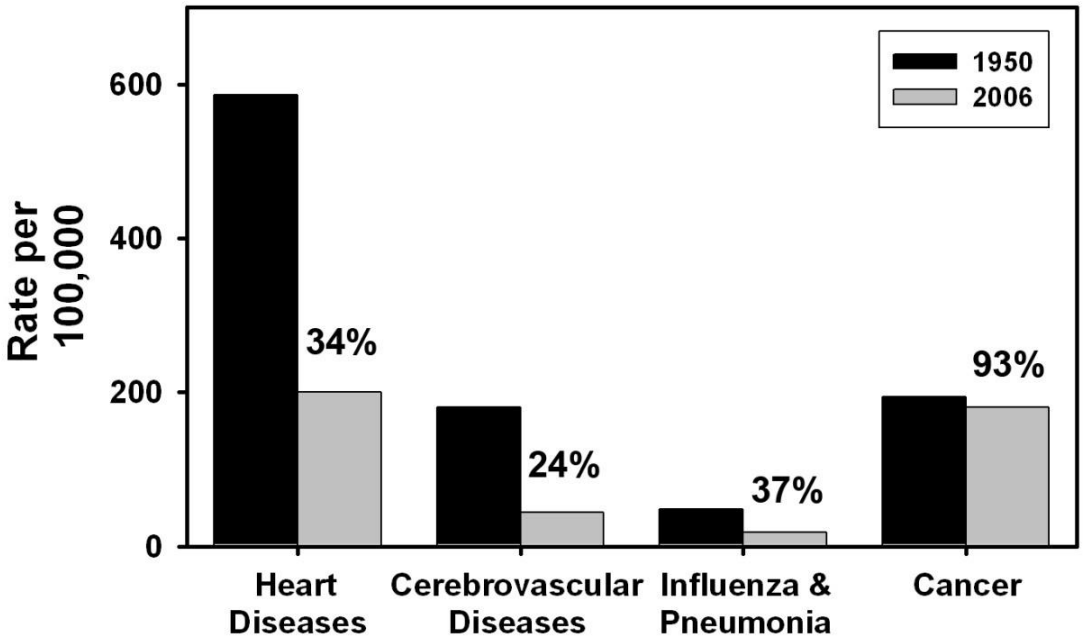

Figure 1.1. Decrease in death rates for 4 major causes of morality in the United States. Cancer has seen only a slight decrease in death rate over the past 50 years in comparison to other common causes of mortality, such as heart disease. From ACS [1].

There has been a remarkably steady and rapid decline in the cardiovascular disease mortality rates for all ages over the past few decades, with heart disease even falling below the cancer rate for people under the age of 85 (Figure 1.2). While there have certainly been advances in the treatment of heart disease, this rapid decline is likely due to a combination of advances in both therapeutics and early diagnostics, in addition to preventative measures. Early stage risk factors, such as blood pressure and

cholesterol levels, have also been determined to help identify patients that may be at risk for the disease early on, when treatment or prevention is much more successful.

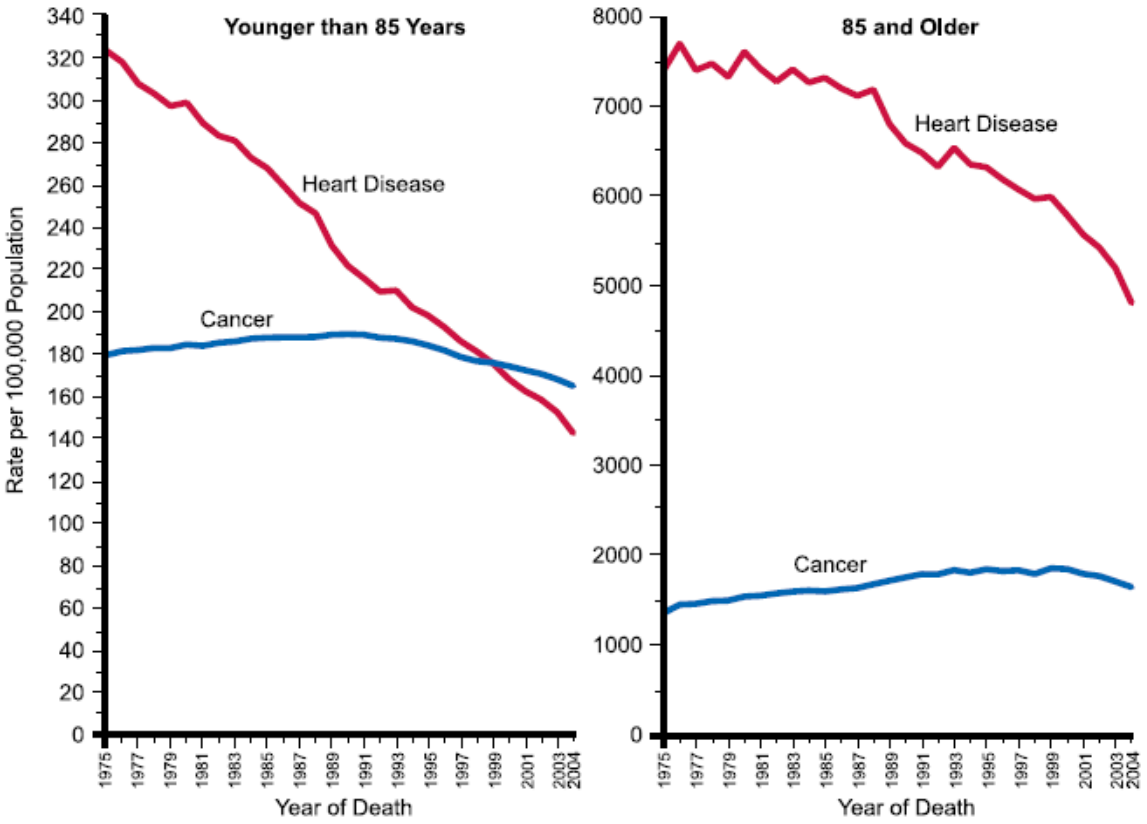

Figure 1.2. Death rates for cancer and heart disease, 1975—2004. Heart disease mortality has seen a steady decline in all age groups. Cancer mortality, however, is relatively steady, with a moderate decrease over the past 15 years. From Jemal et al [4].

In contrast, early stage detection and prevention methods for cancer are far less developed. While significant progress has been made in the treatment and management of the disease, substantial hurdles still remain because of its complexity and heterogeneous nature. Because of new research efforts and recent advances in diagnostic technologies, there is an opportunity to bring the idea of "personalized medicine" to fruition. Personalized medicine is defined as the diagnosis and treatment of patients on a case-by-case basis using molecular information specific to that patient.

This method can be used to generate a patient-specific disease fingerprint, gleaned from advanced diagnostic techniques, which can guide clinicians in the diagnosis as well as treatment of the disease. Although current cancer diagnostic methods merely hint at a patient's underlying molecular problems, advances in nanotechnology may be the stimulus needed to make personalized medicine a reality.

1.3 THE MOLECULAR COMPLEXITY OF CANCER

Research in the fields of molecular and cell biology, biochemistry and medicine has led to many advances in our understanding of cancer and cancer biology as well as new avenues for enhanced treatment and better diagnostics. However, this work has also exposed the very complex and heterogeneous nature of cancer, and revealed many hurdles to the successful diagnosis and treatment of the disease. Increasingly, research efforts are being focused on studying the disease on the molecular level and understanding the very complex causes and pathways involved in the biology of cancer. Because of these efforts, therapeutics as well as diagnostics have begun to focus on the molecular level of the disease and are looking at a cocktail of biomarkers and therapeutic targets rather than a single disease marker.

Acquired Traits of Cancer Cells

Early work in cancer biology led to the discovery of a number of cancer genes, divided into oncogenes and tumor suppressors, which play a crucial role in the regulation of cell growth in normal cells, Mutations in these genes result in either a gain of function (oncogenes) or loss of function (tumor suppressor genes) and can act in coordination and lead to unregulated growth of the cell and cancerous behavior [5]. More recent work has bolstered the idea that tumorigenesis is a multistep process, where each step reflects a genetic aberration responsible for the eventual transformation

of healthy cells into cancer cells. It has been suggested that for many cancers, there are between four to seven rate-limiting alteration events necessary for this ultimate transformation [6], and pathological analysis of patient organs has revealed lesions that could represent the intermediate steps along the progression to invasive cancer [7]. Together, these discoveries indicate that a series of genetic mutations in genes important in the regulation of cell growth lead to a gradual and progressive conversion of normal cells into invasive cancer cells [7, 8]. It has been hypothesized that the vast number of cancer types can be broadly characterized by six functional alterations that affect cancerous cell growth [3]: (1) self-sufficiency in growth signals, (2) insensitivity to growth inhibitors, (3) evasion of apoptosis, (4) limitless replication potential, (5) sustained angiogenesis, and (6) tissue invasion and metastasis.

Independence from External Growth Signals

Noncancerous cells rely on growth factors or signals from their environment or surrounding cells to induce mitosis and proliferation. These signals are relayed to the cell through an intricate pathway of receptors as well as downstream proteins that carry the signal and affect the cell growth pathways. However, cancer cells are able to bypass these control measures and proliferate independent of external growth signals. This can occur through a variety of molecular alterations, including changes in the receptor proteins (structure, number, or type) [9-12] or downstream signaling molecules [13-17] or an acquired ability to produce growth factors that are self-stimulatory [18]. In addition, antigrowth signals abound to maintain homeostasis in normal cells and prevent abnormal cell growth. These signals are transmitted in much the same manner as growth signals, through receptor molecules and downstream pathways. Many of these pathways are associated with the cell cycle clock [3], in particular, the retinoblastoma protein (pRb), p107 and p130 [19, 20], and are responsive to a number of antigrowth

factors, particularly TGFβ [21, 22]. Disruption of these pathways removes a layer of control from the normal cell cycle, allowing uncontrolled growth to proceed.

Avoiding Programmed Cell Death

Other traits that aid in the transformation of a normal cell to a cancerous one are the ability to evade apoptosis and the ability to circumvent intrinsic limits on their multiplication. Apoptosis is programmed cell death, a method organisms use to remove damaged or diseased cells in an organized manner. A cell with DNA damage, mutations or alterations to other important cell pathways may "decide" to undergo apoptosis via a pathway mediated by p53, a tumor suppressing gene, if it is beyond repair. Loss of function mutations in this gene or others in the pathway can result in a cell's ability to avoid programmed cell death [23-27], allowing the cell to grow unchecked. Mounting evidence suggests that the disruption of the apoptosis pathway is a hallmark of most, if not all, types of cancer [3, 28]. However, while the traits described above decouple the cell from the normal signaling controls on cell growth, they are typically insufficient to induce cancer transformation on their own. This is due to an independent limitation on the replicative potential of cells [29], known as the Hayflick limit. Cells that break free from the normal growth confinements imposed by the cell cycle regulatory pathways invariably undergo massive cell death unless they acquire the ability to bypass the Hayflick limit [30]. Although the process is not completely understood, one necessary alteration seems to be the upregulation of telomerase, an enzyme responsible for maintaining the telomeres at the end of chromosomes [31]. These are believed to function as an internal biological clock for the cell, determining its ability to divide and proliferate.

Finding New Nutrient Sources

As the cancer cells multiply, nutrient supply becomes a limiting factor because the diffusion of oxygen and other nutrients is limited across tissue. To bypass this limitation, tumor cells must acquire the ability to induce the growth of blood vessels, enabling them to access the required nutrients. Work over the past few decades has shown that growth factors, such as VEGF and FGF1/2 play a significant role in a tumor's ability to recruit new blood vessels [32]. Finally, the ability of a cancer to metastasize and invade also allows the diseased cells to find new sources of nutrients and is important in determining the eventual survival rate of the patient. Metastasis is a complex process involving many proteins and is thought to account for approximately 90% of human cancer deaths [33].

Cancer Heterogeneity

As described above, the progression cells undergo to reach a cancerous state is an extremely complex process, allowing for considerable heterogeneity. Figure 1.3 shows a simplified schematic of some of the potential pathways involved in the transformation towards malignancy. In addition to the complexity of cancer cells, tumors typically consist of a number of other healthy cell types, including immune and endothelial cells as well as fibroblasts. This heterogeneity makes both diagnosis and treatment extremely complex

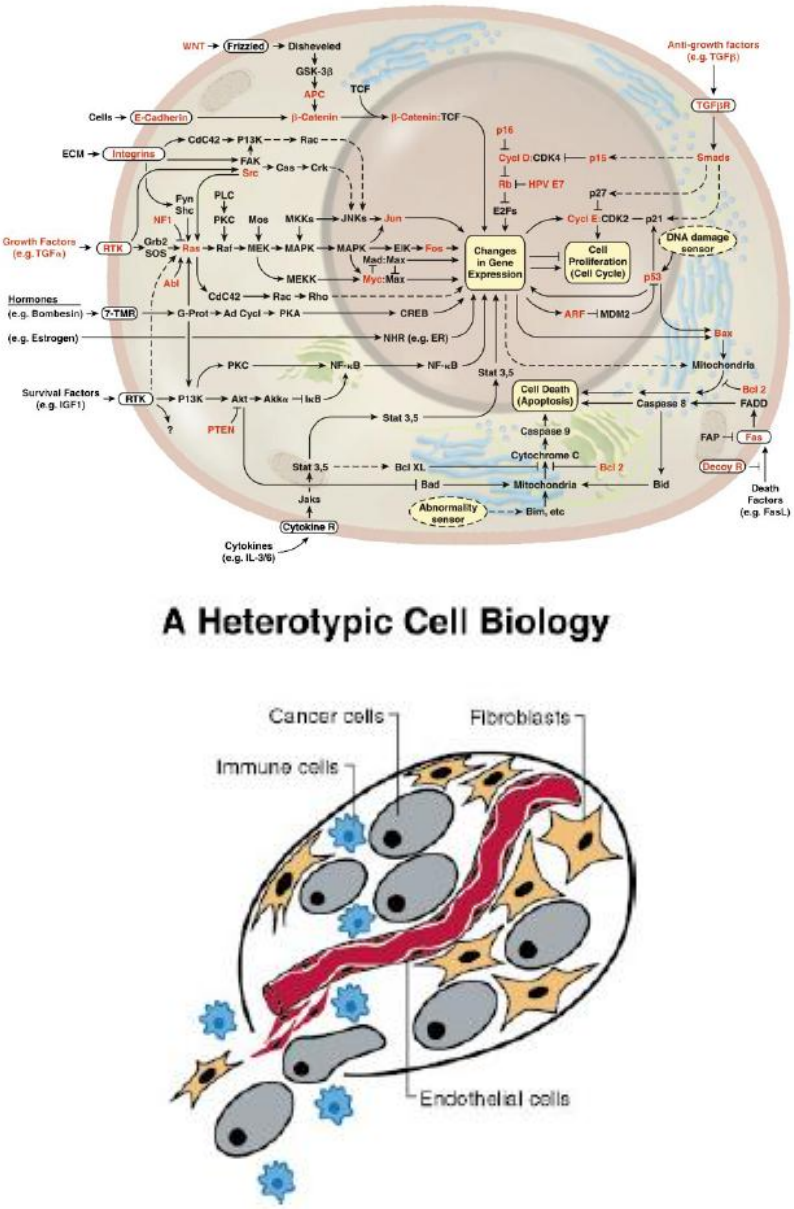

Figure 1.3. The complexity of cancer biology. Schematic showing the complex molecular pathways involved in the regulation of cell growth and death (top) and the heterogeneous nature of tumors, consisting of cancer cells as well as immune and endothelial cells and fibroblasts (bottom). Adapted from Hanahan et al [3].

1.4 NANOTECHNOLOGY AND IMPLICATIONS FOR THERAPEUTICS AND DIAGNOSTICS

One field of technology that has shown surprising promise for use in cancer diagnostics and therapeutics is nanotechnology [34]. It is the field of technology that deals with the control of matter on the "nanoscale", where at least one dimension is less than 100 nm. Nanotechnology is a multidisciplinary field with significant contributions from engineering, materials science and chemistry. It has also been greatly influenced by biochemistry and molecular biology, where biomolecules are in the same size regime as nanoparticles, as shown in Figure 1.4. This size similarity allows for very unique interactions between nanoparticles and biomolecules, such as DNA or protein, and has led to exciting technologies with applications in diagnostics and therapeutics as well as an increased understanding of cell biology. New discoveries in nanotechnology, biology and medicine have led to a plethora of nanodevices with a broad range of applications in the biomedical field, including drug delivery vectors, biomolecule sensing and molecular and cellular imaging [35].

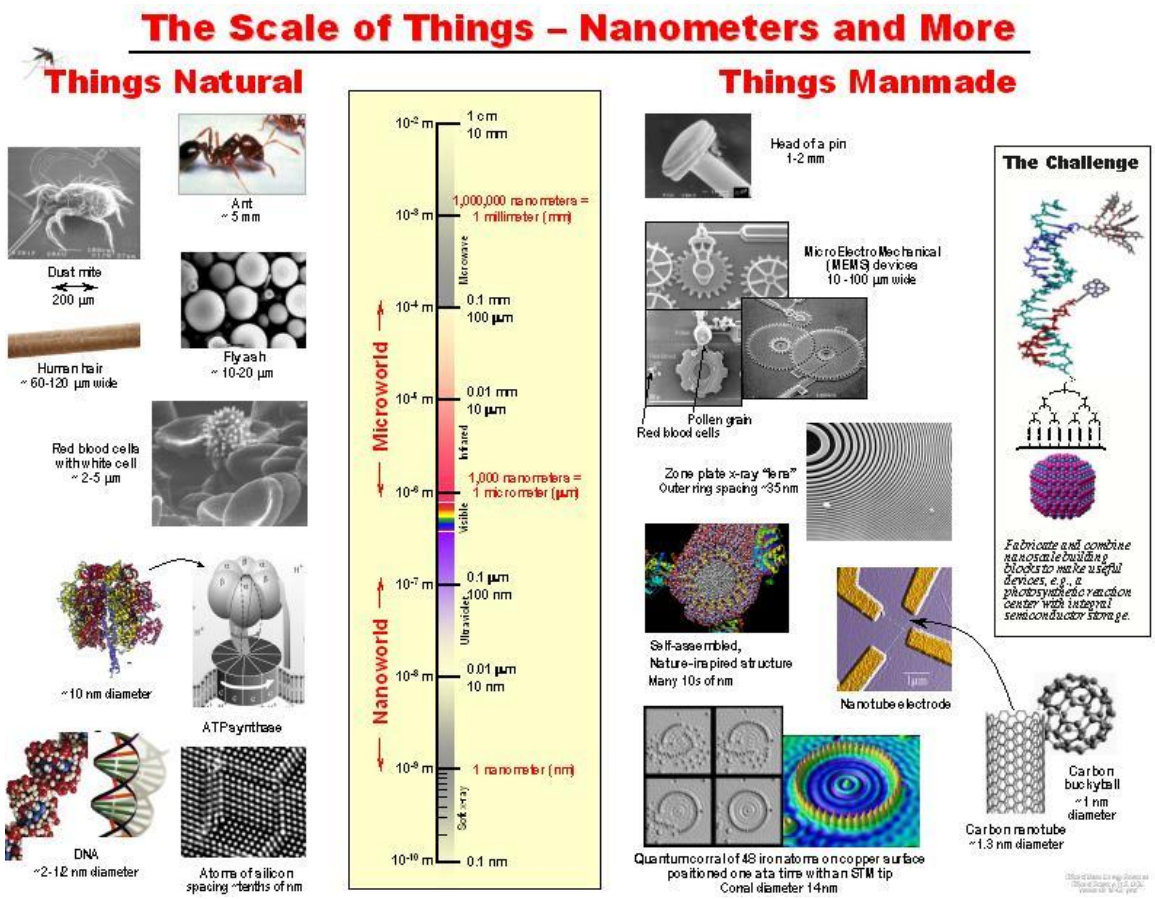

Figure 1.4. The nano scale. Schematic showing the size scale of objects compared to the nanoscale size regime. Complex molecular machines, DNA, and proteins are on the same size scale as nanoparticles and exhibit unique interactions with biomolecules for interesting diagnostic applications. From US DOE [36].

Nano-Diagnostics

A variety of nanoparticles have been proposed for use as *in vitro* and *in vivo* diagnostic contrast agents because of their unique physical properties. In particular, semiconductor and metal nanoparticles have great potential to provide advanced diagnostic platforms for ultrasensitive and multiplexed detection of disease markers and probe disease on the molecular level. Paramagnetic iron oxide nanoparticles have been successfully used *in vivo* as MRI contrast agents for the detection of metastases and have been shown to outperform gadolinium based techniques in some applications [37-

40]. Gold nanoparticles have also been explored as potential imaging agents for use *in vivo*. Preliminary studies show the particles are highly sensitive and can be optically detected through the skin in animal models [41]. While the use of nanoparticles for *in vivo* diagnostic applications has progressed over the past decade, significant hurdles, such as biodistribution and toxicity, continue to limit their utility. This is especially true for nanoparticles containing toxic materials, such as quantum dots (QDs), which often contain cadmium, lead or mercury. Extensive studies will be required before FDA trials are even considered for the *in vivo* use of these particles. *In vitro* diagnostics, however, eliminates these hurdles as an issue. As a result, significant work has been performed to translate these technologies from the bench to the clinic. SERS active gold nanoparticles and QDs have received an incredible amount of attention and work is ongoing to develop new applications for the use of these particles *in vitro [42-55]*.

Nano-Therapeutics

Cancer therapy is expected to be significantly impacted by the development of new nanotechnologies [56-58]. The use of nanoparticles as therapeutic carrying agents provides for a platform technology that can be used for the delivery of both hydrophilic and hydrophobic (which are difficult to administer) molecules as well as biologics such as proteins or nucleic acids [59-63]. The ability to load multiple drug molecules inside a single particle also enables the delivery of larger payloads than with simple administration of naked drug, providing a more effective delivery. Nanoparticles themselves can also have a therapeutic effect. Gold nanoshells have been used to heat tumors upon external stimulation, inducing cell death in tissues where it accumulates [64, 65].

Because of the high surface area to volume ratio for nanoparticles, a substantially higher loading can also be achieved. This is particularly effective for

coating the nanoparticles with multiple targeting moieties, increasing the affinity of the nanoparticles to the targeted tissue. In addition, the size of the nanoparticles alone enhances the delivery of the payload to the cancerous tissue through the EPR effect [66, 67]. Angiogenesis in tumors leads to the formation of "leaky" blood vessels, allowing nanoparticles to escape into the tumor environment and access the diseased cells. Inadequate lymphatic drainage also aids in retaining the particles in the tumor environment, further enhancing the accumulation of drug in the cancerous cells.

1.5 DISSERTATION STRUCTURE

This dissertation concentrates on the development of polymer-coated nanoparticle imaging agents for diagnostics applications and has been organized into 8 chapters. Each chapter focuses on a particular aspect of the development of these imaging agents and discusses the approaches and results in detail. Below is a brief description of each chapter.

Chapter 1- Here, we provide a brief background about cancer and current diagnostic technologies as well as nanotechnology and its potential to revolutionize the diagnostic field.

Chapter 2- This chapter provides a detailed discussion of semiconductor quantum dots (QDs) and how advancements in their development will have a tremendous impact on the use of nanotechnology in medicine.

Chapter 3- Here, we present the design and development of low molecular weight amphiphilic polymers for the coating of hydrophobic QDs and other nanoparticles and how these polymers affect the optical and colloidal properties of QDs in water.

Chapter 4- In this chapter, we discuss the use of these amphiphilic polymers in the simultaneous synthesis and coating of QDs in a one-pot fashion as well as an *in situ* capping method for growing a passivating shell.

Chapter 5- This chapter focuses on the use of the amphiphilic polymers in the synthesis of other inorganic nanoparticles, specifically gold nanoparticles (AuNPs) and SERS particles.

Chapter 6- Here, we investigate the effects of surface charge on the nonspecific binding of nanoparticles in tissues, cells and biological fluids. We also discuss the development of a novel hydroxyl-based surface coating for the elimination of this binding in biological samples.

Chapter 7- In this chapter, we investigate conjugation techniques for the coupling of targeting molecules to the surface of hydroxyl-QDs and their potential use in tissue staining applications.

Chapter 8- Finally, we discuss potential areas for further development of these technologies as well as future directions of cancer nanotechnology for diagnostic as well as other applications.

1.6 CONCLUSIONS

Recent advances in diagnostic technologies as well as our understanding of new disease biomarkers have made possible the idea of “personalized medicine”, where a patient is treated based on their specific disease fingerprint, enabled by advanced diagnostic methods. While this remains a challenge, it is clear that patient survival is significantly improved if the disease can be detected at a very early stage and known disease markers can be identified for potential therapeutic targeting and cancer classification.

CHAPTER 2

QUANTUM DOTS FOR USE IN BIOLOGICAL ENVIRONMENTS

2.1 ABSTRACT

Quantum dots (QDs) are nanometer-sized particles made of semiconductor materials which have interesting optical and electronic properties, enabling a wide array of unique applications. In particular, their fluorescence properties make them ideal for use in a number of biological assays, where ultrasensitive detection is needed. Advances in QD synthesis and surface coatings have led to a dramatic increase in interest from the biological and biomedical community and a number of important studies have been conducted. In this chapter, we discuss the synthesis of high quality QDs and their novel optical properties. We also describe the current state of art for coating the nanoparticles and transferring them to water. In addition, novel uses of QDs for both *in vitro* and *in vivo* applications are reviewed and current challenges and opportunities for the use of QDs in biological systems are discussed.

2.2 INTRODUCTION

Breakthroughs in the understanding of molecular and cellular biology have fueled the push for more advanced tools to probe cells on the molecular level. While fluorescent dyes and proteins have proven to be exceptional molecular imaging agents [68-70], there are many applications in biology where their deficits impede discovery. In particular, their tendency to photobleach under exposure to light significantly hinders their use in long term tracking studies in living cells [49, 71-73], although biologists have discovered ways to use this phenomena as an assay tool [74-76]. In addition, most fluorescent molecules have a relatively small stokes shift and can only emit under a

narrow excitation source. These problems prevent the multiplexing of fluorescent dyes to a large extent. Recent advances in nanotechnology have allowed the use of nanoparticles in a variety of applications, including biology and medicine. Polymer based nanoparticles as well as metal particles have seen a dramatic increase in interest from the medical community for both therapeutic applications as well as diagnostics and molecular imaging. Quantum dots (QDs) are an exciting new class of fluorescent nanoparticle made from semiconductor materials, such as cadmium selenide (CdSe) or indium arsenide (InAs), and have been used in a broad range of applications, including solar energy conversion[77, 78], light emitting diodes[79], displays and biomedical imaging[53, 80-85] and detection[42-45, 86]. This very broad interest is driven by their unique electronic and optical properties, including high signal brightness, resistance to photobleaching, and simultaneous excitation of multiple fluorescence colors [46, 48, 87, 88], making them exceptional for use as optical imaging agents compared to traditional organic dyes.

2.3 SEMICONDUCTOR NANOCRYSTALS

Semiconductor nanocrystals, also know as quantum dots, are typically made of II-VI or III-V semiconductor materials and are generally less than 10 nm in diameter. Many of the unique electronic and optical properties mentioned above are the result of a phenomenon called “quantum confinement”, from which a QD derives its name. When a semiconductor material is excited (for a QD, this typically involves the absorption of photons), electrons are able to leave the valence band and enter the conduction band at a higher energy level. The electron and the hole left behind when it enters the conduction band form a pair called an exciton. A material’s exciton Bohr radius is defined as the physical separation between the electron and the hole of the exciton. For

bulk semiconductor, this is extremely small compared to the size of the material, allowing the exciton to move throughout the material.

However, a QD's size is such that it is smaller than its material's exciton Bohr radius, in a size regime where the bandgap of the material can be tuned by changing the size of the nanoparticle. By decreasing the nanoparticle size to below the exciton Bohr radius, the exciton is confined, increasing the bandgap of the nanocrystal. This increase in bandgap has a direct impact on the energies involved in the production of photons from the material and means emitted light is at a higher energy than for the bulk material, resulting in light emission at a lower wavelength (blue-shifted emission). Because of this unique effect, the fluorescence emission color of the QDs can be tuned by simply altering the particle's size, providing nanoparticles with fluorescence emission in the visible light range as well as the near-infrared. CdSe QDs, the most studied for biological applications, has a bulk bandgap of 1.74 eV, corresponding to far red emission. By decreasing the nanoparticle's size, the fluorescence emission wavelength can be decreased to cover most of the visible light range, from red (particle diameter of approximately 5-6 nm) to blue (particle diameter of approximately 2 nm), as seen in Figure 2.1a.

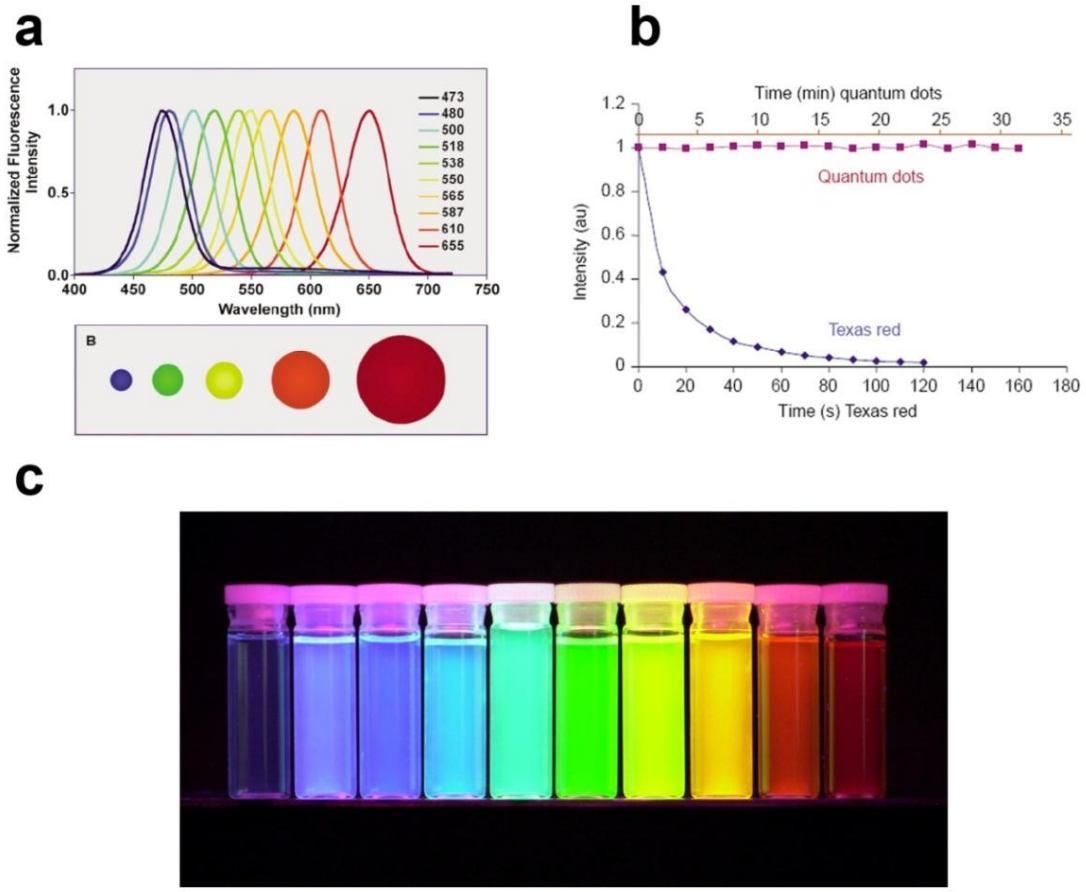

Figure 2.1. Unique optical properties of quantum dots: (a) size tunable fluorescence emission by altered nanoparticle size (from Smith et al [89]), (b) excellent photostability and resistance to photobleaching as compared to organic dyes (from Gao et al [90]), (c) simultaneous excitation of multiple fluorescence colors spanning the entire visible range, allowing highly multiplexed staining of disease biomarkers (from Han et al [47]).

QDs with very high quantum yields can be produced using improved synthetic procedures developed by our lab and others [91-94]. This, in addition to the much larger absorption cross-section of the QDs, results in a particle that is at least 20 times brighter than an organic fluorophore [95]. Resistance to photobleaching is another important feature that is necessary for use in clinical applications. Unlike organic dyes, which can begin to photobleach immediately upon exposure to light [96], the constant fluorescence intensity of QDs make them ideal imaging and biosensing agents where consistent measurements are essential (Figure 2.1b).

For multiplexed assays, which are extremely important for advanced diagnostic applications, the ability to simultaneously excite multiple QD colors with a single excitation source (Figure 2.1c) makes them far superior to organic dyes and allows for the simultaneous measurement of multiple disease markers. These properties, as seen in Figure 2.1, make QD probes well suited for multiplexed molecular profiling of intact cells and clinical tissue specimens in comparison to organic dyes.[54, 55, 90, 97-100]

2.4 COATING STRATEGIES AND TRANSFER TO WATER

Considerable advances have been made in the chemical synthesis and preparation of high quality, monodispersed QDs [91, 101, 102], especially with the use of organometallic and chelated cadmium precursors [103, 104], noncoordinating solvents [105], and inorganic passivating shells [106, 107]. These advances have led to the production of nanoparticles with very narrow size distributions (fluorescence emission FWHM < 25 nm) and high quantum yields (QY > 75%). While the resulting QDs have superb physical and optical properties, the highest quality nanoparticles typically have hydrophobic surface ligands (Figure 2.2) are often and are unsuited for use in biological environments [84, 108, 109]. To address this problem, a number of surface encapsulation and water solubilization strategies have been used to transfer QDs to aqueous solvents including direct ligand exchange of the hydrophobic surface ligands with hydrophilic small molecules, and indirect surface encapsulation techniques using silica, lipids, block copolymers and low molecular weight amphiphilic polymers [53, 80, 81, 83, 110-113].

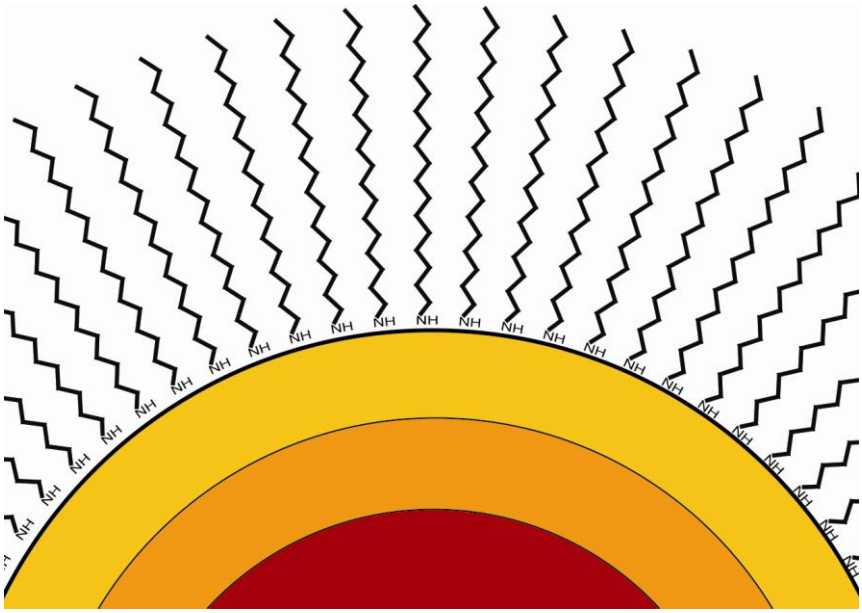

Figure 2.2. Schematic structure of a core-shell quantum dot with hydrodynamic surface ligands for stabilization. For water solubilization, the hydrophobic ligands must either be coated with an amphiphilic material or exchanged for surface ligands that are hydrophilic.

Ligand Exchange with Small Molecules

One of the first successful methods employed to transfer hydrophobic QDs to water was a direct ligand exchange method [81]. This procedure entailed transferring the nanoparticles to a solvent capable of displacing the hydrophobic surface ligands and coordinating with the surface of the nanocrystals. Thiol functional groups were found to strongly coordinate with the inorganic shell of the nanocrystal, making compounds containing these functional groups, such as mercaptoacetic acid, ideal for initial transfers to water. By using small molecules for the transfer to water, the physical and hydrodynamic size of the nanoparticles was also kept to a minimum, as seen in Figure 2.3, important for some biological applications. However, QDs produced in this manner tend to be unstable after a matter of days, leading to particle aggregation and precipitation. Further advances have been made for this transfer strategy, using other

functional groups to coordinate with the QD surface and ligand molecules capable of multivalent coordination to the surface to improve the stability of the particles [48, 110, 111, 114]. In addition, biocompatible molecules such as amino acids, proteins, etc. have also been used for direct ligand exchange and QD coatings [82, 115].

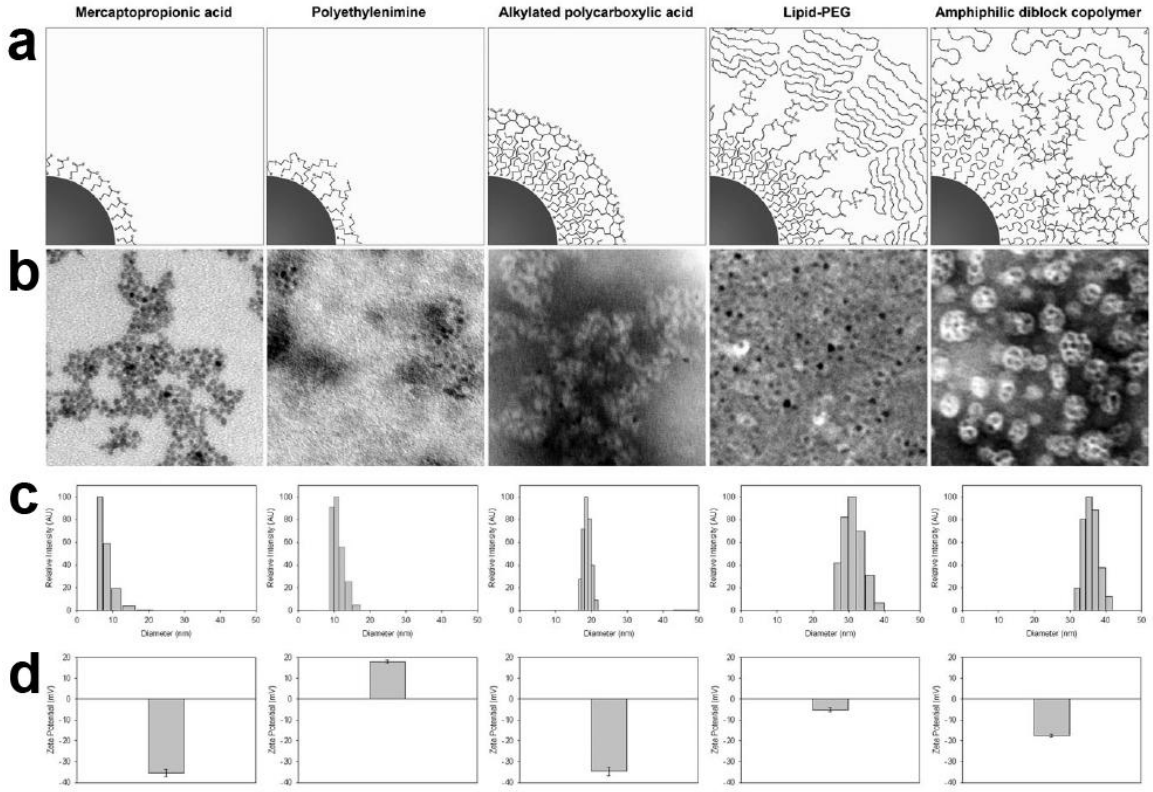

Figure 2.3. Quantum dot coatings and colloidal properties (from Smith et al [116]). (a) Schematics showing a variety of common quantum dot coatings used for transfer to water, including (left to right) mercaptoproprionic acid, polyethylenimine, alkylated polycarboxylic acid, lipid-PEG and amphiphilic diblock copolymers. (b) Transmission electron micrographs (TEM) of coated quantum dots in water, counterstained to show organic coating layer. (c) Dynamic light scattering data reveals nanoparticle hydrodynamic sizes ranging from ~ 8 nm to over 30 nm. (d) Nanoparticles can be designed with a range of surface charges, depending on the functional groups present on the surface.

Polymer Coatings

A second strategy for the transfer of QDs to aqueous environments involves the coating of the hydrophobic nanoparticles with a small amphiphilic polymer. The overall design strategy is to use polymers that are capable of interacting with both the hydrophobic surface of the nanoparticle as well as the aqueous environment. A number of polymers have been used for this technique, including low molecular weight polymers [53, 108], block copolymers [117, 118], and triblock copolymers [84]. Particles transferred using these techniques tend to have higher quantum yields than other particles, likely due to the protective layer of the hydrophobic segments of the polymer and the original surface ligands. These particles are also much more stable than ligand exchanged QDs, due to the multiple interactions between the polymer and the QD surface. One notable downside to these strategies is a substantial increase in particle size, as seen in Figure 2.3. Retaining the original hydrophobic surface ligands adds an additional 1-2 nm to the overall particle size. In addition, the bulky polymers can significantly add to the overall size, resulting in particles that could be as much as 2-3 times as large as particles prepared using standard ligand exchange methods.

The coating techniques described above have allowed a number of exciting biological studies to be conducted and progress has been made in the use of QDs for ultrasensitive detection in solution as well as in cells, tissues and *in vivo*.

2.5 QUANTUM DOT-BASED ASSAYS FOR CLINICAL APPLICATIONS

QDs are of particular interest for diagnostics and molecular imaging because of their small size and unique fluorescence properties, as described above. As a result, many groups, including our own, have reported the use of QDs in a variety of applications, including live cell imaging and tracking [73, 119-121], single molecule tracking [122, 123], cell and tissue staining [53, 54, 81] and *in vivo* imaging [83-85].

Solution Assays

A number of unique solution based assays have been developed using QDs as ultrasensitive imaging agents. Because of their extremely bright fluorescence (a single QD particle can be seen under standard fluorescence microscopy), QDs enable the detection of analytes at extremely low concentrations, increasing the sensitivity of many standard assays. In addition, QDs in multiple colors and in varying ratios can be embedded into polymer or silica microspheres [43, 47, 86], resulting in an optical barcoding system that can be used for distinguishing hundreds or thousands of unique analytes. Another important QD trait exploited to develop sensitive detection assays is their large stokes shift and broad excitation profiles, which allows multiple QDs to be excited simultaneously using a single, high energy excitation source. By using nanoparticles with two different colors and instrumentation capable of detecting photon coincidence, QDs can be used as ultrasensitive probes for the detection of many analytes and large particles, as seen in Figure 2.4b [45], and can also be used to detect binding events. This technology has been used to detect virus particles at the single virus level and can distinguish variations in viral surface proteins to determine virulence in a sensitive manner in real-time [44].

The ability to excite multiple QDs simultaneously as well as their uniform and bright fluorescence has also been exploited to perform single molecule detection and

molecular imaging at resolutions much greater than theoretically possible with standard optical imaging. Because the fluorescence intensity profile of a QD can be modeled as a Gaussian distribution, algorithms can be developed to pinpoint the location of the particle in a very precise manner. By using QD conjugated probes of different colors (red and green) and image processing algorithms, DNA length can be analyzed at the single molecule level and at nanometer resolutions (Figure 2.4a), far below the diffraction limit associated for traditional light microscopy [42]. This technique can also be used to detect the binding of nucleic acid pairs at extremely low levels, providing an assay capable of ultrasensitive detection.

Cell and Tissue Staining

Cell and tissue staining is another application that has received considerable attention for the use of QDs. As mentioned earlier, organic dyes diminish in fluorescence upon exposure to light and can be quenched in seconds to minutes. This, in addition to their lower fluorescence intensity, makes them difficult to use for long term tracking of molecules in live cells. The fluorescence properties of QDs, on the other hand, make them ideally suited for this type of application. Of particular interest for these applications are their photostability and the ability to excite multiple QD colors simultaneously. For single molecule tracking, photostability is of utmost importance when selected an imaging agent. QDs have been shown to maintain a stable fluorescence intensity under bright excitation for over 30 minutes, enabling them to be used for long term molecule tracking [121-123].

In addition to interesting molecular studies in cells, tissue staining is proving to be an exciting application for QDs [54]. The potential for multiplexing opens the possibility of a QD revolution for molecular imaging in cells and pathological analysis of tissues, as seen in Figure 2.4d. Where traditional techniques allow for only a single dye or stain for

marker detection, QDs enable the detection of multiple markers simultaneously. In fact, up to five biomarkers have been simultaneously imaged in clinical tissue samples [100], with the potential for even higher degrees of multiplexing. In addition to higher brightness and stability, the fluorescence emission spectrum of QDs is well suited for use in complex samples. The QD spectra can be approximated as a normal distribution with a narrow peak, unlike dyes, which have broader peaks and tailing effect on the lower energy side of the curve. This makes it easier to subtract background autofluorescence from the image and isolate the desired signals. The optical stability of QDs also makes them attractive for this application, where samples are often stored and may be revisited at a later time for a second opinion or reanalysis.

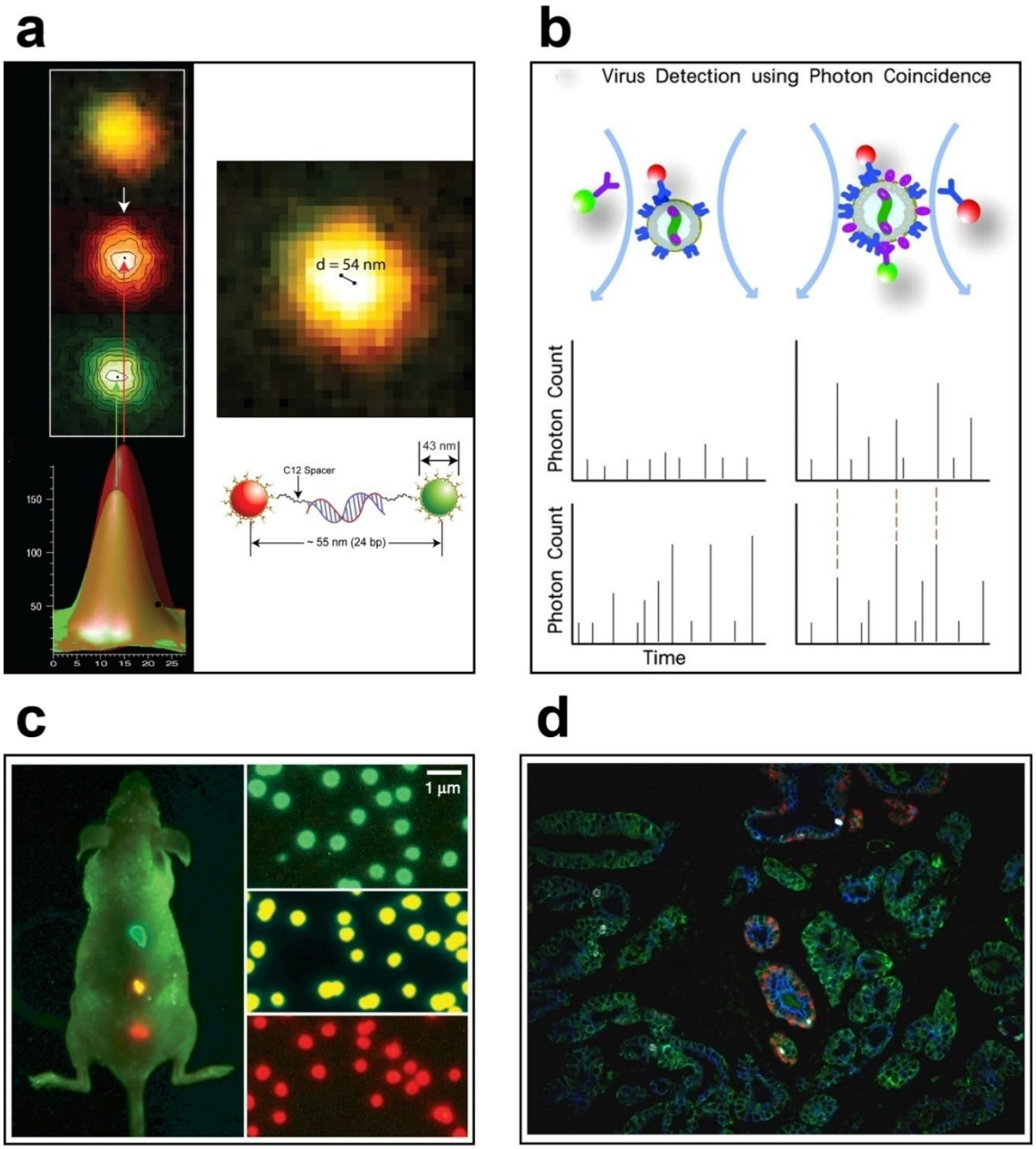

Figure 2.4. Biomedical applications of quantum dots. Quantum dots have utility in a number of diagnostic and ultrasensitive molecular imaging applications in tissue and *in vivo* environments, as well as in solutions. (a) Nanometer-scale mapping of single DNA chains by microscopy. By using quantum dot conjugated probes and image processing algorithms, DNA length can be analyzed at nanometer resolutions, far below the diffraction limit associated for traditional light microscopy (from Agrawal et al [42]). (b) Quantum dots in two colors enable ultrasensitive virus detection at single particle levels using photon coincidence (from Agrawal et al [44, 45]). Quantum dots are also extremely useful for multiplexed molecular imaging (c) *in vivo* (from Gao et al [84]) and (d) in clinical tissue samples (image courtesy of Dr. Jian Liu).

In Vivo Imaging

The unique optical properties of QDs have also allowed their use in many exciting *in vivo* applications, including live cell tracking and tumor detection. QDs with a PEG coating have been used in *Xenopus* embryos to track cells during development and were found to be stable, slow to photobleach and nontoxic during the course of the experiment [83]. QDs were injected into an individual blastomere during early cleavage stages and fluorescence could be tracked to the tadpole stage of development. This exciting new tool for lineage tracking could lead to an enhanced understanding in the field of embryology. QDs have also been employed in the tracking of cancer cells in mouse models [120]. Tumor cells were loaded with QDs and then intravenously injected into mice. These labeled cells were tracked as they extravasated into the lung and were shown to behave identically to unlabelled cells, providing a powerful method to study cancer metastasis. The ability to track cells *in vivo* is expected to be an important research tool for a broad range of fields, including oncology, embryology, and immunology.

In addition to studying labeled cells, molecular imaging *in vivo* using QD technology has also been reported. QDs coated with PEG and targeted to prostate-specific biomarkers have been delivered intravenously into animal models and were shown to accumulate in the subcutaneous tumor (Figure 2.4c) [84]. This was the first report of simultaneous targeting and imaging of QDs for *in vivo* applications. Since that work, there have been a number of exciting studies showing the utility of QDs as *in vivo* imaging agents. In particular, type II QDs (a new class of QDs capable of emission in the near infrared) were shown to function well *in vivo* and could improve the depth limitation seen with type I QDs [85]. This limitation significantly hinders the utility of QDs emitting in the visible range, where tissue and other components can strongly absorb.

Research by our group and others is ongoing to develop new QD probes capable of near-infrared emission with quantum yields suitable for use in deep tissue imaging [124].

2.6 CHALLENGES AND OPPORTUNITIES

Critical advances in the development and use of QDs and similar nanoparticles have made their use in biological and medical applications imminent. Particularly, techniques for coating and water solubilizing high quality nanoparticles have substantially contributed to their adoption by biological researchers. While the progress made in this field is monumental, significant challenges remain. Even nanoparticles designed for use in cells, tissues and *in vivo* exhibit problems such as potential toxicity. Usefulness as an *in vivo* clinical imaging agent, where the potential toxicity of cadmium-containing QDs is of major concern and the ultimate fate of nanoparticles in the body is unclear, remains to be seen for human patients. Many preliminary studies have shown that toxicity issues for QDs *in vivo* are of some concern [125, 126]. Although this could eventually prevent their use *in vivo*, immunohistological and cellular and tissue staining is performed on *in vitro* or *ex vivo* clinical samples, where heavy metal toxicity is inconsequential. As a result, the use of multicolor QD probes for tissue staining and biomarker detection is likely one of the most important and clinically relevant applications in the near term [54, 55, 99, 110].

However, a significant hurdle for the use of QDs in this clinical setting is that the water soluble probes tend to be “sticky” and often bind nonspecifically to cellular membranes, proteins, and extracellular matrix materials. These nanoparticles also show strong binding to components in blood, plasma and serum, significantly limiting their use in these samples. This nonspecific binding problem causes a high fluorescence background signal that degrades the signal-to-noise ratio and limits staining specificity and detection sensitivity. It can also lead to false positive staining for biomarkers in cells

and tissues. Recent work has shown that size and surface chemistry play a critical role in determining the binding properties of QDs and other nanoparticles. These discoveries present an opportunity for the design of new QD probes that are functional in a range of clinical environments.

As coating strategies continue to develop, new applications for these technologies will certainly emerge. Techniques to minimize the size of the particles as well as provide complete protection of the nanoparticle may enable the use of QDs *in vivo*. It has been shown that small molecules (less than 6 nm) are able to be cleared from the body by renal filtration. Designing nonstick nanoparticles that are stable and have a completely protected nanocrystal core could clear the way for the first human trials for this technology. New coatings could also lead to multifunctional probes, which can provide imaging capabilities in multiple modalities (such as MRI, CT, PET, etc.) as well as deliver a drug payload to the targeted disease tissue.

Ultimately, these developments will lead to an era of personalized medicine, where the diagnosis and treatment of a patient will be done on an individual basis, based on the patient's disease profile. These technologies will also dramatically reduce the time required to diagnosis and treat a patient, rapidly improving patient care.

2.7 CONCLUSIONS

QDs have been shown to have great potential in the fields of biology and medicine, in particular cancer diagnostics. However, challenges remain before the adoption of QDs in clinical applications becomes widespread. In this work, the interaction of polymers and nanoparticle surfaces as well as how surface chemistry affects the interaction of nanoparticles and biomolecules will be addressed. Bright and stable nanoparticles are needed to deliver optimal performance for imaging and sensing applications. This work will explore polymer-coatings for QDs and describe the

parameters for optimizing nanoparticle stability and optical performance. The use of these low molecular weight polymers in a one-pot nanoparticle synthesis method will also open a new avenue for the production of high quality nanoparticles for the clinical market. Nonspecific binding will also be addressed by examining nanoparticle surface chemistry and its effects on the interaction of nanoparticles with biological molecules such as proteins, nucleic acids and organelle membranes. The results of these studies provide a novel QD suitable for ultrasensitive and multiplexed detection of disease biomarkers in biological fluids, cells and tissues.

CHAPTER 3

SYNTHESIS AND CHARACTERIZATION OF AMPHIPHILIC POLYMERS FOR QUANTUM DOT COATING

3.1 ABSTRACT

Because high quality quantum dots (QDs) are typically synthesized in high temperature, oily solvents, the resulting nanocrystals are hydrophobic and unsuitable for use in biological environments. To phase transfer the nanoparticles to water, a variety of techniques have been developed, including polymer coating. In this chapter, we have developed and optimized the polymer synthesis and purification techniques to develop low molecular weight polymers for use in nanoparticle coating applications. We have also extensively characterized the polymers to determine parameters important for their use with QDs and other nanoparticles, including solubility, critical micelle concentration (CMC), conjugation percentage and hydrodynamic size in solution. After successfully coating and water solubilizing the QDs, water purification procedures were developed to yield highly fluorescent, monodisperse nanoparticles. The colloidal and optical properties of the nanoparticles were then analyzed, particularly absorption and fluorescence, quantum yield and hydrodynamic size. We have also systematically altered the polymer synthesis and coating procedure to determine the effects of the polymer parameters on the nanoparticle coating process and optimized the stability and optical properties for use in biological applications. It was found that an amphiphilic polymer with 40% of the carboxylic acid functional groups modified with a 12 carbon aliphatic chain was ideal for QD coating, yielding monodispersed, single particles with quantum yields of 60% or higher.

3.2 INTRODUCTION

Advances in polymer science and chemistry have not only increased the fundamental understanding of the behavior of molecules on a nanometer level, but also led to the development of a number of new and exciting applications for this technology. Significant breakthroughs in medicine, materials and energy have been achieved because of the progression of polymer technology. Specifically, polymers have made substantial contributions to the development of drug delivery technologies [127-132], clinical imaging agents [133-139], organic LEDs or other optoelectronic devices [140, 141], and drug eluting stents [142, 143],to name just a few applications. Amphiphilic block copolymers (typically with one segment that is hydrophilic and one that is hydrophobic) have been extensively studied for use in biomedical applications. These polymers have also been studied on a more fundamental level, examining the complex morphologies they can self assemble into (Figure 3.1), to aid in the design of complex, polymer-based technologies. One major driving force for the self assembly of amphiphilic polymers into micelles or other particle-like aggregates in polar solvents (such as water) is the interaction between the hydrophobic and hydrophilic segments of the polymer with the aqueous environment. Free energy is decreased as hydrophobic segments of the polymer are buried in the interior of the nanoparticle and shielded from the aqueous surrounding by the hydrophilic segments [144], driving the spontaneous assembly of the polymers into a variety of confirmations.

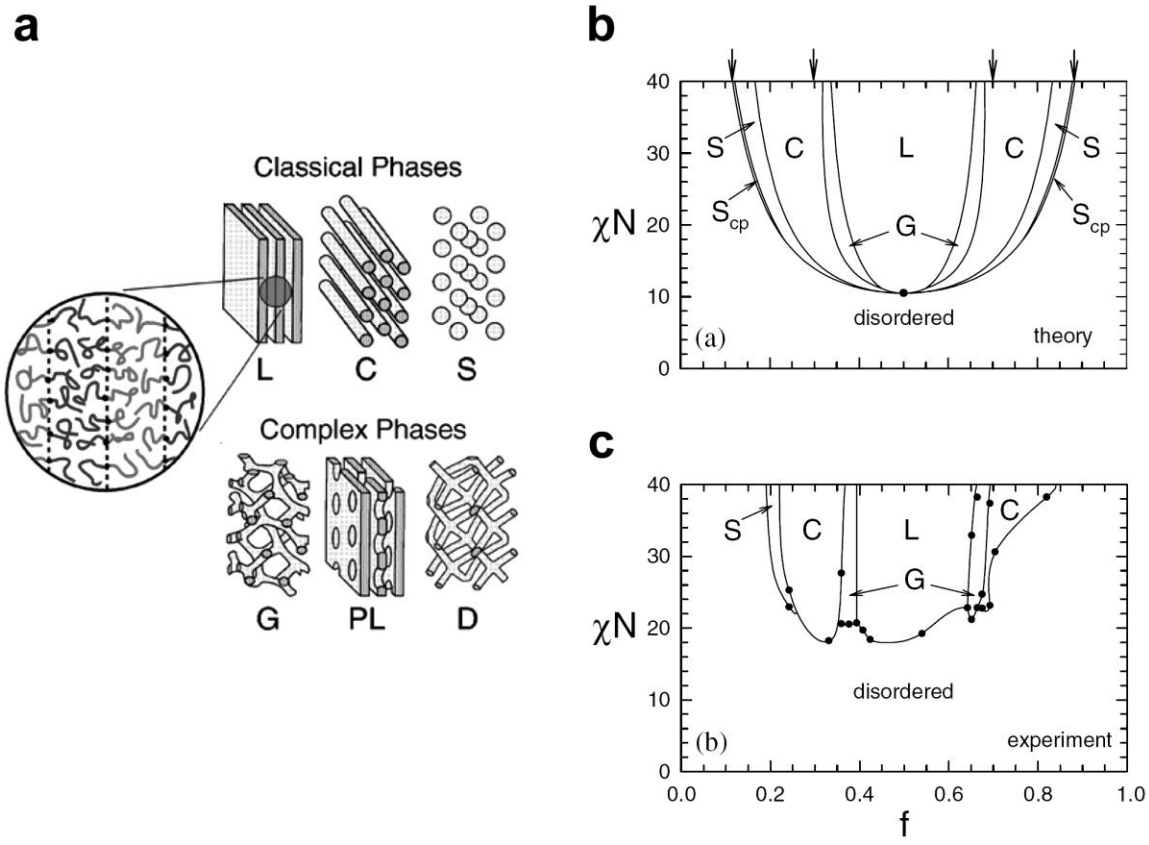

Figure 3.1. Self-assembly of block copolymer melts. (a) Illustration of six common morphologies taken by block copolymer melts, divided into classical phases (lamellar, cylindrical, and spherical) and complex phases (gyroid, perforated-lamellar and double-diamond) [145]. (b) Theoretical and (c) experimental phase diagrams using polystyrene-polyisoprene diblock copolymers, where f is the fraction of one block and χN, the Flory-Huggins parameter, is the mean field approximation of the local interactions between polymer segments [145-149]. Experimental measurements match well with the theoretically predicted phases. From Matsen et al [145].

Many groups have taken advantage of this assembly process and used these polymers for the encapsulation and soubilization of a number of hydrophobic materials for use in aqueous solutions, including drugs and imaging contrast agents. In particular, block copolymers have been extensively used by our group and others for the coating and water solubilization of QDs and other hydrophobic nanoparticles [116, 118, 150]. Using a variety of techniques, polymer micelles can be loaded with as few as one

nanoparticle to tens or hundreds of particles, providing a diverse tool for the design of single or multimodal imaging agents.

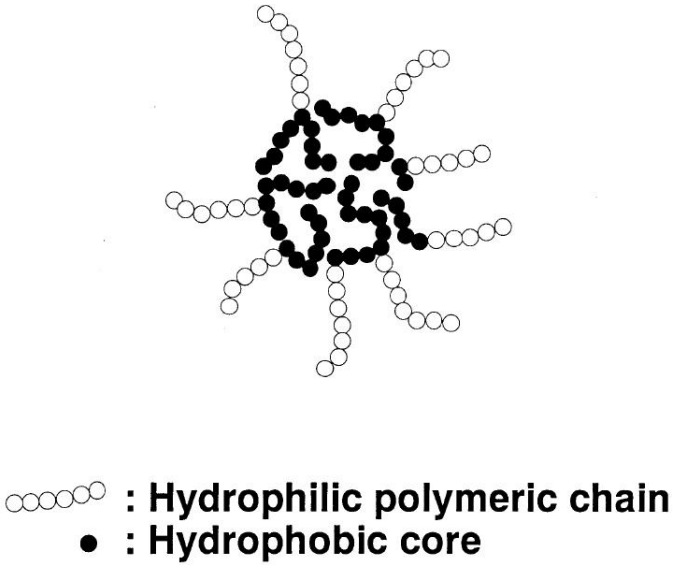

Figure 3.2. Illustration showing a graft copolymer with small polymer segments randomly "grafted" to a backbone polymer [151]. Hydrophobic and hydrophilic portions of the polymer can drive the self-assembly of nanoparticles [152]. From Sakuma et al [151].

Although block copolymers are an excellent tool for the development of micellar contrast agents, these particles tend to be large because of the large size of the amphiphilic polymers. Graft copolymers (shown in Figure 3.2) have been studied in less detail for these types of applications but are extremely promising. While block copolymers have their segments attached end to end, graft copolymers have a "backbone" polymer with smaller polymer units randomly "grafted" along its length. This could allow for interesting interactions with the surface of nanoparticles, with the backbone wrapping around the particle while the grafts interact with the hydrophobic surface ligands present. In addition, small, "pseudo" graft copolymers could be produced that utilize a small polymer backbone with molecules serving as the "graft"

segments. We have hypothesized that these small polymers can effectively coat the surface of nanoparticles and allow for an extremely small polymer coating

To successfully cover the surface of the nanoparticle with a polymer-coating suitable for use in biological applications, the polymer must be designed in such a way that enables interaction with both the hydrophobic ligands on the surface of the particle and the aqueous environment. Based on these criteria, we hypothesized that an amphiphilic polymer with long hydrocarbon chains capable of noncovalent interactions with the surface ligands and a hydrophilic backbone to interact with the aqueous environment could render the nanoparticles water soluble. Furthermore, hydrophobic and hydrophilic interactions between the nanoparticle surface, the amphiphilic polymer and the aqueous solvent are able to drive the self assembly of the polymer on the surface of the QDs, completely encapsulating the nanoparticle. In addition, by varying the length of the hydrophobic regions of the polymer, the degree of hydrophobicity and the polymer : QD ratio, both the stability and optical properties of the particles can be tuned.

In this chapter, we have developed and optimized the polymer synthesis and purification techniques to develop low molecular weight polymers for use in nanoparticle coating applications. We have also extensively characterized the polymers to determine parameters important for their use with QDs and other nanoparticles, including solubility, critical micelle concentration (CMC), conjugation percentage and hydrodynamic size in solution. After successfully coating and water solubilizing the QDs, water purification procedures were developed to yield highly fluorescent, monodisperse particles. The colloidal and optical properties of the nanoparticles were then analyzed, particularly absorption and fluorescence, quantum yield and hydrodynamic size. We have also systematically altered the polymer synthesis and coating procedure to determine the effects of the polymer parameters on the nanoparticle coating process and optimized the

stability and optical properties for use in biological applications. It was found that an amphiphilic polymer with 40% of the carboxylic acid functional groups modified with a 12 carbon aliphatic chain was ideal for QD coating, yielding monodispersed, single particles with quantum yields of 60% or higher.

3.3 METHODS

Amphiphilic Polymer Synthesis

The amphiphilic polymers used in these studies were synthesized using standard carbodiimide chemistry. Poly(acrylic) acid (MW = 1800 Daltons) and a primary alkylamine (hexadecylamine, octylamine, decylamine, dodecylamine, tetradecylamine, hexadecylamine or octadecylamine) were dissolved in dimethylformamide (DMF) at a molar ratio of 2:5 primary alkylamine to carboxylic acid. Dicyclohexylcarbodiimide (DCC) was dissolved in a minimum amount of DMF and added dropwise to the solution in a slight molar excess to the primary alkylamine present. The reaction solution was mixed vigorously for 24 hours to give an amphiphilic polymer with 40% of the carboxylic acid functional groups modified with an aliphatic chain (Figure 3.3).

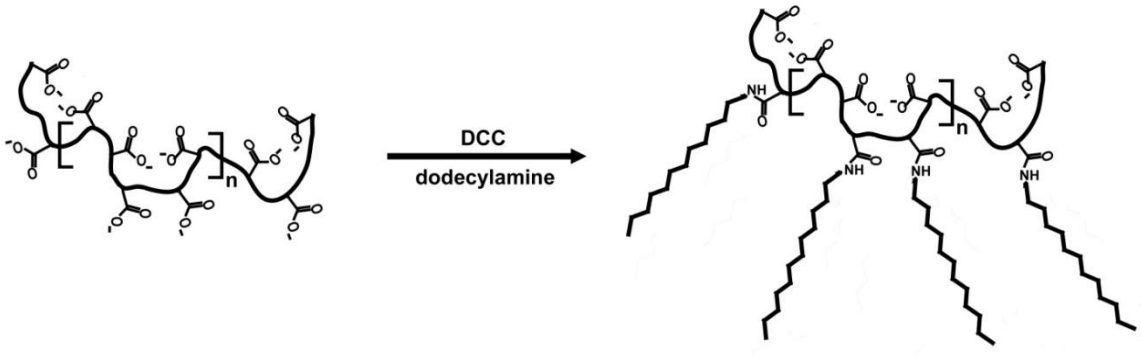

Figure 3.3. Reaction scheme for an amphiphilic polymer to be used for synthesis and coating of nanoparticles for biological applications. The hydrophobic carbon chains are able to intercalate into the hydrophobic surface ligands of the nanoparticle, coating the surface and leaving carboxylic acid functional groups for water solubilization and particle stabilization.

Polymer Purification

The polymer solution was cooled in an ice bath to facilitate the precipitation of the dicyclohexylurea (DCU) byproduct. The insoluble DCU was removed using vacuum filtration, leaving a transparent, slightly yellow filtrate. The polymer filtrate was then added dropwise to a solution of aqueous sodium hydroxide (pH ~10) under vigorous stirring to yield a slightly cloudy aqueous solution. Vacuum filtration was again used to remove any insoluble contaminants (trace DCU, unreacted DCC and alkylamine), resulting in a slightly opaque solution. Under vigorous stirring, hydrochloric acid (HCl) was added dropwise to precipitate the polymer product. This mixture was vacuum filtered to collect the precipitated product and washed with deionized (DI) water to remove any residual aqueous contaminants. The purification process was repeated 3 times by redissolving the product in aqueous sodium hydroxylde (pH ~ 10), filtering to remove insoluble contaminants, acidifying to precipitate the polymer and finally collecting the precipitate through filtration. The polymer precipitate was then freeze dried to remove trace amounts of water, giving a dry, white powder.

Polymer Conjugation Titration Assay

25 mg of purified amphiphilic polymer was transferred to a 125 mL Erlenmeyer flask. The polymer was then dissolved using 50 mL of ethanol (EtOH). The flask was moved to a stir plate and a stir bar was added to completely mix the sample. 2 drops of a 2% Phenolphthalein solution (in EtOH) were added to the sample as a color indicator. Separately, a 0.05 M solution of aqueous sodium hydroxide (NaOH) was prepared. The polymer sample was titrated with aqueous NaOH under vigorous stirring until the solution retained a faint pink color, noting the volume of NaOH used. Moles of NaOH were used to calculate the moles of COOH present and the conjugation percentage of the polymer.

Critical Micellar Concentration

A 0.6 M solution of pyrene was prepared in acetone. Polymer solutions ranging from 0.5 µg/mL to 1 mg/mL were separately prepared in water (pH ~8). 1 mL aliquots of the pyrene/acetone solution were transferred to glass vials and the acetone was evaporated overnight under reduced pressure. 1 mL of the polymer concentration series were added to the vials and the samples were vortexed. The samples were then heated at 80ºC for 2 hours to equilibrate the partitioning of pyrene into the polymer micelles. The vials were then wrapped with foil to prevent light exposure and allowed to cool to room temperature overnight. The samples were analyzed using a spectrofluorometer, with excitation and emission wavelengths of 339 nm and 390 nm, respectively.

Polymer Hydrodynamic Size

Dynamic Light Scattering (DLS) data, used to determine the polymer aggregates hydrodynamic size in water, was obtained on a Brookhaven Instruments 90 Plus Particle Analyzer. Amphiphilic polymers with aliphatic chains from 8 to 18 carbons long were dissolved in basic water (pH ~8) at a concentration of 5 mg/mL. The samples were vortexed and sonicated and then filtered through a 0.45 µm filter to remove dust or other contaminants present. 500 µL aliquots were then taken and measured using DLS. Experiments were carried out for 2 minutes with 3 replicate runs and analyzed using the Number Multimodal Size Distribution mode.

Quantum Dot Synthesis

Cadmium selenide (CdSe) QDs were synthesized in a noncoordinating solvent as reported in previously published procedures. The nanocrystal cores were purified using liquid-liquid extraction with hexane and methanol (MeOH) 3 times. The purified nanoparticles in the hexane layer were then transferred to a centrifuge tube and precipitated using an excess of acetone. The solution was centrifuged at 7000g for 15 minutes to collect the insoluble QDs. After resuspending in chloroform ($CHCl_3$), the QDs were transferred to a mixture of octadecene (ODE) and octadecylamine (ODA) and heated under vacuum to remove any volatile solvents. An inorganic passivating shell of cadmium sulfide (CdS) and zinc sulfide (ZnS) was then grown on the nanocrystals using organometallic precursors at ~220ºC, as described in literature. The crude QD solution was then rapidly cooled to room temperature and transferred to glass vials and stored long term at -20ºC.

Quantum Dot Coating and Transfer to Water

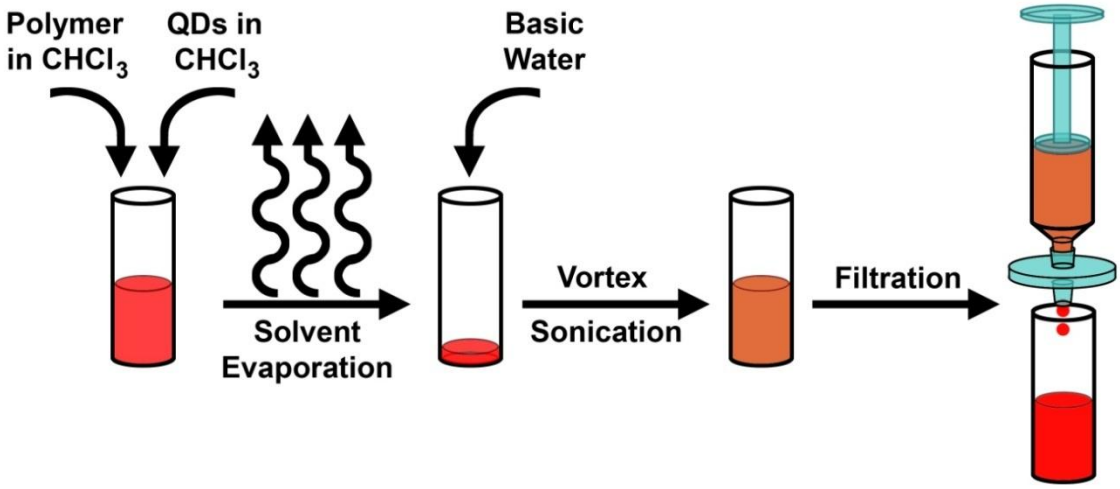

Figure 3.4. Quantum dot coating and water purification schematic. Both hydrophobic quantum dots and polymer were dissolved in chloroform ($CHCl_3$) and mixed in a vial. The $CHCl_3$ was evaporated under reduced pressure, leaving a polymer/quantum dot film. Basic water (pH 10) was added and the solution was vortexed and sonicated to dissolve the coated quantum dots, leaving a slightly opaque solution. Filtration through a 0.2 μm filter resulted in a highly fluorescent, transparent solution.

An aliquot of crude QDs was diluted into hexane and purified using liquid-liquid extraction from hexane and MeOH as described above. The nanocrystals were then precipitated using acetone and centrifuged at 7000 g for 15 minutes to form a QD pellet. The pellet was then resuspended in a minimal amount of $CHCl_3$. Separately, an amphiphilic polymer (poly(acrylic acid)-dodecylamine, PAA-DDA) was dissolved In $CHCl_3$ at a concentration of 10 mg/mL. The QD and polymer solutions were mixed in a glass vial at a molar ratio of 500:1 polymer to QD (Figure 3.4). The solution was vortexed to ensure complete mixing and the $CHCl_3$ was slowly removed under reduced pressure overnight, leaving a thin polymer/QD film in the vial. Basic water (pH ~10) was added to the vial and the solution was vortexed and sonicated in a bath sonicator for 10 minutes to completely resuspend the polymer coated QDs in water, resulting in a slightly

cloudy solution. The QD solution was then filtered through a 0.2 μm filter to remove any insoluble contaminants, yielding a transparent, fluorescent solution.

Water purification of quantum dots

Water soluble QDs were transferred to a cellulose ester 100 kDa MWCO dialysis tube (Spectra/Por) and dialyzed against 2 L of 50 mM Borate Buffer for 7 days, exchanging the buffer daily. The purified solution was then concentrated under reduced pressure using a rotavapor at reduced pressure and ~15ºC.

Verification of Polymer Removal

Polymer removal from QD samples was determined by TEM. Purified and unpurified QD samples were prepared and filtered to remove any dust contaminants. 5 μL of the samples were then pipetted onto a carbon TEM grid. The solvents were slowly wicked away with filter paper after 15 minutes and the grids were then counterstained with a 1% phosphotungstic acid solution (pH adjusted to 6) for 30 seconds. The staining solution was slowly wicked away and the grids were imaged and compared to determine the degree of polymer removal. FPLC was also used to confirm polymer removal from QD samples. A pure polymer solution was first analyzed to determine it's elution time. Samples of purified and unpurified QD solutions were then analyzed using FPLC and the change in intensity of the polymer peak was observed.

Fluorescence microscopy of single quantum dots

A 50 nM solution of QDs was prepared for microscopy. The sample was sonicated to disperse any aggregates and filtered to remove contaminants. 1.5 μL of the purified QD solution was pipetted onto a glass coverslip. A second coverslip was placed

on top to form a thin film between the coverslips, which was allowed to dry overnight. The coverslips were then separated and imaged on a fluorescent microscope at 100x.

Polymer effects on quantum dot fluorescence intensity

Amphiphilic polymers with carbon chain lengths from 8 to 16 carbons were prepared and used to coat 630 nm QDs at varying QD : polymer ratios. The QDs were transferred to water and purified as described above. The samples were then diluted to 200 nM and fluorescence intensity spectra were recorded using a spectrofluorometer. Fluorescence intensity was taken as the area under the curve of the fluorescence spectrum.

pH Stability of Polymer-Coated Quantum Dots

A 100 nM solution of QDs was prepared in DI water and vortexed and sonicated for 15 minutes to redisperse any aggregates. The sample was then filtered using a 0.2 μm filter to remove any large contaminants. Separately, a 0.1 M solution of citric acid and a 0.2 M solution of sodium phosphate dibasic (Na_2HPO_4) were prepared in water. These solutions were mixed in various ratios to produce buffers ranging from pH 2.5 to 7.5. 900 μL of the buffers were pipetted into glass vials. 100 μL of the QD sample were then transferred to the vials, which were then vortexed briefly to mix the solutions. Fluorescence measurements were taken using a spectrofluorometer before and after filtering though a 0.2 μm filter and the ratios were then plotted.

Quantum Dot Size Analysis

QD size was independently analyzed using 3 separate techniques. Counterstained TEM was used to image both the nanocrystal core as well as the polymer shell surrounding the core. These images were analyzed using ImageJ to

determine a size distribution for the sample and an average size for the coated particles. DLS was used as described above to measure the hydrodynamic diameter of the nanoparticles. QD samples were prepared at 50 nM and filtered using a 0.2 μm filter immediately before reading the sample to eliminate dust. FPLC was also used to determine the hydrodynamic size of the QDs. Briefly, globular protein standards with known hydrodynamic diameters were measured and elution time was noted and used to develop a standard curve. QD hydrodynamic size was then analyzed using FPLC elution times and the protein standard curve.

3.4 RESULTS AND DISCUSSION

Because the optical and colloidal properties of quantum dots (QDs) are heavily influenced by the protection of the surface and surface ligands of the nanocrysal, we hypothesized that these important properties can be optimized by coating with an amphiphilic polymer specifically designed for encapsulating the QD and interacting with the hydrophobic surface. In particular, we speculated that the hydrophobic component of the polymer was particularly important for an optimally designed amphiphilic polymer. This is the portion of the polymer responsible for driving the self assembly of the coating through strong noncovalent interactions with the surface of the nanoparticle. By altering the hydrophobic component as well as the ratio of hydrophilic : hydrophobic portions of the polymer, we can maximize the noncovalent interactions between the polymer and the surface ligands to increase the colloidal stability and further improve the optical properties of the nanoparticle. This component also has a significant impact on the free polymers behavior in water, affecting the purification of the polymer-coated QDs as well.

Polymer Development and Selection

In order to develop a polymer-coating suitable for encapsulating and solubilizing hydrophobic QDs or other nanoparticles, several important parameters were considered. High quality QDs typically have hydrophobic surface ligands with long hydrocarbon chains such as hexadecylamine or oleylamine, as shown previously in Figure 2.2. The polymer to be used for nanoparticle coating must have a hydrophobic component capable of strong noncovalent interactions with these surface ligands. An amphiphilic polymer containing a number of long hydrocarbon chains was determined to be ideal for coating the nanoparticle surface, as they can intercalate into the hydrophobic ligands on the surface as the hydrophilic polymer backbone wraps around the nanoparticle. These also provide the added benefit of protecting the surface of the nanocrystal from the biological environment. Fully extended, the surface ligands and polymer-coating provide a barrier of approximately 1.5 nm between the aqueous environment and the surface of the nanocrystal. Protection of the nanocrystal surface from water, oxygen or other compounds that could react with the nanocrystal and cause surface defects or oxidation[116] is extremely important in preserving the excellent optical properties exhibited by high quality QDs. By providing a hydrophobic barrier, similar to the fatty acid barrier of a cell membrane, many of these damaging species can be effectively blocked from reaching the nanoparticle surface. The polymer also stabilizes the hydrophobic ligands and prevents dissociation from the surface, further preserving the outstanding optical properties seen before transfer to water.

When designing the polymer, the hydrophilic : hydrophobic ratio was another important parameter to consider. Because of their extremely small size, nanoparticles have a very small radius of curvature. This high curvature greatly affects the way ligands behave on the surface of the particle and interact with each other. It was necessary to design the polymers with a hydrophobic conjugation percentage low

enough to allow the polymer backbone to conform to the curvature of the nanoparticle. A 40% conjugation ratio (40% of the original carboxylic acid functional groups conjugated to hydrophobic carbon chains) was determined to be acceptable for strong interactions with the hydrophobic surface while maintaining good nanoparticle coverage.

The polymer must also contain a hydrophilic portion capable of interacting with the surrounding aqueous environment and rendering the coated nanoparticle water soluble. There are a number of functional groups suitable for nanoparticle stabilization and water solubilization, such as carboxylic acids, amines and silica functional groups. Carboxylic acids were chosen because of the availability of high quality poly(acrylic acid) polymers for use as a polymer backbone and the relatively simple chemistry associated with these functional groups. They have also been shown to provide excellent colloidal stability for the nanoparticles [81] and resist particle aggregation through electrostatic repulsion. Based on the above criteria, amphiphilic polymers with a backbone containing carboxylic acid functional groups as well as a number of long, hydrophobic carbon chains was chosen for further study.

Polymer Synthesis and Purification

Because poly(acrylic acid), which contains carboxylic acid functional groups, and a number of long chain alkylamines are readily available, these were chosen as starting materials for the synthesis of amphiphilic polymers for further studies. Carbodiimide chemistry was used to couple a portion of the carboxylic acids to the primary amine of primary alkylamine molecules (as shown above in Figure 3.3). This chemistry is often used in peptide synthesis for the formation of amide bonds between the carboxylic acid and amine groups of amino acids and in the activation of carboxylic acids towards ester formation. N,N'-dicyclohexylcarbodiimide (DCC) was used as the carbodiimide dehydration agent because of its solubility in dimethylformamide and the insolubility of its

hydrolysis byproduct, dicyclohexylurea (DCU), for easy purification. A number of parameters for the polymer synthesis were studied to optimize the procedure for a variety of conjugation ratios and alkyl chain lengths. Reaction temperature was found to be critical and was optimal at 45ºC, with unpredictable results occurring above 75 ºC.

Synthesis and purification of a number of amphiphilic polymer variants (varying the hydrophobic portion of the polymer) was performed, as described above. Polymers were produced with alkyl chains varying in length from 8 carbons to 18 carbons, while keeping the conjugation percentage (percentage of original carboxylic acid functional groups modified with an alkylamine) at approximately 40%. Table 3.1 shows the amphiphilic polymers produced as a result of these synthesis procedures.

Table 3.1. Amphiphilic polymer variants used in these studies. Amphiphilic polymer were produced with alkyl chains varying in length from 8 carbons (PAA-OA) to 18 carbons (PAA-ODA). Conjugation percentages and molecular weight were calculated by titrating the remaining carboxylic acid functional groups of the polymer.

Nomenclature	Carbon Chain Length	Conjugation %	Molecular Weight
PAA-OA	**8**	**46**	**3040**
PAA-DA	**10**	**42**	**3220**
PAA-DDA	**12**	**45**	**3630**
PAA-TDA	**14**	**42**	**3800**
PAA-HDA	**16**	**37**	**3815**
PAA-ODA	**18**	**38**	**4135**

An important step in the polymer preparation was the removal of DCU, a byproduct of the carbodiimide coupling. Several strategies were investigated for byproduct removal, including centrifugation and filtration. Our studies have shown that maximum byproduct removal was achieved by cooling the reaction solution and subsequently vacuum filtering using an 11 micron filter. The polymer was further purified using a precipitation technique to remove excess reactants and byproducts. Prepared

polymers with carboxylic acid functional groups remaining were expected to be soluble in slightly basic water because the pKa of a carboxylic acid is approximately 5. At a pH above this value, most of the carboxylic acids will be deprotonated and negatively charged, making them very water soluble. While the product does have a significant hydrophobic character, the polymer is able to form small micelles or self-aggregates and remains water soluble due to the negative charge of the carboxylate functional groups. Aliquots were taken of the polymer and mixed with slightly basic water, yielding a slightly opaque solution. Upon shaking the vial, the solution appeared very soapy and a number of bubbles formed, indicating the polymer was dissolved and able to act as a surfactant. The polymers solubility in water allowed for an easy purification of the hydrophobic impurities remaining in solution (such as DCU byproduct, unreacted DCC, and unreacted alkylamine) using simple vacuum filtration. After filtering, the polymer could be collected by a simple precipitation procedure. By adding acid (dilute HCl) to the polymer solution to decrease the pH to below 5, the majority of the carboxylic acid groups become protonated (and neutral) again, dramatically reducing their solubility in water. This, in addition to the insolubility of the hydrophobic alkyl chains, forces the polymer to precipitate, where it can be easily collected using vacuum filtration and freeze dried to remove any remnants of water. Filtering at this step also allows for the removal of any water soluble contaminants or byproducts as well as the DMF solvent used in the original synthesis.

Polymer Characterization and Analysis

In order to measure the success of the reaction and quality of the polymer product, several characterization techniques were employed. First, polymer solubility was tested in chloroform. Unmodified, or only slightly modified, poly(acrylic acid) is not soluble in hydrophobic solvents such as chloroform. Solubility in chloroform was used

as an indirect verification of the successful conjugation of alkyl groups to the polymer backbone. For a more quantitative assay of the degree of conjugation as well as the molecular weight, titration assays were conducted to measure the remaining carboxylic acid functional groups. A volume of NaOH with known concentration was used to titrate the polymer sample. Phenolphthalein was used as an indicator to determine the moles of NaOH needed to completely titrate the carboxylic acids. Based on these values, and the known molecular weights of the original poly(acrylic acid) polymer and alkylamine, conjugation percentages and molecular weights could be calculated:

$$grams_{POLY} = (mol_{COOH})(MW_{PAA\,monomer}) + \left(mol_{alkylamine}\right)\left(MW_{alkylamine} - MW_{water}\right)$$

Equation 3.1

With the moles of COOH known, solving Equation 3.1 for the moles of alkylamine allowed us to estimate the conjugation percentage of the polymer (Conj.%) and the molecular weight (MW_{POLY}) of the polymer using Equations 3.2 and 3.3, respectively.

$$Conj.\% = \frac{mol_{alkylamine}}{(mol_{alkylamine} + mol_{COOH})}$$

Equation 3.2

$$MW_{POLY} = (1 - Conj.\%)MW_{PAA\,monomer} + (Conj.\%)(MW_{alkylamine} - MW_{water})$$

Equation 3.3

The polymers' critical micellar concentration (CMC) was also measured experimentally to analyze the behavior of the polymers in solution. A pyrene fluorescence assay was used to determine the minimum concentration necessary for the polymers to aggregate into micelles or micelle-like conformations. This assay relies on

the different fluorescence characteristics of pyrene, a hydrophobic compound, depending on the properties of the surrounding medium. In polar solvents, such as water, the fluorescence intensity of the molecule is visible but relatively weak. However, in the presence of a hydrophobic environment, such as the interior of a micelle with a hydrophobic core, the fluorescence of the molecule changes and significantly increases, as seen in Figure 3.5a.

At low polymer concentrations (concentrations below the CMC), the polymer molecules are free in solution and are unable to encapsulate the fluorophore, subjecting the pyrene to the polar environment of water. As the polymer concentration increases to values above the CMC, the polymer molecules are able to capture pyrene in the interior of the micelle, providing a hydrophobic environment to increase the fluorescence. For this assay, the fluorescence intensity of the pyrene was plotted as a function of the log of the polymer concentration. CMC was taken as the concentration where fluorescence begins to increase, as seen in Figure 3.5b. For the polymers used in these experiments (see Table 3.1), there was a slight difference in the measured CMC values. Most polymers had a CMC of approximately 0.01 mg/mL to 0.1 mg/mL, with PAA-DDA (shown below, Figure 3.5b) having a CMC of approximately 0.05 mg/mL.

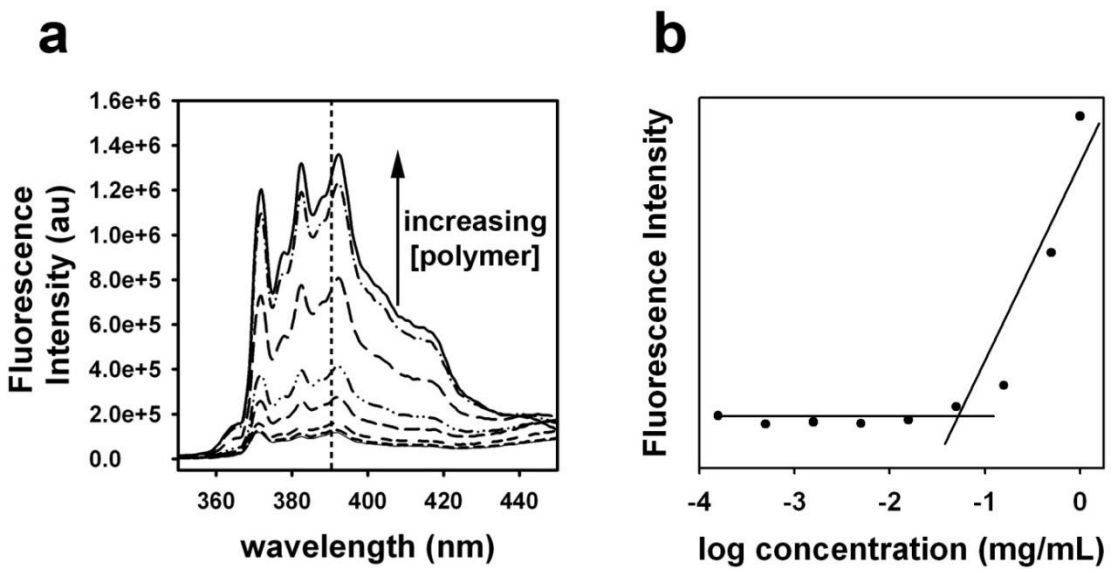

Figure 3.5. Polymer critical micelle concentration (CMC). (a) Pyrene fluorescence spectra for increasing polymer concentrations, noting fluorescence intensity at 390 nm (dotted line). (b) Pyrene fluorescence intensity at 390 nm as a function of polymer concentration. CMC is noted as the point of inflection where fluorescence intensity begins to increase.

Dynamic light scattering (DLS) was also used to determine the behavior of the polymer when dissolved in water. A sample of the amphiphilic polymer was prepared in basic water at a concentration of 5 mg/mL (approximately 2 orders of magnitude higher than the CMC) and measured using DLS to observe the formation of polymer aggregates. A representative size histogram is presented in Figure 3.6a, showing a relatively narrow size distribution for the purified polymer sample. Polymers with hydrocarbon chain lengths from 8 to 18 carbons (Table 3.1) were measured and the mean hydrodynamic diameter was analyzed as a function of carbon length (Figure 3.6b). Hydrodynamic diameter was shown to significantly increase as a function of the hydrophobic carbon chain length for the size ranges measured in this study. For conjugation percentages held relatively constant, increasing the carbon chain length dramatically increases the hydrophobic content of the amphiphilic polymer, relative to

the hydrophilic backbone. With a larger hydrophobic component to shield from the aqueous environment, the formation of larger particles is necessary.

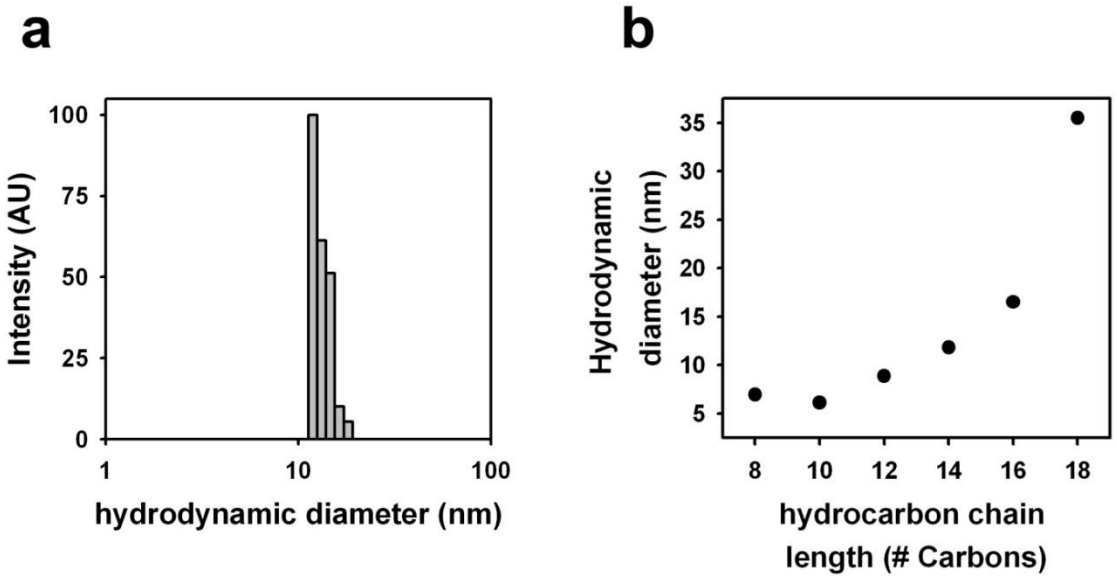

Figure 3.6. Hydrodynamic size of polymer aggregates in water, as measured by dynamic light scattering (DLS). (a) Size histogram of poly(acrylic acid)-*g*-dodecylamine hydrodynamic diameter in water, showing a narrow size distribution. (b) Polymer aggregate hydrodynamic diameter as a function of hydrocarbon chain length.

Phase transfer of Quantum Dots to Aqueous Solution using Amphiphilic Polymers

With the successful synthesis of a library of amphiphilic polymers, further experiments were performed to study and optimize the polymer coating process for hydrophobic QDs. These studies focused on the process of encapsulating the hydrophobic QDs with the polymer, as well as purification of the water soluble QDs and characterization techniques. There are a variety of procedures that can be used to drive the self assembly of the polymer-coating on the nanoparticles' surface, including emulsion, dialysis and solvent evaporation [84, 108, 110, 112, 117, 150, 153-159]. For this work, solvent evaporation proved to be the most effective and simple method for

forming high quality, polymer-coated QDs in water. For the solvent evaporation method to be successful, a solvent must be chosen that is able to dissolve both the polymer as well as the hydrophobic QDs. Additionally, the solvent must have a relatively low boiling point to allow for evaporation in a timely manner with little to no heating required. Chloroform was chosen as the ideal solvent for this procedure because of its low boiling point (61ºC) and ability to dissolve both QDs and polymer effectively. Hydrophobic QDs were purified using liquid-liquid extraction and phase transferred into chloroform. Separately, amphiphilic polymer was dissolved in chloroform and added to the QD solution. After thorough mixing, the sample was placed under vacuum and the solvent was slowly removed. As the solvent is removed, the hydrophobic alkyl chains are slowly driven to intercalate with the surface ligands on the QD, resulting in a polymer-coated nanoparticle. After complete removal of the solvent, basic water is added to deprotonate the free carboxylic acids and render the coated QDs soluble in water.

Based on a geometric model of the amphiphilic polymer and the QD surface area, it is estimated that each QD can be optimally covered with approximately 150 polymer molecules, resulting in a nanoparticle with approximately 2500 carboxylic acid groups (each polymer molecule has ~15 COOH groups for the 40% conjugation ratio used in these studies). A molar ratio of 1000 : 1 polymer molecules per QD was used for the coating procedure to give a slight excess of polymer in solution (a concentration slightly less than one order of magnitude over the optimal ratio) and ensure the surface of the QDs was completely covered. This results in an excess of free polymer that must be subsequently removed after dissolving in water to give a pure nanoparticle solution.

After successfully transferring the coated QDs to water, a number of purification techniques were employed and compared to determine the most appropriate for QD purification. Because both the QDs and amphiphilic polymers were independently purified prior to coating, purification schemes focused on the removal of free polymer in

solution without adversely affecting the optical or colloidal properties of the QDs. Ultracentrifugation has been extensively used in the past as a method to separate aqueous constituents with different densities. Studies were conduced to determine the efficacy of ultracentrifugation in the separation of polymer coated QDs from free polymer. Our initial results were moderately successful, with QDs forming a pellet on the bottom of the centrifuge tube while free polymer remained in the supernatant. Decanting the polymer containing supernatant and resuspending in buffer resulted in a QD solution with little to no free polymer. However, the centrifugation process resulted in moderate aggregation of the nanoparticles with a portion of the sample unable to redisperse in solution. In addition, smaller aggregates dispersed in solution were subsequently removed during a final filtration through a 0.2 μm filter, resulting in a lower than expected yield for the final product.

To combat these problems, ultracentrifugation was used with a density gradient (sucrose gradient solution in centrifuge tube) to separate QDs and polymer without aggregating the nanoparticles. This technique is common for separating protein molecules and has been successfully used in a number of applications. By using a sucrose gradient, QDs were prevented from precipitating and were successfully purified from the free polymer in solution. Nevertheless, a number of disadvantages remained when using ultracentrifugation. Foremost, sample throughput was extremely small, allowing the preparation of only a small amount of nanoparticles at one time. In addition, use of the sucrose gradient introduced impurities (sucrose) that must be later removed, increasing the time required for the purification.

In an effort to increase the throughput of QD preparation, dialysis was studied as a potential purification method. A significant advantage of the dialysis method is the ability to process large sample sizes in a single batch. Other advantages include the gentle nature of this purification technique (virtually eliminating the aggregation problem

seen when using ultracentrifugation) as well as the inexpensive materials and equipment needed, in comparison to the centrifugation methods. Dialysis using a large molecular weight cut off (MWCO) of 250 kDa was shown to be successful in removing excess polymer but was relatively slow, taking days to weeks to completely remove the free polymer. While considerably longer than ultracentrifugation techniques, sample throughput was higher because of the increased sample size and improved product recovery. QD quality was also improved, with virtually no aggregation observed in the process.

Dialysis cut off size was chosen based on results from the polymer characterization studies described above, which show free polymer aggregates that are 10 nm or less in diameter when using PAA-DDA as the coating polymer. Using this MWCO size, significant polymer reduction was seen after a few days, with complete removal observed after approximately 10 days. To improve upon this procedure and increase both the maximum sample volume as well as processing time, an ultrafiltration procedure was developed. Ultrafiltration across a small membrane under pressure works by the same principle as dialysis and proved to purify the QDs in a much more rapid manner, completing the purification in a matter of hours instead of days or weeks. Another important advance is the ability to process very large volumes of nanoparticles in a single batch, with batch sizes of over 300 mL possible using inexpensive equipment and larger batches possible with larger equipment.

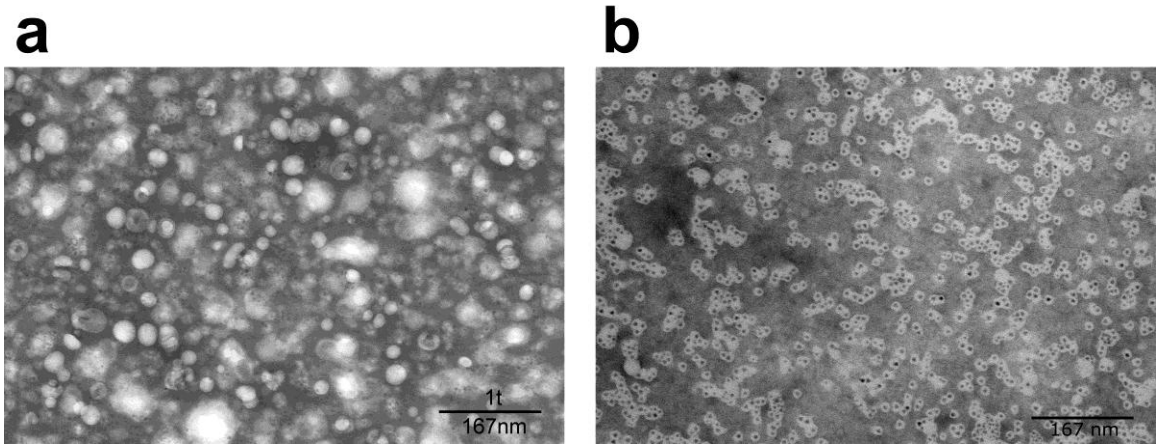

Figure 3.7. Removal of excess polymer from water solubilized quantum dots. (a) Negatively stained TEM of unpurified quantum dots, showing large excess of free polymer in solution. (b) After purification, little to no free polymer is seen in solution, revealing monodisperse quantum dots with a uniform polymer coating.

To analyze the success of the QD purification using dialysis and ultrafiltration, TEM was used to visually inspect the samples before and after the process. Samples were taken and negatively stained to visualize the polymer in solution and surrounding the QDs. As seen in Figure 3.7a, free polymer was clearly visible in unpurified samples, with aggregates appearing in white and obscuring the view of the nanoparticles. In contrast, TEM images taken after the sample was purified showed virtually no excess polymer in solution (Figure 3.7b). In fact, monodisperse nanoparticles are clearly visible, with the polymer shell appearing in white and the nanocrystal core appearing in dark black. Using this technique, we were able to confirm the presence of the polymer shell coating, as predicted in our hypothesis. Based on these results, large quantities of purified water soluble QDs with a polymer coating can be produced in a rapid fashion.

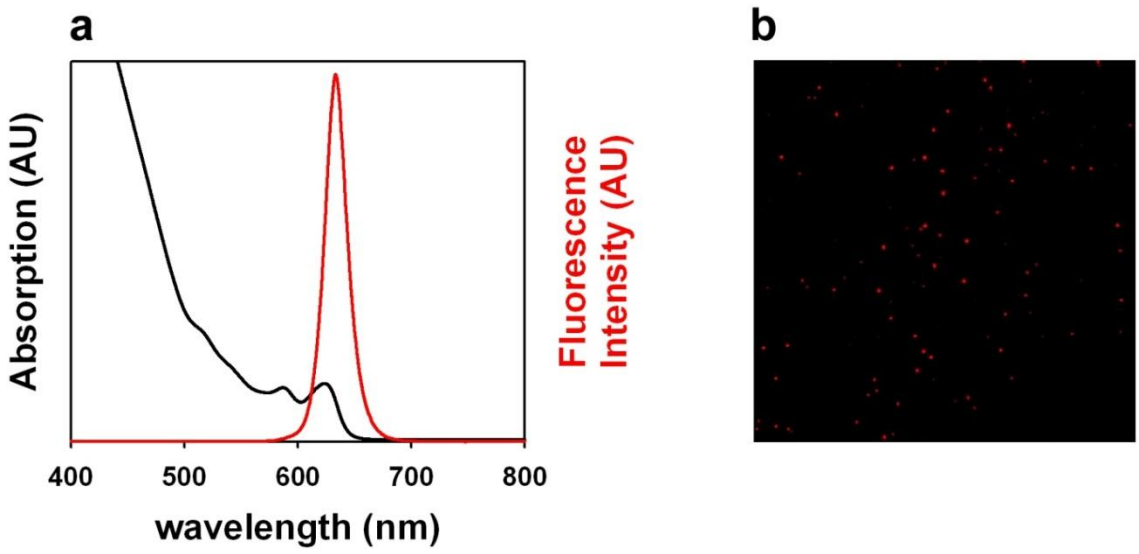

Figure 3.8. Characterization of quantum dot optical properties. (a) Absorption (black) and emission (red) spectra of coated quantum dots in water with narrow peak widths, indicating a very monodisperse sample. (b) Fluorescence micrograph showing well dispersed quantum dots. The nanoparticles exhibited characteristic fluorescence blinking associated with single particles.

To verify that the optical and colloidal properties of the QDs were maintained upon coating, phase transfer into water and purification, samples were taken and characterized by several methods. Absorption and emission spectra were taken before and after polymer coating to determine if there was a loss of fluorescence or a change in the fluorescence peak. Polymer encapsulation and phase transfer to water has no significant effects on the quantum dot's fluorescence properties and the particles remain very bright with a narrow (<25 nm full width half max) emission peak (Figure 3.8a). The particles are also well dispersed with little to no aggregation, as revealed by fluorescence microscopy (Figure 3.8b). The presence of single particles was further

verified by a characteristic blinking behavior for immobilized QDs on a glass slide, indicative of well dispersed single particles [160].

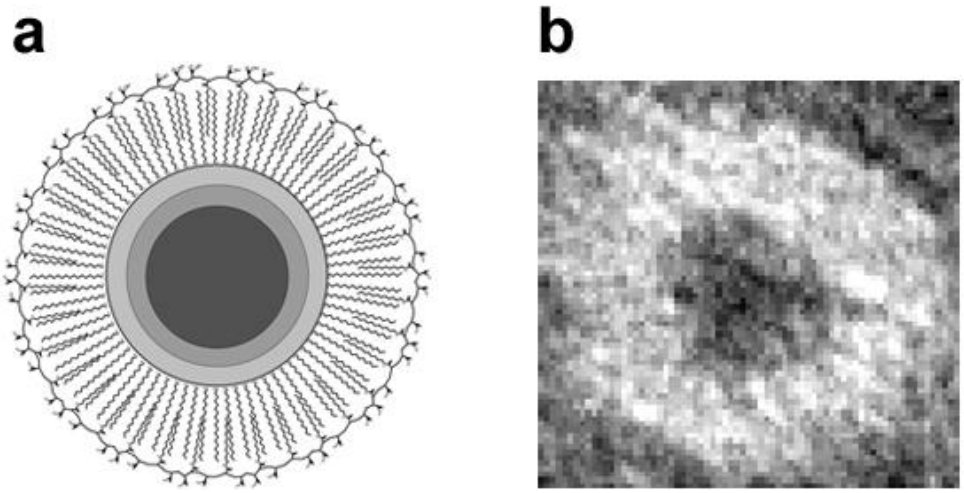

Figure 3.9. Confirmation of polymer coating thickness and particle size. (a) Schematic showing a geometric model of the quantum dot nanocrystal with surface ligands and polymer coating, predicting a shell thickness of approximately 2 nm and an overall diameter of 12-13 nm. (b) Transmission electron micrograph (TEM) showing a single quantum dot particle in water. The TEM grid was negatively stained with PTA to provide contrast to visualize the polymer (in white). The polymer shell had a measured thickness of approximately 2 nm and the overall particle diameter was approximately 13 nm.

Transmission electron microscopy (TEM), dynamic light scattering (DLS) and fast protein liquid chromatography (FPLC) were also used to independently determine the nanoparticle size in solution and study the polymer coating. TEM was performed on purified QD samples, as described above. After analyzing the image on a particle-by particle basis, size histograms were generated to determine the mean diameter of the particles, revealing a particle diameter of approximately 12-13 nm. These values strongly agree with the expected values based on a geometric model of the polymer coated QD (Figure 3.9a), which predicted a nanoparticle diameter of 13 nm. Indeed, TEM images of single polymer-coated QDs are nearly identical to the predicted structure

(Figure 3.9). TEM further reveals a polymer shell with a thickness of approximately 2-3 nm, closely matching the predicted values (Figure 3.9b).

In addition to TEM, DLS and FPLC were used to determine the hydrodynamic size of the nanoparticles in solution. The hydrodynamic size is expected to be slightly larger than the size predicted by the model and confirmed using TEM. This is due to the electrical double layer surrounding the charged nanoparticles in water, slightly increasing their measured size in solution. DLS results indicate a nanoparticle size of approximately 14 nm, slightly larger than that shown in TEM, as expected. Further studies using FPLC were also conducted to verify the hydrodynamic size measurement (Figure 3.10). Globular protein standards with known hydrodynamic diameters and molecular weights were measured in the instrument and elution times were noted and used to develop a standard curve (Figure 3.10b). QD samples in water were then analyzed and elution times were noted to determine the hydrodynamic size. QDs eluted at 27.5 min, corresponding to an equivalent size of approximately 550 kDa and 14 nm hydrodynamic diameter based on the protein standards, corroborating the data obtained using DLS. Based on the results from these methods, it was determined that the polymer-coated QDs have a diameter of approximately 13-14 nm. TEM also confirmed the presence of a polymer coating on the nanoparticles, showing a coating thickness of approximately 2-3 nm, agreeing well with predicted values.

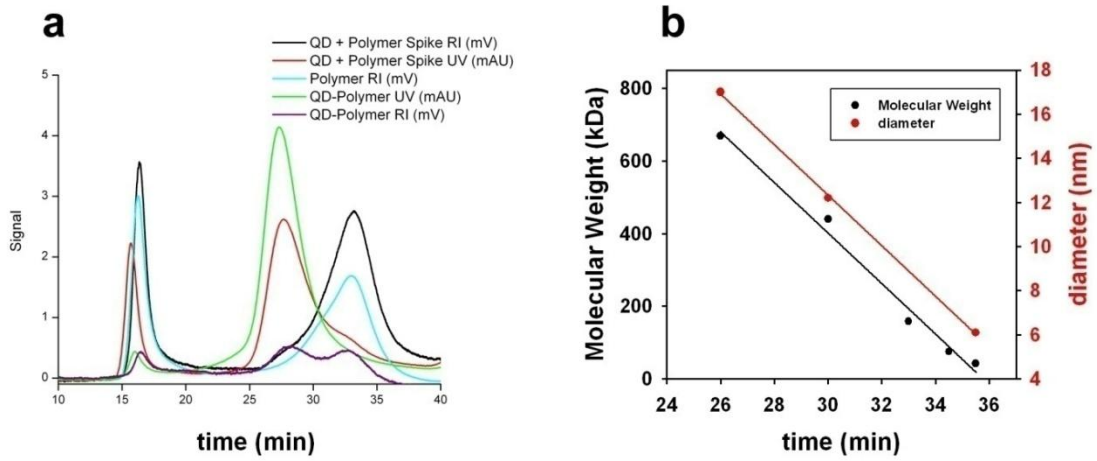

Figure 3.10. Analysis of excess polymer removal and quantum dot hydrodynamic size using Fast Protein Liquid Chromatography (FPLC). (a) A significant decrease is seen in the polymer elution peak in purified quantum dot samples (~34 min, purple curve) compared to samples containing excess polymer (black curve), confirming the removal of excess polymer. (b) Quantum dots eluted at 27.5 min, corresponding to an equivalent size of 550 kDa and 14 nm hydrodynamic diameter based on protein standards, matching well with dynamic light scattering measurements.

Colloidal stability of the polymer-coated QDs was analyzed to determine the nanoparticles' utility in a range of environments. Purified QDs were diluted into 50 mM borate buffer (pH ~ 8.5) and stored at 4ºC to determine their stability under long term storage. QDs showed little to no aggregation under these conditions and retained their optical and colloidal properties for over 1 year. Long term storage at -20ºC was also studied as a potential preservation method for the prepared QD samples. QDs in water were diluted into glycerol (final solution 50% glycerol) and stored at -20ºC for 6 months. Glycerol acts as an antifreeze agent, preventing problems previously seen when storing aqueous QD samples at temperatures below the freezing point of water (aggregation, decrease in stability). Samples stored with glycerol performed extremely well and maintained the colloidal stability and excellent optical properties observed in freshly prepared samples.

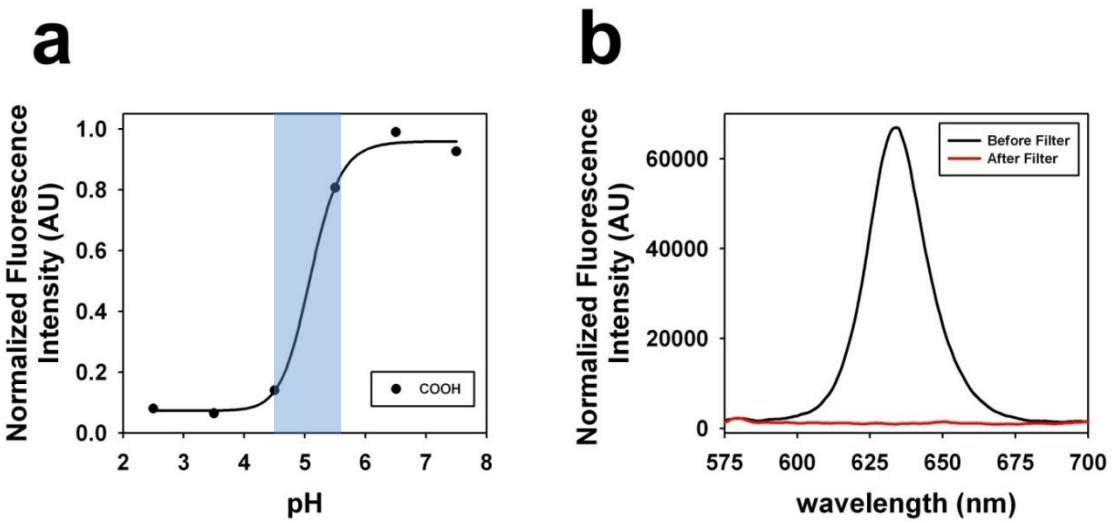

Figure 3.11. pH stability analysis of quantum dots. (a) Fluorescent intensity of filtered QDs as a function of pH, normalized using unfiltered samples. Shaded blue region represents the range of pKa values for COOH. (b) Fluorescence spectra of filtered (red) and unfiltered (black) QD samples at pH ~2.5.

In addition, acid/base stability was analyzed to determine the effects of pH on the stability of the nanoparticles (Figure 3.11). QD samples were diluted into buffers at a range of pH values and fluorescence intensities were measured before and after filtration through a 0.2 μm filter to determine stability. Filtering samples allowed for the removal of any aggregates formed as a result of the surrounding environment, where aggregation would indicate instability of the particles in the solvent. Fluorescence intensity of the samples decreased in a sigmoidal fashion as the pH decreased, indicating colloidal instability at low pH, as seen in Figure 3.11a. This curve matches almost identically with published titration curves of common carboxylic acid containing molecules, such as acetic acid, which has a pKa of ~4.75 [161]. These results are not surprising, as the colloidal stability of the polymer-coated QDs presented in this chapter are strongly dependent on the protonation of the carboxylic acid functional groups on the surface of the particles. As the pH decreases, the carboxylic acid groups become protonated and are no longer charged, reducing the electrostatic repulsion necessary to

keep the nanoparticles in solution. At a pH equal to the pKa of the carboxyl groups (pH at which 50% of the functional groups are protonated), the charge is no longer strong enough to provide colloidal stability and the particles aggregate. Interestingly, fluorescence measurements taken before filtration show the particles remain extremely bright (as seen in Figure 3.11b), indicating the polymer coating is able to protect the surface of the nanocrystal for a wide range of pH values. These data suggest that simple surface chemistry modifications could be sufficient to designing nanoparticles with increased utility in acidic environments. Indeed, recent work by our group has shown that changing the surface chemistry of the nanoparticles can greatly affect the stability of particles in a variety of environments [110, 116, 162].

Effects of Polymer Chain Length on QD Optical Properties

Finally, studies were conducted to determine the effect, if any, of the amphiphilic polymer hydrocarbon chain length on the optical properties of the QDs. Amphiphilic polymers with carbon chain lengths from 8 to 16 carbons were used to coat QDs, which were then phase transferred and purified as described above. Fluorescence intensity measurements were then taken and plotted to determine the effects of polymer concentration as well as chain length on the QD fluorescence properties. As seen in Figure 3.12, low polymer concentrations, regardless of carbon chain length, resulted in poor fluorescence intensity from the purified nanoparticles. For these samples, the polymer concentration was likely insufficient to completely cover and protect the nanoparticles for transfer into water, exposing the QD surface to oxidizing and other damaging compounds and resulting in diminished or nonexistent fluorescence. As the polymer concentration increase, fluorescence intensity plateaus as expected, when the QD surface is sufficiently covered in polymer. Another interesting finding is the dependence on carbon chain length. The fluorescence intensity of the samples

increases as the carbon chain increases, to a value of 12 carbons (corresponding to PAA-DDA). However, further increasing the hydrocarbon chain length results in a significant decrease in the QD fluorescent intensity. It is hypothesized that the increased length of the long hydrocarbon chains significantly hinders the intercalation of the polymer into the surface ligands present on the nanoparticle. This results in an incomplete coverage of the particle, reducing the colloidal stability of the particles and leaving unprotected pockets available for attack by reactive molecules.

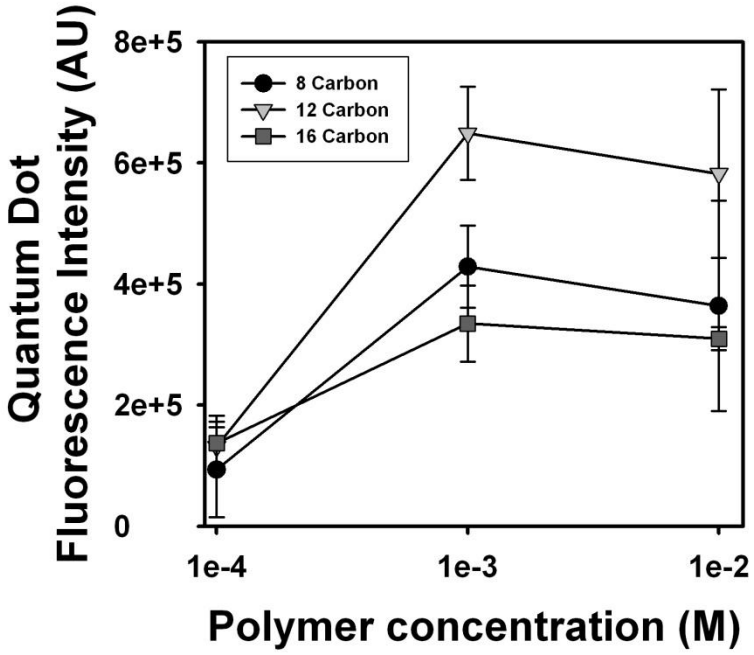

Figure 3.12. Quantum dot fluorescence intensity as a function of polymer concentration and carbon chain length. Using low polymer concentrations resulted in insufficient coverage and protection of the nanoparticles and decreased fluorescence intensity, which plateaus with higher polymer concentrations. Polymers with 12 carbon hydrophobic chains were shown to be optimal for maximum fluorescence intensity.

3.5 CONCLUSIONS

In this chapter, we have described the design, development and synthesis of amphiphilic polymers suitable for coating hydrophobic nanoparticles and transferring

them to water. Our studies have also shown that QDs perform very well when phase transferred to aqueous solutions using amphiphilic polymers. Nanoparticles coated with a thin polymer shell show no shifting in emission color and almost no loss of fluorescence intensity compared to QDs that are solubilized using other strategies, such as ligand exchange with small hydrophilic molecules. The polymer-coated particles are also very stable in solution, showing no aggregation after more than 12 months. This is likely due to polymer stabilization of the surface ligands and prevention of ligand dissociation, which can lead to aggregation. Of particular interest, QDs with a polymer shell provide an additional benefit of protecting the surface of the particle from the surrounding aqueous environment, where water, oxygen or other compounds could react and cause surface defects or oxidation [116]. This is accomplished by the hydrophobic layer from the surface ligands and hydrophobic portions of the coating polymer. Although this coating provides considerable protection of the excellent properties of the QDs, a small group of molecules are able to reach the surface and cause some damage to the QDs [162, 163]. Research is ongoing to enhance the polymer coating to provide further protection to QDs in extremely harsh environments.

CHAPTER 4

AMPHIPHILIC MULTIDENTATE POLYMERS FOR ONE-POT SYNTHESIS, ENCAPSULATION AND SOLUBILIZATION OF QUANTUM DOTS

4.1 ABSTRACT

Quantum dot (QD) nanoparticles are expected to have many applications in a broad range of fields, from medicine to digital displays and energy. While significant progress has been made in the production of high quality nanocrystals, compromises are generally made in scale, ease of production or quality. For the successful use of these particles in a number of applications, high quality particles must be produced in a simple, scalable process. In this chapter, we show the development of multidentate precursor ligands for high quality nanocrystal production and the use of these ligands for a one-pot synthesis procedure for QDs. By using these polymer precursor ligands, the growth kinetics of the synthesis can be tightly controlled, allowing the production of very uniform particles as well as very small nanocrystals. The QDs produced using this method are also resistant to Ostwald ripening, making the particles extremely stable. By using high boiling point, hydrophilic solvents (such as PEG) in addition to excess amphiphilic polymer, we are able produce water soluble QDs in a true one-pot synthesis procedure. In addition, this synthetic procedure allows for in-situ growth of an inorganic passivating shell on the QD core, opening the possibility of bandgap engineering and providing a large dynamic range for QD emission from the visible to the near infrared.

4.2 INTRODUCTION

Semiconductor quantum dots (QDs) are currently under intensive research for a broad range of applications, ranging from molecular and cellular imaging to solar energy conversion [53, 77, 78, 80-85]. The development of high quality synthesis procedures is particularly important for the incorporation of nanoparticles into a number of these applications. Significant advances have been made in the colloidal synthesis of highly crystalline and monodispersed QDs, especially with the use of organometallic and chelated cadmium precursors [103, 104], noncoordinating solvents [105], and inorganic passivating shells [106, 107]. However, these synthesis procedures are generally time consuming with many steps and the resulting nanocrystals are typically hydrophobic and must be rendered water soluble post-synthesis through a variety of encapsulation or ligand exchange processes for many important applications [84, 108, 109].

Aqueous synthetic procedures have been used as alternative approaches to prepare QDs suitable for use in biological environments. These methods typically use small thiol-containing molecules or polymers with carboxylic acid functional groups as stabilizing agents and surface ligands [164-170] and water soluble precursors for cadmium and tellurium. While aqueous synthetic techniques are commonly used because of their simplicity and relative safety, this approach generally yields suboptimal QDs with lower fluorescence brightness and a higher size polydispersity than can be achieved with the high-temperature organic procedures. Moreover, the colloidal and optical stability of QDs prepared using aqueous procedures are typically lower than QDs prepared using other procedures.

High quality synthesis of QDs and other nanoparticles often involve the use hydrophobic carboxylate ligands to coordinate the precursor atoms in solution and bind the nanoparticle surface for stabilization during the synthesis procedure [104]. It was observed that the low molecular weight amphiphilic polymers used previously for the

coating of hydrophobic QDs (described in Chapter 3) were similar in structure to the hydrophobic carboxylate ligands used during QD synthesis to coordinate the precursor atoms in solution and bind the nanoparticle surface for colloidal stability (Figure 4.1). Based on this observation, it was hypothesized that the amphiphilic polymers could serve as multidentate ligands in the synthesis of high quality nanoparticles, allowing for a high degree of size control and increased nanoparticle stability. Furthermore, by using an excess of polymer during the synthesis procedure and a noncoordinating amphiphilic solvent that is miscible with water, free polymer molecules could encapsulate the nanoparticles and render them suitable for immediate transfer to aqueous solutions.[171]

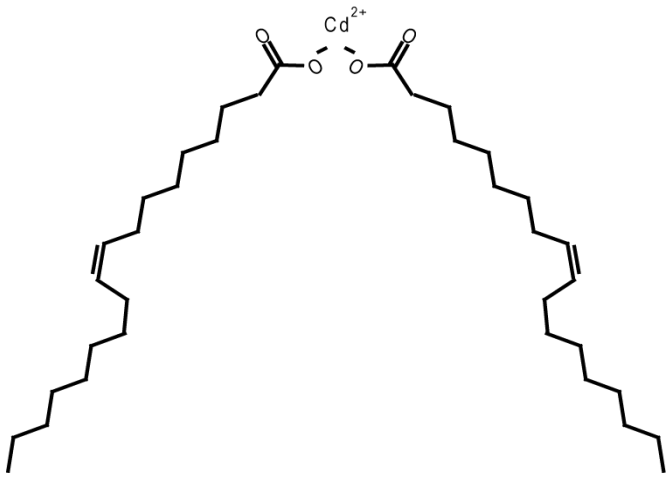

Figure 4.1. Cadmium Oleate, a common cadmium precursor for quantum dot synthesis, is formed by reacting cadmium oxide with oleic acid at elevated temperatures. The amphiphilic polymers discussed previously provide both the carboxylic acid functional groups used for coordination with the cadmium atom and aliphatic carbon chains, making them useful in precursor formation.

Here, we show an “all-in-one” strategy for the simultaneous synthesis, encapsulation, and solubilization of high-quality QDs. This one-pot method is based on the use of amphiphilic multidentate ligands and noncoordinating solvents such as low-

molecular weight polyethylene glycol (PEG) (MW = 350 Daltons). The multidentate polymer ligands contain aliphatic chains and carboxylic acid functional groups, and were found to act as both a cadmium precursor ligand and a nanoparticle surface stabilizer, leading to improved control of chemical reaction kinetics, increased resistance to Ostwald ripening and increased colloidal stability. In addition, by performing the synthesis in noncoordinating amphiphilic solvents such as PEG, nanoparticles can be immediately phase transferred to water, making this a true one-pot procedure. When exposed to water, excess polymer molecules spontaneously encapsulate and solubilize the QDs without any additional materials or steps. Furthermore, this synthetic procedure allows for in-situ growth of an inorganic passivating shell on the nanocrystal core, enabling one-pot synthesis of both type-I and type-II core-shell QDs [172].

In this chapter, we have developed multidentate polymer precursors and determined their effectiveness in the synthesis of QDs. In addition, we have studied the effects of using the multidentate polymer ligands on the reaction kinetics of QD synthesis and nanoparticle properties in comparison to traditional synthetic procedures for QDs in organic solvents. We have also examined the effects of the polymer and solvent in successfully transferring the nanoparticles to water. Additional studies were conducted to optimize the growth of an inorganic passivating shell on the nanoparticles *in situ*, to provide a true one-pot synthesis procedure for core-shell QDs in aqueous solvents.

4.3 METHODS

Polymer Synthesis

The amphiphilic polymer PAA-DDA (~ 3500 Daltons) was synthesized using standard carbodiimide chemistry, as described above. Briefly, 518 mg of poly(acrylic) acid (MW = 1800 Daltons) and 533 mg of dodecylamine (2:5 ratio of alkylamine:COOH) were dissolved in 20 mL DMF. 609 mg of dicyclohexylcarbodiimide dissolved in a minimum amount of DMF was added dropwise and the solution was mixed vigorously for 24 hours to give an amphiphilic polymer with 40% of the carboxylic acid functional groups modified with a 12-carbon aliphatic chain. The polymer was purified using the water precipitation method previously described.

Synthesis of Cadmium Telluride (CdTe) Cores Using Mulitdentate Polymer Ligands

Approximately 170 mg (0.6 mmol COOH groups) of the amphiphlic polymer (~ 3500 MW, described above) was dissolved in 0.5 mL ODE at 100°C under vacuum to remove volatile compounds and dissolved gases. 12.84 mg (0.1 mmol) CdO was added and the solution was heated to 200°C under Argon to form the carboxylate precursor. 3.5 mL ODE were added to dilute the solution and the remaining steps were carried out under an inert environment using standard airless procedures. The solution was heated to 300°C and a Tellurium precursor solution (0.05 mmol Te dissolved in 25 µL tributylphosphine and 1 mL ODE at 200°C) was quickly injected under vigorous stirring to initiate nanocrystal growth. Reaction progress was monitored by taking 100 µL aliquots at various time points using standard airless techniques and rapidly cooling to room temperature to halt the nanocrystal growth.

No-Injection Synthesis of CdTe QDs

Both Cd and Te precursor solutions were prepared, as described above. The Te precursor solution was then added to the Cd solution at low temperatures (~150ºC). The reaction mixture was purged under vacuum to remove oxygen and the remaining steps were conducted under an Argon environment. The reaction mixture was then slowly heated to 240ºC to initiate nucleation and facilitate nanocrystal growth. Reaction progress was monitored by taking 100 µL aliquots at various time points using standard airless techniques and rapidly cooling to room temperature to halt the nanocrystal growth.

Reaction kinetics of CdTe core synthesis

QD synthesis using multidentate polymer ligands was performed as described above. Aliquots were taken using standard air-free techniques at various time points and rapidly cooled in cold solvent to halt the reaction. Fluorescence emission and absorption spectra were obtained using a spectrofluorometer and Uv-Vis absorption spectrometer, respectively. Reaction kinetics were compared to QDs prepared under identical conditions, using traditional monovalent ligands.

One-pot synthesis of water soluble quantum dots using hydrophilic solvents

Approximately 170 mg (0.6 mmol COOH groups) of the amphiphlic polymer (~ 3500 MW, described above) were dissolved in 1.5 mL PEG (350 MW) at 100°C under vacuum to remove water and dissolved gases. 12.84 mg (0.1 mmol) CdO were added and the solution was heated to 200°C under Argon to form the carboxylate precursor. 2.8 mL PEG were added to dilute the solution and the remaining steps were carried out under an inert environment using standard airless procedures. The solution was then heated to 300°C and a Tellurium precursor solution (0.05 mmol Te dissolved in 25 µL

tributylphosphine and 1 mL PEG at 200°C) was quickly injected under vigorous stirring to initiate nanocrystal growth. Reaction progress was monitored by taking 250 µL aliquots at various time points using standard airless techniques and rapidly cooling to room temperature to halt the nanocrystal growth.

Quantum Dot Size Analysis

TEM was used to image the nanocrystal core and determine the mean size and size distribution of the prepared QDs. Briefly, QDs prepared using the one-pot method in PEG were precipitated using centrifugation and resuspended in $CHCl_3$ at a concentration of ~100 nM. The sample was sonicated to disperse any loose aggregates and a 1.5 µL aliquot was pipetted onto a carbon TEM grid and allowed to dry. The sample was imaged using TEM and these images were analyzed using ImageJ to determine a size distribution for the sample and an average size for QDs.

In-situ capping of CdTe core QDs with CdSe

CdTe cores were synthesized in PEG with multidentate polymer ligands as described above. The reaction was allowed to proceed to completion to deplete the Te precursor in solution (monitored by observing shift in fluorescence spectra). The solution was then cooled to 180-200°C for the CdSe capping procedure. A 0.1 M selenium precursor solution was prepared using standard airless technique. Briefly, 78.96 mg Se was dissolved in 250 µL trubutylphosphine and 9.75 mL PEG at 50°C and then cooled to room temperature. 2 mL of the Se precursor solution was added dropwise over the course of an hour while the core solution was vigorously stirred and the fluorescence and absorption spectra were observed to monitor the shell deposition.

4.4 RESULTS AND DISCUSSION

Multidentate Precursor Preparation

Based on the successful coating of hydrophobic QDs with low molecular weight, amphiphilic polymers (Chapter 3), it was hypothesized that these polymers might enable a one-pot method for high quality QD synthesis and immediate phase transfer to water. These polymers contain both carboxylic acid functional groups (necessary for coordination with cadmium ions) and long hydrophobic carbon chains that bind and protect the nanocrystal surface and provide colloidal stability in organic solvents, which are necessary to act as a cadmium coordinating ligand. From these observations, a series of experiments were developed to test the feasibility of preparing multidentate polymer ligands for use in QD synthesis procedures. Schematic structures of the proposed multidentate cadmium ligands and the self-encapsulated, water soluble QDs are shown in Figure 4.2.

An important precursor in the proposed synthesis procedure is the cluster of chelated cadmium ions (Figure 4.2a), formed by dissolving the amphiphilic polymer and cadmium oxide or cadmium acetate in a noncoordinating solvent such as octadecene (ODE) at elevated temperatures. Cadmium ions are chelated between neighboring carboxylic acid functional groups on the polymer, providing a polymer precursor containing multiple cadmium ions (cadmium polyate). The reactivity of this precursor plays a key role in controlling both the nucleation and growth kinetics of the nanoparticles and can be tuned by altering the structure of the polymer. By increasing the length of the polymer backbone and the density of hydrophobic side chains, a dramatic steric hindrance effect was observed, resulting in homogeneous nucleation and growth, whereas the use of traditional monovalent ligands under similar conditions leads to uncontrollable and heterogeneous results. Based on our initial studies, we have found that a 40 percent graft percentage (40% of the carboxylic acid groups are modified

with hydrophobic aliphatic chains) of a 12 carbon hydrocarbon group is optimal for controlled nanoparticle growth and potential transfer of the QDs to water and other solvents. For the remainder of this work, PAA-DDA was used for the multidentate precursor studies as well as the QD synthesis procedures.

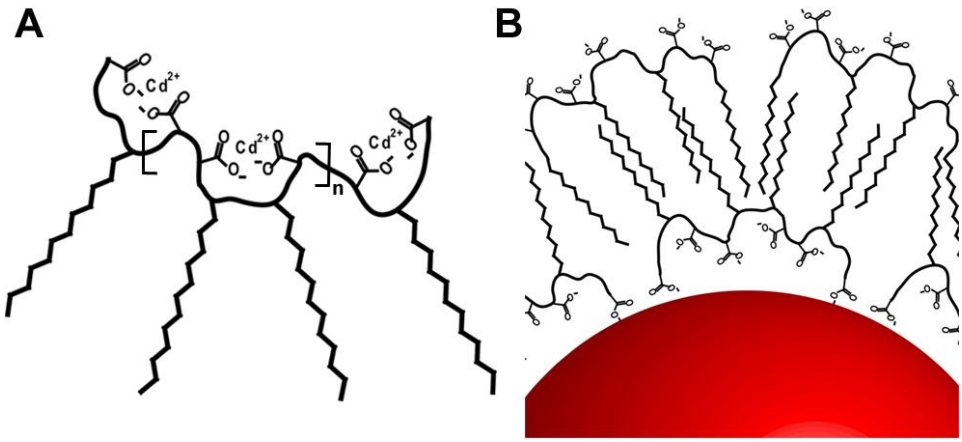

Figure 4.2. (A) Schematic structure of the amphiphilic multidentate ligand with multiple chelated cadmium ions. (B) Diagram showing multidentate ligand binding to the quantum dot surface. The resulting nanocrystals are spontaneously encapsulated and solubilized by a second layer of the same multidentate polymer upon exposure to water.

QD Synthesis and Reaction Kinetics

After preparing the multidentate polymer precursor, experiments were conducted to determine the optimal reaction parameters for QD synthesis and analyze the nucleation and growth kinetics observed when using polymer ligands. QDs were prepared under conditions identical to the monovalent synthesis procedure, replacing cadmium oleate precursors with the multidentate cadmium precurors described above. Upon anlaysis of the growth kinetics of polymer-prepared QDs, a number of interesting properties were observed. By increasing the concentration of polymer in the reaction mixture (effectively increasing the COOH:Cd ratio), a decrease in the nucleation and

growth kinetics was observed (Figure 4.3a). This was unexpected, as an analysis of the reaction kinetics seen in monovalent synthesis techniques [105] reveals the opposite effect.

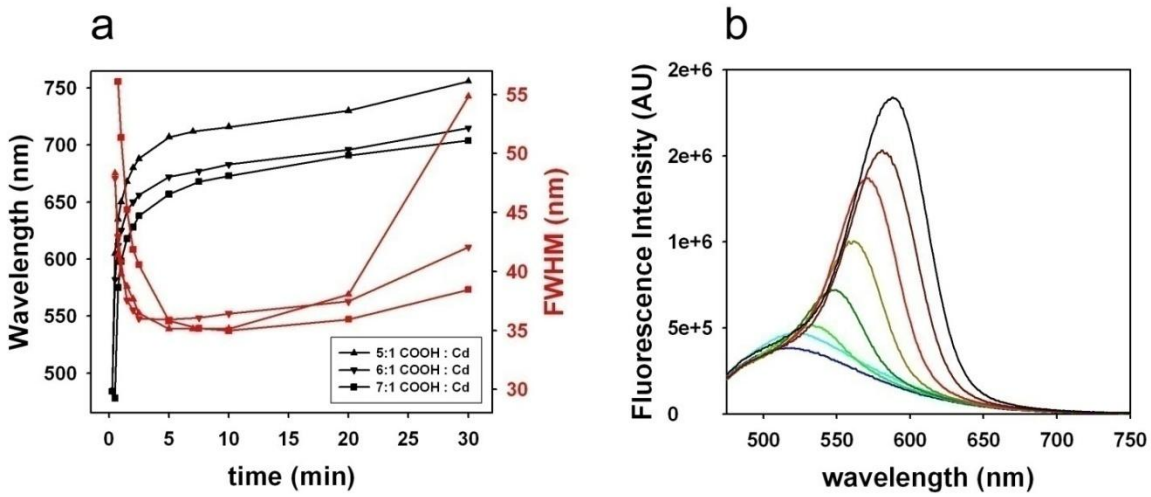

Figure 4.3. Unique growth properties of polymer synthesis procedure. (a) Fluorescence wavelength and full width half max (FWHM) as a function of time and polymer concentration, showing a decrease in nanoparticle growth rate with increasing polymer precursor concentration (opposite effect seen with monovalent precursors). (b) Preparing a reaction flask containing both precursors and then rapidly increasing temperature results in nucleation of nanoparticles without the need of an injection step, which is necessary for synthesis using monovalent precursors.

It is hypothesized that this significant difference is the result of steric hindrance from the multidentate polymer precursors. Using monovalent ligands for cadmium precursors, steric hindrance plays no significant role in the kinetics of nanoparticle nucleation or growth because the precursor is always composed of two oleic acid molecules coordinating a single cadmium ion, regardless of the oleic acid concentration. By increasing the concentration of oleic acid, only the reactivity of the cadmium chelate is affected by increasing the concentration of carboxylic acids present in the solution. Conversely, by altering the concentration of the multidentate polymer when preparing the cadmium precursor, the structure of the cadmium polyate is significantly altered. At

low polymer concentrations, the structure most likely obtained is one in which multiple cadmium ions are coordinated by a single polymer, as shown in the schematic representation in Figure 4.2a. However, as the concentration of the polymer increases, the number of cadmium ions per polymer decreases and the probability that a cadmium ion may be coordinated by carboxylic acid groups from separate polymers is higher. This phenomena essentially allows the tuning of the effective molecular weight of the precurosr by changing the polymer : cadmium ratio. Because of this increase in molecular weight, steric hindrance plays a significant role in the reaction kinetics. With increased steric hindrance, both nucleation and nanocrystal growth kinetics are retarded despite an increase in the concentration of carboxylic acids in solution, enabling an interesting method for controlling the nanoparticle growth.

Another interesting property of the polymer procedure for QD synthesis is the ability to perform “no-injection” nucleation of nanocrystals. For typical synthetic procedures using monovalent precursors, a solution of an anion chalcogen precursor (sulfur, selenium, tellurium) is prepared separately and then rapidly injected into the hot cadmium precursor solution to initiate nanoparticle nucleation and subsequent growth. This presents a problem for the scale up of these reaction procedures, as it is increasingly difficult to rapidly inject larger volumes of chalcogen precursor and the time needed for the solution to mix completely increases. This can lead to a more polydisperse product, lowering the quality of the resulting nanoparticles. By using the cadmium polyate precursor, the chalcogen precursor can be separately prepared and added at low temperatures and allowed to mix completely. After a homogenous solution is obtained, the temperature can then be increased to induce nucleation of the nanoparticles, as seen in Figure 4.3b. This development provides a potential path towards large scale production of QD nanoparticles that would be needed for a number of important applications.

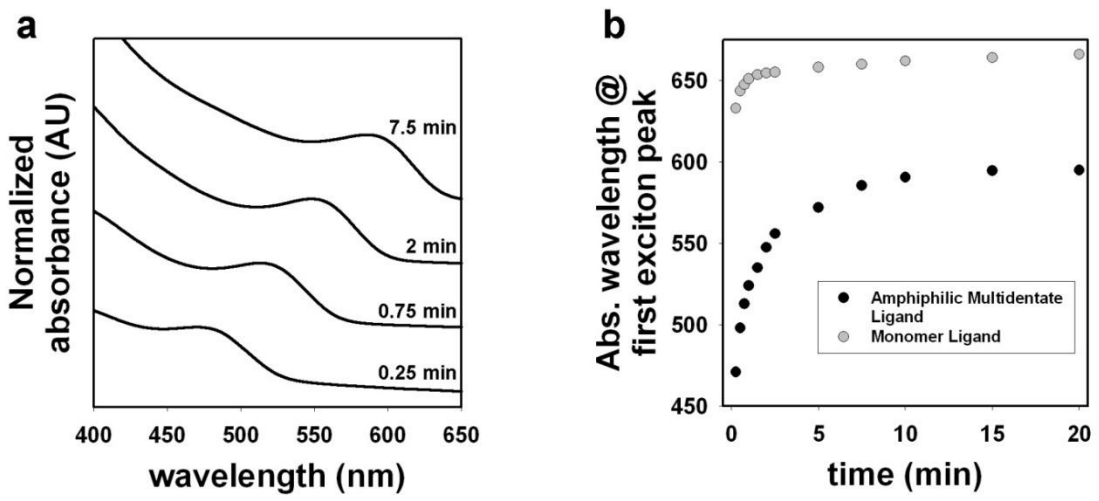

Figure 4.4. Reaction kinetics of CdTe core synthesis. (A) Temporal evolution of the absorption spectra for CdTe cores synthesized using the amphiphilic multidentate ligand procedure. (B) Reaction kinetics of the multidentate ligands compared to traditional monodentate ligands.

Next, the overall growth rate of the nanoparticles synthesized using multidentate ligands was directly compared to procedures using monodentate oleic acid precursors. CdTe core synthesis reactions were carried out under identical conditions, with a COOH : cadmium ratio of 6:1 for both procedures (Figure 4.4). The polymer synthesis procedure resulted in a very slow nanocrystal growth, as evidenced by the absorption spectra taken over time (Figure 4.4a). In fact, depending on the polymer concentration, the nanocrystals were still growing after more than 10 minutes at 270ºC. In contrast, QDs synthesized with oleic acid precursors grew very rapidly and were much quicker to plateau (Figure 4,4b). This again is attributed to the increased steric hindrance of the polymer ligands as well as multivalency. As the nanoparticles are formed and grow, it is hypothesized that the polymer is able bind the surface of the QD in a multivalent fashion (see diagram in Figure 4.2b). Assuming the k_{on} and k_{off} rates are similar for carboxylic

acids in oleic acid and the amphiphilic polymer when binding to the nanoparticle surface, multivalent binding will result in an effective k_d (dissociation constant) that is lower than for monovalent binding (meaning an effectively higher binding affinity). Because of this higher affinity, the deposition of cadmium and chalcogen monomers on the surface of QDs protected by polymer ligands is expected to be significantly slowed, which is consistent with the data. In addition, a single amphiphilic polymer is more than 12 times the size of an oleic acid molecule (~3500 Da vs. 282.5 Da), which may also slow the kinetics down through steric effects.

One-pot synthesis

After successfully synthesizing QDs using the multidentate polymer ligands, a sample of the QDs in the crude reaction mixture (containing octadecene, TOP, excess polymer) was transferred to water to determine if the nanoparticles could be immediately phase transferred through a spontaneous coating with excess polymer (Figure 4.5). After vigorously mixing, a two phase system was obtained, with ODE and QDs in the hydrophobic layer and water and impurities in the hydrophilic layer, as seen in Figure 4.5b, right. It was determined that the presence of the ODE solvent hindered the transfer of these nanoparticles to water, regardless of the concentration of excess polymer in solution. To combat this problem, it was necessary to select a different solvent that was capable of acting as a noncoordinating solvent for the QD synthesis and an “adjuvant” for immediately transferring the prepared particles to water. Low molecular weight PEG was identified as a potential reaction solvent because of it’s similarity to the structure of ODE (Figure 4.5a), its miscibility with a number of solvents (especially water) and its relatively high boiling point, important for producing high quality particles. PEG provides not only an inert and noncoordinating environment for quantum

dot synthesis at high temperatures, but also acts as an “adjuvant” to facilitate nanoparticle dispersion in a variety of solvents.

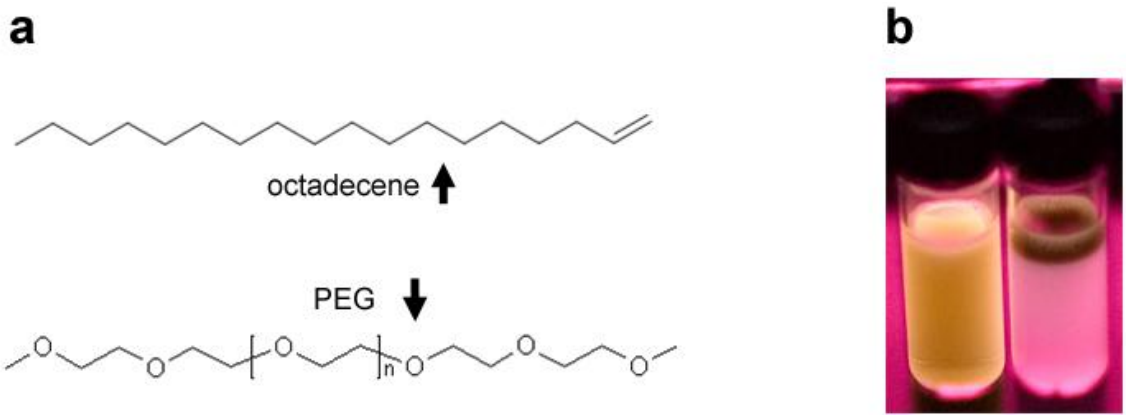

Figure 4.5. Phase transfer of polymer synthesized quantum dots to water. (a) Typical high temperature synthesis procedures use high boiling point, oily solvents such as octadecene (ODE), which is immiscible in water, making transfer of QDs to water difficult. Polyethylene glycol (PEG) was identified as a potential substitute because of its high boiling point and excellent water miscibility. (b) Phase transfer of quantum dots to water using PEG (left) and ODE (right). Hydrophobic solvents such as ODE result in 2 solvent phases, making water transfer difficult.

After successfully synthesizing QDs using PEG as a replacement for ODE, an aliquot of the crude reaction mixture was transferred to water and thoroughly mixed. As seen in Figure 4.5b, left, the crude solution was completely miscible with water and the prepared QDs remained colloidally stable and fluorescent. By optimizing the balance between the hydrophobic and hydrophilic portions of the polymer, the resulting nanocrystals are solubilized by a second layer of excess polymer when the reaction mixture is exposed to water or buffer (Figure 4.2b). However, if the hydrophobic grafting percentage is too high, the number of surface carboxylic acid functional groups becomes too low for water solubilization.

Indeed, the QDs produced using this method show “amphibious” behaviors and were soluble in a wide range of hydrophilic and hydrophobic solvents including water,

DMF, acetone, and chloroform. It was hypothesized that the nanoparticles were coated with excess polymer to transfer them to polar solvents, such as water. Solubility in hydrophobic solvents is likely due to the hydrocarbon chains from the polymer ligands being exposed to the solvent. To test this hypothesis, an aliquot of crude QDs in PEG was taken and transferred to two separate centrifuge tubes. One tube was immediately phase transferred to water, yielding water soluble fluorescent nanoparticles, as expected. The second sample was cooled and centrifuged to precipitate the QDs. After removing the supernatant (along with the excess polymer), buffer was added to water solubilize the QDs. Samples prepared in this manner resulted in an aggregated sample with QDs insoluble in water, verifying the need for excess polymer in solution. However, the QD pellets were soluble in a number of nonpolar solvents, such as chloroform, consistent with our hypothesis.

As described above, the improved control in nanoparticle growth kinetics seen with the polymer precursor ligands allowed for a more precise tuning of the nanoparticle size and fluorescence emission wavelength across a wide range (Figure 4.6a). In fact, QD fluorescence emission could be consistently controlled within as little as 2 nm. The use of these amphiphilic polymer precursors also provides a new route to ultrasmall QDs; for example, small CdTe cores emitting in the green range (515 – 525 nm, as small as 1.5 nm) can be produced with narrow size distributions, allowing for a large fluorescence dynamic range from the green to the far red wavelengths (Figure 4.6a). It is worth noting that ultrasmall QDs are often difficult to synthesize with traditional monovalent precursors because of problems with kinetic control of small particles. The QDs coated with the amphiphilic ligands were also strongly resistant to Ostwald ripening, likely due to the multidentate interactions described previously. Each polymer has approximately 15 carboxylic acid functional groups that are capable of coordinating with surface atoms of the QD. By increasing the overall binding affinity through multivalent

interactions and providing steric hindrance, the polymer coating can better stabilize the nanoparticles and reduce ripening. However, some ripening can occur at increased temperatures after substantial periods of time, as shown by the dark red curve obtained after 1 hour at 280°C (Figure 4.6b, slight tailing). Overall, transmission electron microscopy reveals uniform, nearly spherical particles without clustering or aggregation when using the polymer synthesis procedure in PEG (Figure 4.6c), confirming the stability and monodispersity of QDs synthesized and protected with multidentate polymer ligands.

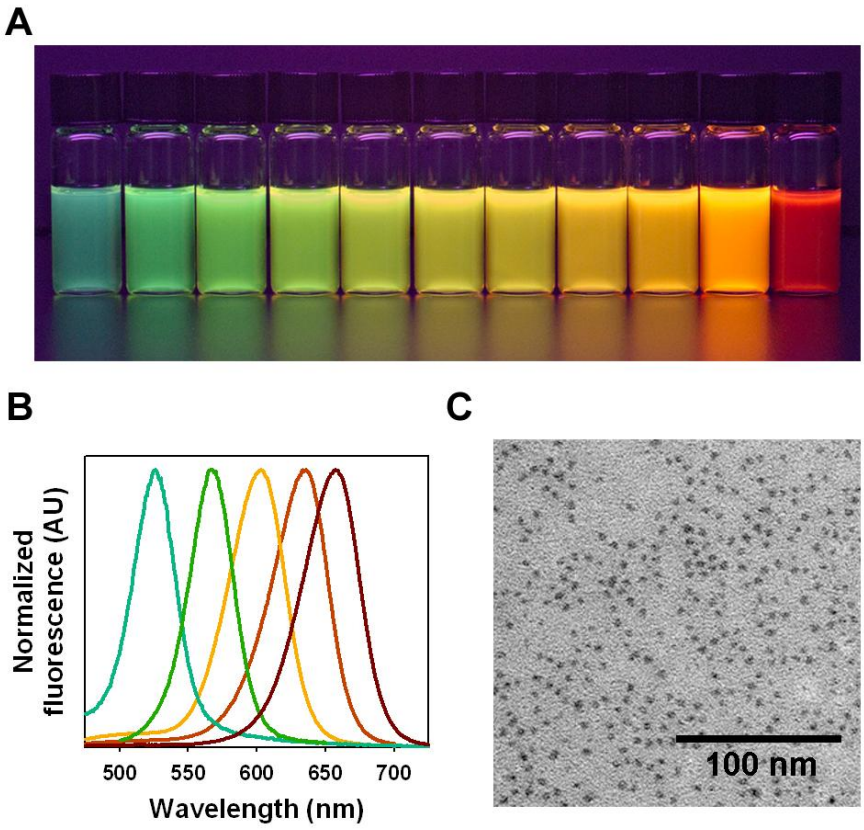

Figure 4.6. Fluorescence emission and electron microscopy structural properties of CdTe core quantum dots prepared by using multidentate polymer ligands in a one-pot procedure. (A) Series of monodispersed CdTe quantum dots, showing bright fluorescence from green to red (515 to 655 nm) upon illumination with a UV lamp. (B) Normalized band-edge fluorescence emission spectra of CdTe quantum dots with 35-50 nm full width at half-maximum (FWHM) (QY ~ 30%). (C) Transmission electron

micrograph of CdTe cores (emission = 655 nm) showing uniform, nearly spherical particles.

Size monodispersity for QDs prepared using multidentate polymer precursors in PEG is comparable to nanoparticles produced using traditional monovalent ligands in high temperature organic solvents. TEM was performed on samples and analyzed to develop a size histogram for the QDs (Figure 4.7). In a characteristic sample, prepared nanocrystals had a mean diameter of 4.2 nm with a standard deviation of approximately 10%.

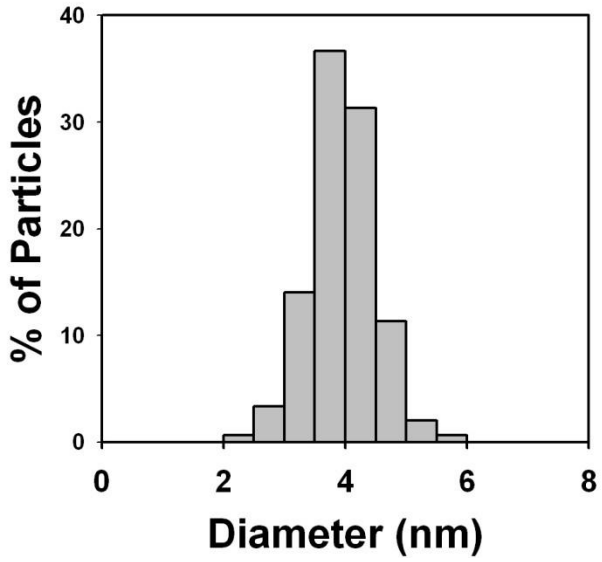

Figure 4.7. Size histogram of CdTe cores. CdTe core QDs were synthesized using the polymer procedure. A transmission electron micrograph was taken and analyzed to determine size distribution of the particles (mean diameter = 4.2 nm, standard deviation ~ 10%).

In-Situ Capping with an Inorganic Passivating Shell

Because QD cores show a propensity to oxidize in water, decreasing their fluorescence intensity and eventually degrading the nanocrystal, we have developed an *in-situ* procedure for capping them with an inorganic passivating shell. Inorganic shells

have the added benefit of increasing the fluorescence quantum yield as well as opening the possibility of bandgap engineering[124, 172] through the selection of an appropriate shell material. Through bandgap engineering, we can design high quality QDs with extended emission ranges, from the ultraviolet into the near infrared. In this procedure, an excess of multidentate cadmium precursor was used to start the core QD synthesis (the mole ratio of cadmium to tellurium is typically 2:1 or higher), and the reaction was allowed to proceed until the limiting species (tellurium) was depleted. After completely removing the tellerium species, an excess of the cadmium precursor is available for incorporation into an inorganic passivating shell with a different chalcogen. CdSe was used as a model shell material for CdTe cores because the band offsets are such that CdTe/CdSe is a type-II core-shell QD with light emission in the near-infrared range.[172] This provides a dramatic shift in the emission spectra as well as significant changes in the shape of the absorption spectra, allowing for definitive evidence that the shell growth was successful.

Fluorescence emission spectra (Figure 4.8a) showed significant red-shifting of the original quantum dot core emission peak, from 650 nm to 810 nm, as the CdSe inorganic passivating shell was grown on the nanocrystal surface (quantum yields were consistent with those reported in literature [172]). Considerable broadening of the emission peak was also observed with the shell growth, consistent with the behavior of type-II QDs. Monitoring of the nanoparticle absorbance spectra also confirms shell growth and transition to type-II behavior (Figure 4.8b). For example, the distinct exciton peak seen in the CdTe cores (red curve) was gradually red-shifted and eventually disappeared during shell deposition. This was expected as the CdTe/CdSe quantum dots should behave as indirect semiconductors near the band edge.

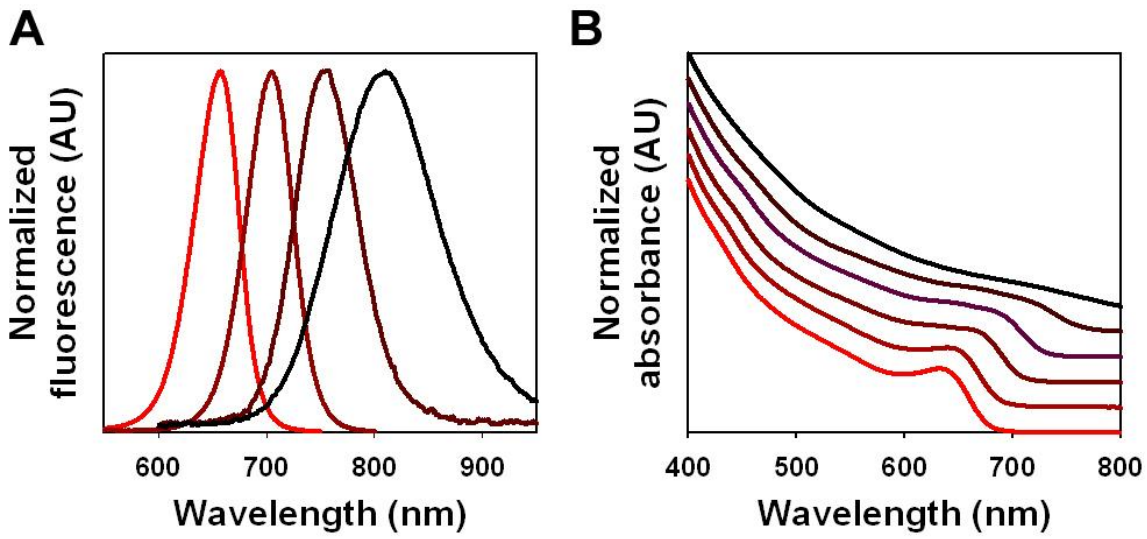

Figure 4.8. Type-II core-shell CdTe/CdSe quantum dots synthesized in a one-pot method. (A) Normalized fluorescence emission spectra showing the transition from CdTe cores (red curve) to CdTe/CdSe core-shell quantum dots emitting in the near-infrared (black curve). (B) Optical absorbance showing the red-shifting and eventual loss of the first exciton peak as the CdSe shell is grown on the CdTe core, typical of type II quantum dots.

4.5 CONCLUSIONS

In summary, we have reported a new, one-pot procedure for preparing high-quality QDs based on the use of amphiphilic multidentate ligands and short polyethylene glycols at high temperatures. The novel features associated with the use of polymeric precursors are better control of the nanocrystals growth kinetics, resistance to Ostwald ripening, and synthesis of ultrasmall dots with blue-shifted emission spectra. This synthetic procedure also allows for in-situ growth of an inorganic passivating shell (CdSe) on the QD core, opening the possibility of bandgap engineering for these nanoparticles and providing a large dynamic range for QD emission from the visible to the near infrared. Finally, by using amphiphilic PEG as a noncoordinating solvent for the synthesis, QDs can be immediately phase transferred to water, with excess polymer coating the nanoparticle surface.

CHAPTER 5

AMPHIPHILIC MULTIDENTATE POLYMERS FOR ONE-POT SYNTHESIS OF SERS ACTIVE GOLD NANOPARTICLES

5.1 ABSTRACT

The interesting electronic and optical properties of gold colloids have led to an explosion of interest in these nanoparticles and a rush to use them in many exciting applications, including biomedical imaging and therapeutics. In particular, the use of gold nanoparticles (AuNPs) as SERS active tags has shown tremendous potential for near-term clinical adoption. Recent work by our group and others has shown that biocompatible coatings are necessary for the development of functional probes suitable for use in biological environments. However, synthetic procedures for the production of high-quality particles must be scaled up to quantities needed for use *in vivo*. In this chapter, we show the development of a novel, one-pot synthetic procedure for the production of SERS active AuNPs using amphiphilic multidenate polymers. The use of these polymeric stabilizers confer many unique properties, including controlled growth kinetics, increased nanoparticle stability and a wide range of possible nanoparticle sizes. The procedure also allows for the *in situ* addition of reporter dyes, spontaneously forming SERS active particles in a one-pot method and yielding AuNPs with high contrast under dark field microscopy and distinct Raman signatures.

5.2 INTRODUCTION

The preparation of gold nanoparticle (AuNPs) solutions has taken place since ancient times [173], although understanding of the process was not possible until recently with the development of highly sensitive instrumentation able to characterize and image the particles. Initial applications for AuNP solutions was in the staining of glass or ceramics red due to the unique absorption properties of colloidal gold solutions. AuNP solutions were also thought to have medicinal properties, and have been used for the treatment of arthritis [173]. Michael Faraday, in 1857, reported the synthesis of colloidal gold through the reduction of chloroaurate [174]. The reduction preparation method has continued to be studied and major improvements were made in the past several decades by Turkevitch *et al.* [175] and Frens [176]. Citrate (Figure 5.1a) has been shown to act as both a reducing agent (to reduce chloroaurate) and a coordinating and stabilizing ligand to bind to the surface of the AuNPs and render them colloidally stable in water. Nanoparticles synthesized using this method are very monodisperse and show a characteristic surface plasmon resonance peak in their absorption spectra, as seen in Figure 5.2b. With the introduction of the citrate reduction method (as well as other synthesis procedures), the preparation of AuNP solutions can be done in a rapid and repeatable fashion.

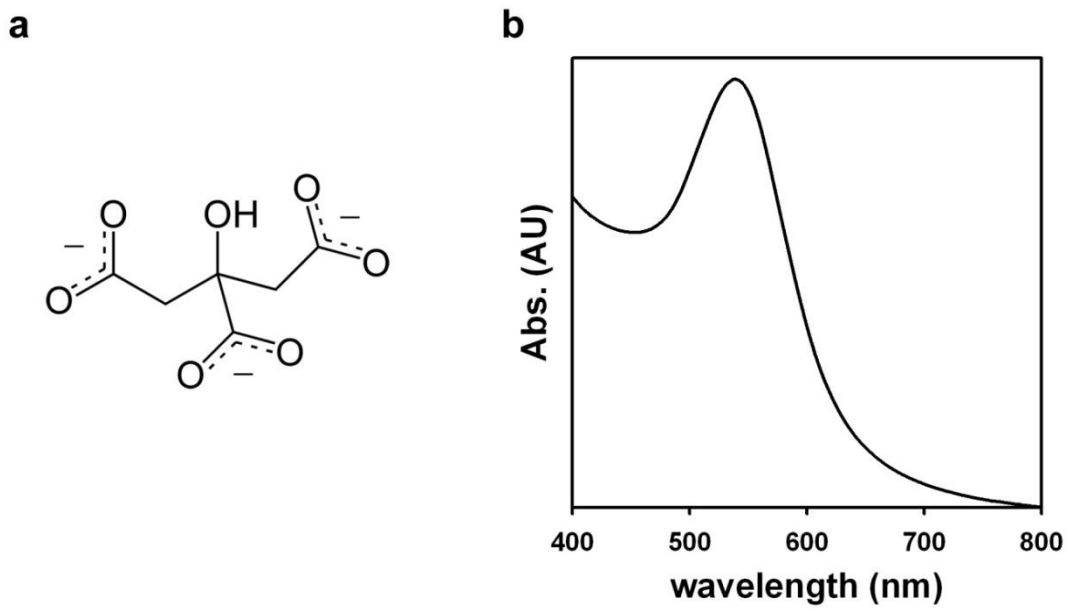

Figure 5.1. Gold nanoparticle synthesis using citrate reduction. (a) Citrate contains carboxylic acid functional groups (also present on the amphiphilic polymer) capable of gold reduction and coordination and stabilization of gold nanoparticle surfaces. (b) Characteristic surface plasmon resonance peak for gold nanoparticles.

The interesting size-dependent electronic, optical and magnetic properties of gold colloids [173, 177-180], in addition to the advances in synthetic preparation techniques, have led to an explosion of interest in these nanoparticles and a rush to use them in many exciting applications. In particular, the use of AuNPs as a biomedical labeling agent has received considerable attention in the past few decades. Because of their strong electron absorbing properties, AuNPs have been used as TEM contrast agents for cell and tissue applications. They have also been used in countless colorimetric assays based on the color change of gold colloid solutions upon aggregation. The use of DNA-conjugated gold particles to detect low concentrations of nucleic acids has been extensively studied and elegant and highly sensitive assay techniques have been developed for this application [51, 181-184] as well as others. One particular assay that has seen considerable commercial success is the home

pregnancy test, many of which utilize gold nanoparticles for a colorimetric determination [185].

Surface Enhanced Raman Scattering (SERS) using AuNPs is a particularly important technique that has generated substantial interest in the research community in recent years [52, 186]. Initial work by our group and others has shown an incredible signal enhancement factor on the order of 10^{14}-10-^{15} [186, 187]. A subset of optically "hot" nanoparticles were also identified which have extremely efficient optical enhancement [188-191]. These discoveries have led to many studies showing single molecule detection using SERS AuNPs. However, biocompatible coatings for the SERS particles were needed for their use in biological and medical applications. Several groups have demonstrated a variety of surface coating techniques, including polydivinylbenzene-coatings [192] and glass shells [193]. While these designs allowed preliminary biological studies to be performed, several limitations remained. Our group has recently developed a new class of SERS nanoparticle tags that directly address many of the limitations of previous efforts. These tags are composed of large gold nanoparticles with dye adsorbed to the surface and a thick PEG-thiol coating to protect the nanoparticle and provide biocompatibility. These SERS particles have been successfully used in a number of applications, including *in vivo* targeting and imaging of tumors in animal models [41].

In this chapter, we show a novel strategy for the one-pot synthesis of high-quality AuNPs and SERS tags. This method is based on the use of amphiphilic multidentate ligands acting as both a reducing agent for the gold solution as well as a surface coating for the prepared AuNPs. By using the polymer based procedure, the reaction kinetics for the synthesis are dramatically changed in comparison to standard citrate reduction, significantly slowing the reaction and allowing interesting control of the synthesis. The prepared particles are also extremely stable in a variety of conditions, including high salt

concentrations and high pH, likely due to the stability of the polymer coating. Furthermore, by changing the initial concentration of polymer in solution, the size of the prepared AuNPs can be tuned, allowing for the synthesis of larger particles with the potential for SERS activity. Indeed, adding a SERS active dye to the large AuNP solution enables SERS signal to be detected.

5.3 METHODS

Synthesis of Gold Nanoparticles Using Multidentate Polymers

The multidentate polymer ligand, PAA-DDA, was synthesized and purified as previously described. A stock solution of the polymer in basic water (pH ~8) was prepared and vortexed/sonicated to completely disperse the polymer. DI water was added to give a final concentration of 0.15 M COOH. Separately, a 50 mM stock solution of gold (III) chloride was prepared in water. For a 10 mL reaction, 50 µL of the 50 mM stock solution was diluted into 9.783 mL DI water and heated to 100ºC under vigorous stirring. 167 µL of the polymer stock solution was quickly added, to give a 10:1 COOH:Au ratio. The reaction was allowed to progress at 100ºC and atmospheric pressure for 24 hours.

Synthesis of Gold Nanoparticles using Citrate Reduction

A stock solution of gold (III) chloride was prepared as described above. Separately, a solution of sodium citrate was prepared in water to yield a solution with a final concentration of 0.15 M COOH (0.05 M citrate). For a 10 mL reaction, 50 µL of the 50 mM stock solution was diluted into 9.783 mL DI water and heated to 100ºC under vigorous stirring. 167 µL of the citrate stock solution was quickly added, to give a 10:1 COOH:Au ratio. The reaction was allowed to progress at 100ºC and atmospheric pressure for 15 minutes (until reaction completion).

Reaction Kinetics of Gold Nanoparticle Synthesis

AuNP synthesis using the multidentate polymer ligands was performed as described above. 500 µL aliquots were taken at various time points and transferred to 1.7 mL eppendorf tubes. The aliquots are rapidly cooled by immediately placing the sample tube in an ice water bath to halt the nanoparticle growth. Absorption spectra were obtained using a Uv-Vis absorption spectrometer. The spectra were analyzed and surface plasmon resonance (SPR) peak and the half width half max (HWHM) of the absorption peak were calculated and plotted. HWHM was defined as the width of the curve from the absorption peak to half of the intensity peak, measured in nanometers. Reaction kinetics were compared to AuNPs prepared under identical conditions, using traditional citrate reduction.

Gold Nanoparticle Size Analysis

AuNP size was analyzed using both DLS and TEM. Unstained TEM was performed as described for QDs. Images of the samples were taken and analyzed using ImageJ to determine a size distribution for the sample and an average size for the coated particles. DLS was used as previously described to measure the hydrodynamic diameter of the nanoparticles. AuNP samples were prepared in water and filtered using a 0.45 µm filter immediately before analyzing the samples to eliminate dust.

Gold Nanoparticle Salt Stability

A stock solution of polymer-coated AuNPs was prepared in DI water, vortexed and sonicated for 15 minutes to disperse any loose aggregates and filtered through a 0.45 μm filter to remove any contaminants. Separately, a 5 M NaCl solution was prepared and serial dilutions were made. Aliquots of the polymer-coated AuNP solution were taken and diluted into the salt solutions at a 1:1 ratio and vortexed to complete mix the solutions, resulting in final NaCl concentration ranging from 2.5 M to 0 M NaCl. Absorption spectra were then taken using a Uv-Vis absorption spectrometer. The procedure was repeated for citrate stabilized AuNPs and the results were compared.

Gold Nanoparticle pH Stability

A solution of AuNPs was prepared and filtered as described above. Basic (pH~10) and acidic (pH~3) buffered solutions were prepared and 1 mL aliquots were transferred to a 1.7 mL eppendorf centrifuge tube. 250 μL aliquots of the AuNP solution were pipetted into the tubes and vortexed to mix completely. The samples were then centrifuged at 5000 g for 10 minutes and observed for evidence of precipitation.

Synthesis of Large Gold Nanoparticles Using Multidentate Polymers

AuNP synthesis using the multidentate polymer ligands was performed as described above. The polymer concentration in the reaction flask was varied to determine the effect of polymer concentration on reaction kinetics and AuNP size. For larger AuNPs, the polymer concentration was reduced to below the CMC of the polymer (~ 0.05 mg/mL).

Dark Field Microscopy of Large Gold Nanoparticles

Large polymer-coated AuNPs were synthesized as described above. A solution was prepared and vortexted/sonicated to resuspend the particles and disperse any aggregates. 1.5 µL of the prepared AuNP solution was pipetted onto a glass coverslip. A second coverslip was placed on top to form a thin film between the coverslips. After waiting 10 minutes for the nanoparticles to settle, the sample was then imaged using an Olympus BX51 microscope for reflective mode dark field microscopy.

SERS Active Gold Nanoparticle Synthesis

Large polymer-coated AuNPs were synthesized as described above. A solution was prepared and vortexted/sonicated to resuspend the particles and disperse any aggregates. Separately, a 4 µM solution of malachite green (MCG) in water was prepared. The MCG solution was added dropwise to a rapidly mixing solution of AuNPs at a molar ratio of ~25,000:1 MCG:AuNP. The AuNPs were allowed to precipitate and then resuspended in 50 mM borate buffer. SERS spectra were obtained using a Advantage Raman Series system (DeltaNu) and compared to polymer-coated AuNPs without MCG as well as a standard MCG spectrum.

5.4 RESULTS AND DISCUSSION

Gold Nanoparticle Synthesis Using Multidentate Polymers

Citrate reduction has become a widely used synthesis procedure for the production of high quality, monodisperse AuNPs for a wide range of sizes. However, AuNPs stabilized with citrate molecules are generally too unstable for use in biological applications and must be coated with other surface ligands or protective molecules to enhance their utility [41, 182, 193]. Based on our success in preparing semiconductor nanoparticles using amphiphilic polymers as multidentate precursors and ligands

(Chapter 4), we have studied the potential for using these polymers in AuNP synthesis. Because the polymer contains a number of carboxylic acid functional groups (as citrate does, Figure 5.1a), it was hypothesized that the polymer could behave in a similar manner, acting as a reducing agent for the gold and a surface ligand/ polymer coating for the gold nanoparticles. In addition, it is expected that the prepared particles will be more stable than citrate stabilized AuNPs due to the multivalent binding of the functional groups on the particle surface and the thickness of the polymer shell.

Preliminary synthesis experiments were performed in water at 100°C with a 10:1 ratio of carboxylic acid functional groups to Au atoms, a common ratio used in the citrate procedure. Analysis of the absorption spectra during the reaction procedure reveals a gradual appearance of a peak at 540 nm, as seen in Figure 5.2a. This peak is characteristic of the plasmon resonance peak seen for AuNPs, indicating the presence of nanoparticles. The reaction solution, originally transparent with no color, also gradually obtained a deep red color, further indicating the successful synthesis of AuNPs. To conclusively determine if the amphiphilic polymer can be used in the synthesis of AuNPs, TEM was used to examine the samples after the reaction was terminated. Analysis of the TEM images revealed a large concentration of spherical nanoparticles, as seen in Figure 5.5a. Upon closer examination of the samples, a number of interestingly shaped particles were observed. Using the polymer synthesis method, nanoparticles with three, four, five and six sides were observed in addition to spherical particles as seen in Figure 5.2b. Although the proportion of particles with these unique shapes was low, further exploration is warranted because of their unique optical and electronic properties [194-196]. Additional studies are needed to determine the parameters required to push the reaction equilibrium towards the formation of these interesting shapes.

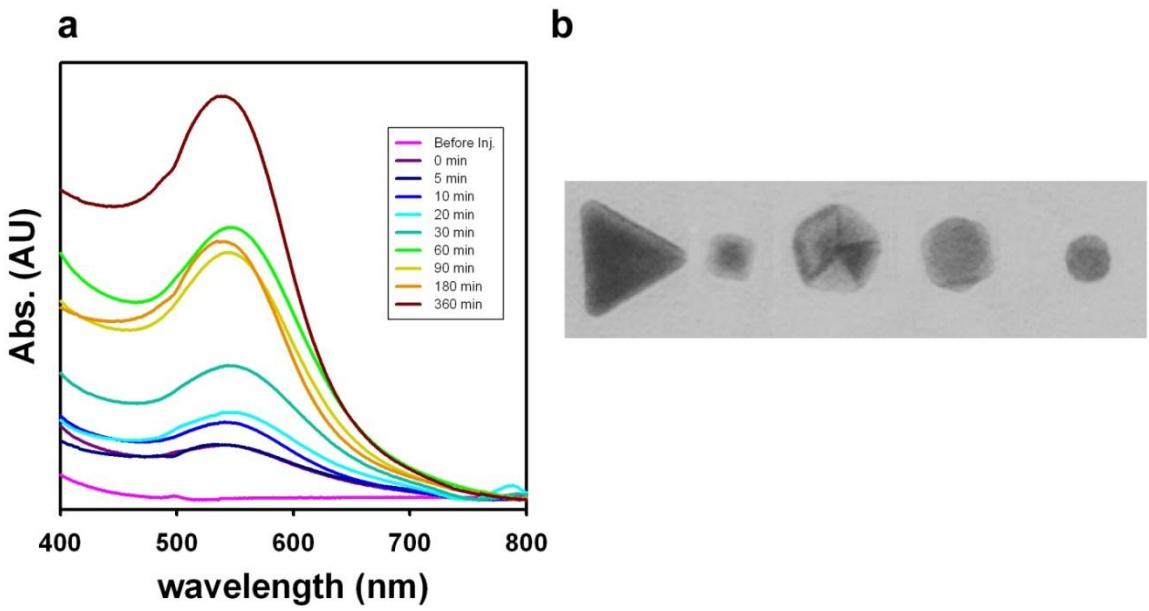

Figure 5.2. Gold nanoparticle synthesis using amphiphilic polymers. (a) Absorption spectra over the course of the synthesis, showing the gradual emergence of a peak at 540 nm, indicating the presence of gold nanoparticles. (b) Nanoparticle synthesis using multidentate polymer results in the formation of a number of interesting shapes, with the majority of the population being spherical.

Another interesting observation made during the initial synthesis procedure was the color shift of the solution. The reaction mixture of aqueous AuNPs synthesized using citrate reduction undergoes a series of color changes before finally obtaining the deep red color associated with colloidal gold particles. The mixture starts as a clear or slightly yellow solution as a result of the chloroaurate precursor used. The solution then develops a dark grey color, which transitions to purple and then finally red, as colloidal gold is formed. Recent work has revealed that the deep grey/purple color of the solution is associated with a transient intermediate consisting of gold nanowires [197]. These transient nanowires eventually bud off, forming citrate-stabilized, spherical AuNPs and a resulting red color. AuNPs synthesized using the amphiphilic polymers, however, do not undergo a grey/purple transition. Instead, the transparent solution gradually develops a pink hue, which slowly intensifies until a deep red color is observed. This can be

observed in the absorption spectra (Figure 5.2a), where the spectra shift only slightly and merely increase in intensity.

Interestingly, altering the concentration of the polymer in solution has dramatic effects on the synthesis process. For synthesis procedures using a polymer concentration between one and five times the CMC, stable gold nanoparticles are difficult to produce. These solutions enter a perpetual grey/purple phase and are unable to transition to the red phase associated with colloidal gold, eventually precipitating after extended heating at 100°C (approximately 6 hours). Although not completely elucidated, the mechanism of AuNP formation using polymer nanoparticles has been shown in this work to be unique compared to the citrate procedure. It is hypothesized that the perpetual grey/purple phase seen in some experiments could be due to the formation of stable gold nanowires. Further studies could reveal this complex mechanism and lead to the synthesis of novel nanomaterials.

Polymer Procedure Reaction Kinetics

Upon successfully synthesizing AuNPs using multidentate polymers, a series of experiments were performed to systematically study the reaction kinetics of the procedure. AuNPs were synthesized using both citrate reduction and the polymer method under identical reaction conditions and samples were taken during the process to monitor the reactions. Synthesis using citrate reduction proceeded as expected, with a transition from clear to grey/purple and finally red within approximately 7.5 minutes. The plasmon resonance peak showed a significant decrease over the course of the reaction, blue-shifting approximately 50 nm as seen in Figure 5.3a. Likewise, the half width half max (HWHM) of the peak dramatically decreased to approximately 40 nm for the prepared nanoparticles. This peak narrowing, as seen in Figure 5.3b, corresponds

with a focusing of the size distribution of the AuNPs, leading to an increase in monodispersity.

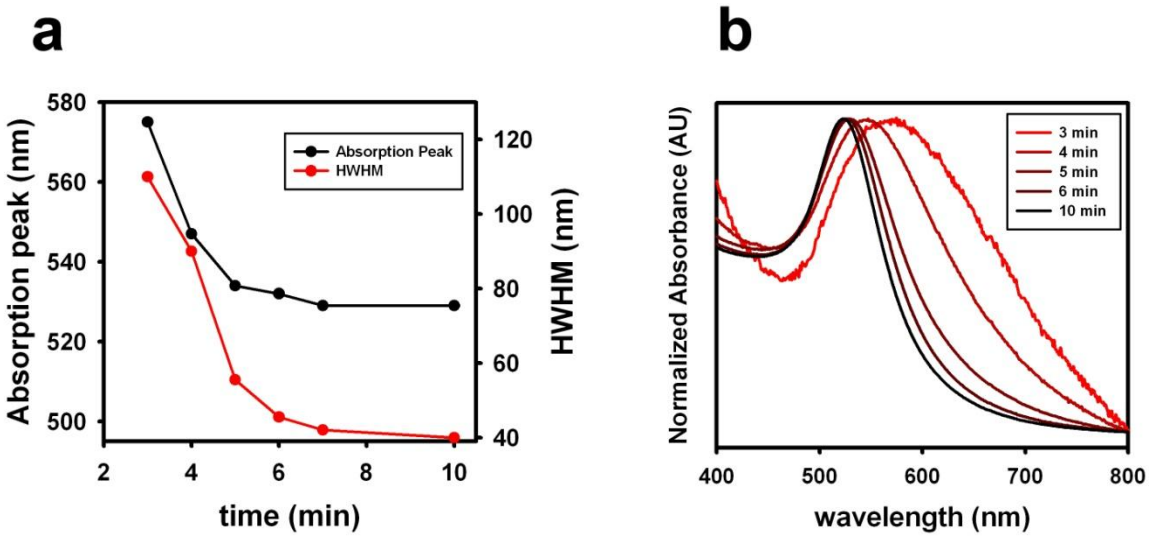

Figure 5.3. Gold nanoparticle synthesis reaction kinetics using citrate reduction. (a) As the reaction progresses, the absorption peak (black) decreases abruptly and plateaus at approximately 530 nm while the HWHM significantly narrows to approximately 40 nm. (b) Normalized absorbance spectra of the prepared nanoparticles over the course of the reaction.

In contrast, the reaction kinetics seen with the use of amphiphilic polymers was significantly retarded, mirroring results seen during the polymer synthesis of QDs (Chapter 4). In fact, the reaction progress was slower than the citrate procedure by nearly two orders of magnitude, requiring approximately 10 hours to reach completion. This considerable decrease in reactivity is likely due to the structure of the polymers in water and their interaction with the AuNPs. The polymer concentrations used in these studies were well above the CMC of the polymer, resulting in micelles or polymer aggregates in solution. As shown in Chapter 3, these polymers form aggregates in water with a size between 5 and 10 nm in hydrodynamic diameter. These macromolecular structures could have a tremendous impact on the properties of the

polymer and the reaction parameters by significantly decreasing the polymer's diffusivity. A decrease in the diffusion coefficient would likely lead to substantially lower nucleation rates.

In addition, because the polymers are in an aggregate form, there is likely shielding of a portion of the carboxylic acid functional groups as they are buried in the interior of the polymer, effectively lowering the COOH:Au ratio in comparison to procedures using citrate. The interaction of these functional groups with the surface of the growing nanoparticles likely plays a major role, as in the case with QDs (Chapter 4). Multivalent binding to the nanoparticle surface results in a much stronger polymer-particle interaction and hinders the access of gold atoms to the surface. The bulky nature of the polymer also contributes to this phenomenon because of steric hindrance, further reducing the growth rate.

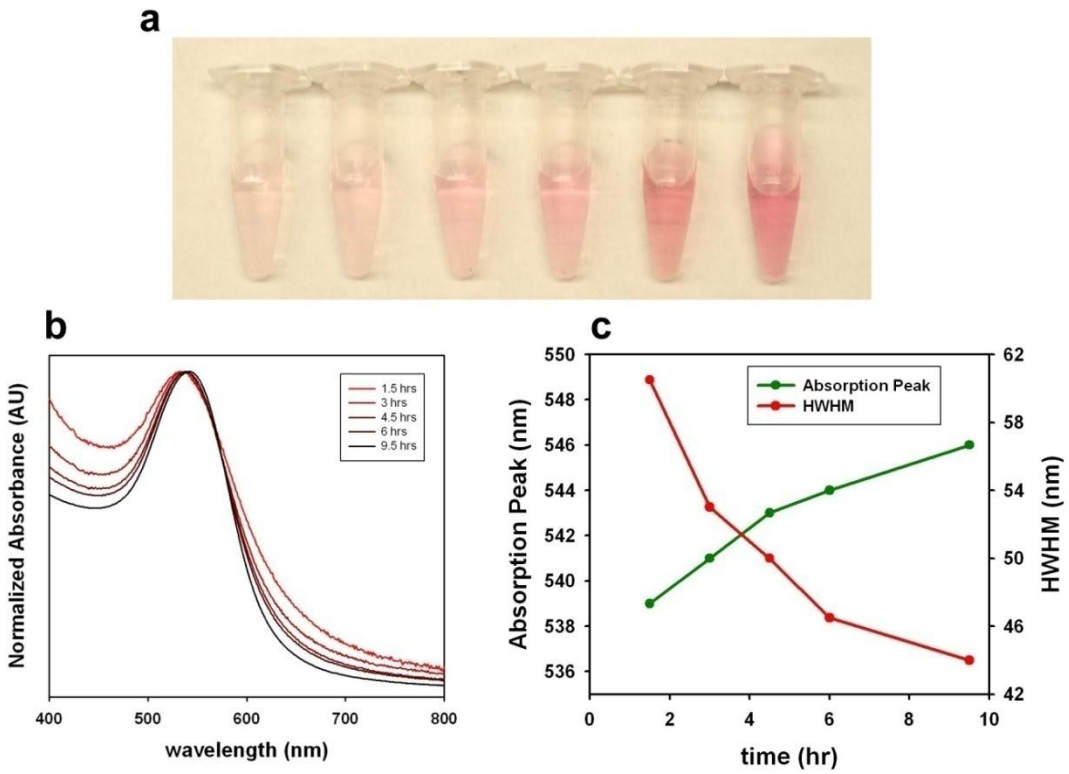

Figure 5.4. Gold nanoparticle synthesis reaction kinetics using polymer reduction. (a) Aliquots taken during reaction procedure at various time points. The samples slowly transition from a transparent to red solution as nanoparticles are formed over the course of approximately 10 hours. (b) Normalized absorbance spectra of the reaction mixture from 1.5 to 9.5 hours. (c) The absorption peak slightly red shifts (green curve) while the monodispersity of the sample, measured by the half width half max (HWHM) in red, significantly narrows as the reaction progresses.

As mentioned above, the reaction appears to bypass the dark grey/purple phase, with simply a gradual appearance of a red color (Figure 5.4a) as the nanoparticles begin to form and the size distribution is focused. This unique aspect of the synthesis mechanism is further demonstrated by the absorption spectra taken during the reaction procedure. Unlike the citrate reduction, which showed dramatic shifts in both the plasmon resonance peak and HWHM, samples analyzed over the course of the polymer reaction show only slight changes in the absorption peak, as shown in Figure 5.4b, red-shifting less than 10 nm over the 10 hour reaction. As in the citrate reduction synthesis procedure, the size distribution of the nanoparticles narrows as the reaction progresses,

reaching a HWHM of almost 40 nm. However, this change was much less significant because of the relatively low initial HWHM in comparison to the citrate method (Figures 5.3a, 5.4c)

The polymer synthesis procedure presented in this dissertation allows very tight control of the growth reaction, enabling the production of AuNPs in a very consistent manner. These experiments further reveal that growth time plays little role in the final determination of the nanoparticle size. Subsequent experiments have revealed a strong dependence on the initial polymer concentration in determining the ultimate size of the AuNPs. These results are discussed in detail below.

Gold Nanoparticle Characterization

To verify the quality and stability of AuNPs synthesized using the polymer method, samples were characterized by a variety of methods and then compared to particles stabilized with citrate. AuNP size was determined using DLS as well as TEM, as described above. The examination of TEM images of the polymer-coated nanoparticle samples (Figure 5.5a) shows a population of well dispersed, spherical particles with no aggregation. Further analysis of the images revealed a nanoparticle size of approximately 20 nm in diameter. These results were verified using DLS, which showed a fairly narrow size distribution with an average particle diameter of 40 nm (Figure 5.5b), considerably larger than that calculated by TEM. This result is not surprising, as the hydrodynamic size of a particle is typically larger than that shown under TEM, due to the thickness of the electrical double layer. In addition, the TEM images do not account for the thickness of the polymer coating, which is likely to be relatively thick because of their confirmation in the synthesis procedure.

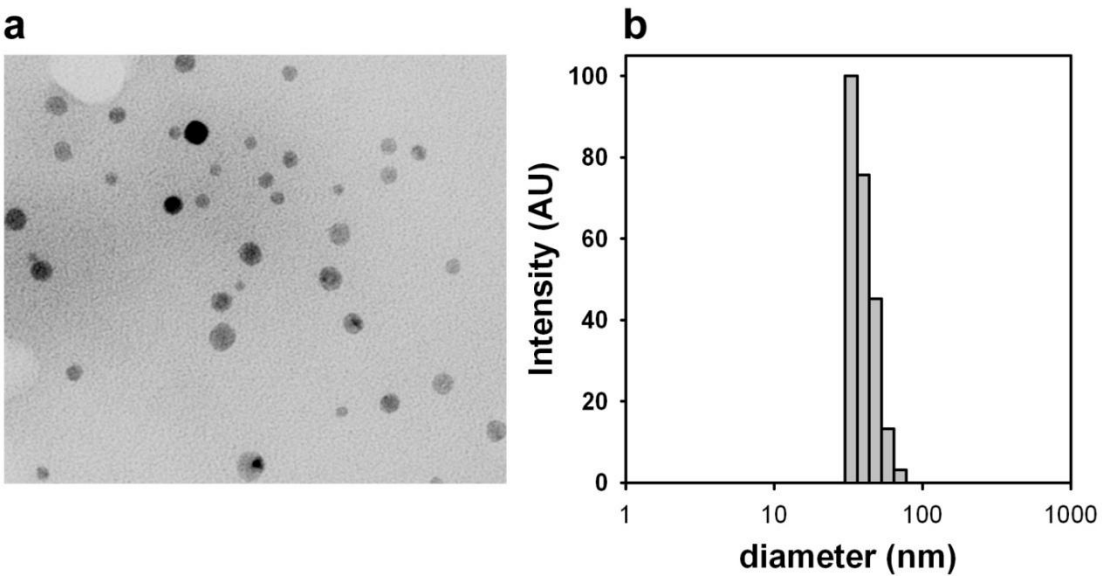

Figure 5.5. Gold nanoparticle size characterization. (a) Transmission electron micrograph (TEM) of gold nanoparticles synthesized using polymer reduction, showing spherical particles with no aggregation. (b) Hydrodynamic diameter histogram of a gold nanoparticle solution, as measured by DLS.

In addition, the stability of the polymer-coated AuNPs was measured in a number of environments. Samples were prepared and transferred to buffered solutions with high and low pH to determine the effect of pH on the colloidal stability of the nanoparticles. AuNPs at high pH showed no signs of aggregation and remained colloidally stable, as seen in Figure 5.6a, left. However, when pH to levels were reduced to below 4, a substantial amount of aggregation was observed (Figure 5.6a, right), as was the case for polymer-coated QDs. This is due to the protonation state of the carboxylic acid functional groups, which are most protonated and less water soluble at low pH.

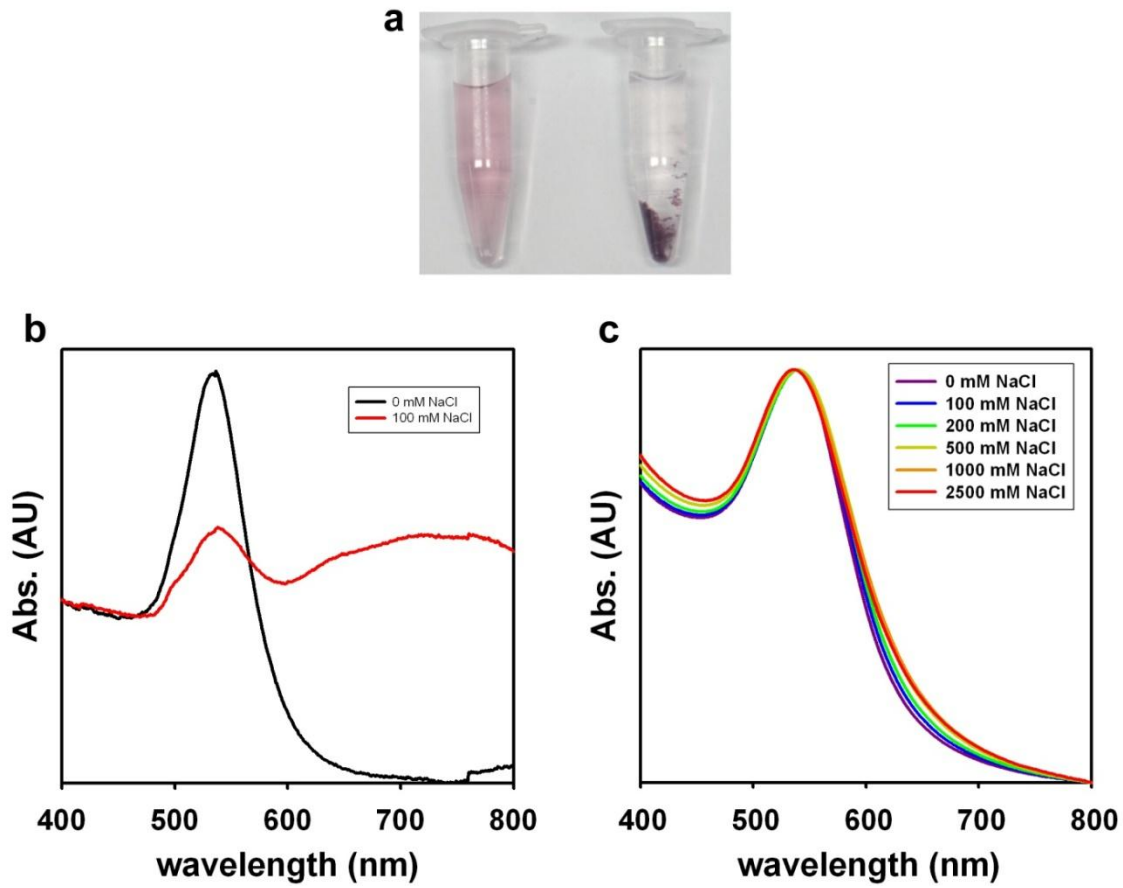

Figure 5.6. Stability of polymer-coated gold nanoparticles. (a) Polymer coated gold nanoparticles are stable at basic pH (left) but precipitate in acid conditions (right). (b) Absorbance spectra of citrate stabilized gold particles in the absence (black) and presence (red) of salt. 100 mM NaCl results in the precipitation of the gold nanoparticles. (c) Absorbance spectra of polymer stabilized gold particles in the presence of salt. Even at 2.5 M NaCl concentration, the gold nanoparticles show little to no aggregation.

The stability of polymer-coated AuNPs was also measured in the presence of salt. AuNP samples were prepared, diluted into solutions with increasing sodium chloride (NaCl) concentrations, and measured using absorption to determine if there was any aggregation. Remarkably, the polymer-coated AuNPs showed virtually no aggregation in the presence of salt, with the characteristic plasmon resonance peak unchanged at salt concentrations as high as 2.5 M. In contrast, AuNPs stabilized with citrate were extremely sensitive to the presence of salt, showing significant aggregation

at NaCl concentrations as low as 100 mM. While the NaCl is able to shield the charge of the nanoparticles, enabling them to aggregate, it is likely that AuNPs coated with a polymer shell are able to resist this aggregation because of the additional steric repulsion from the polymer.

Large Gold Nanoparticles and Synthesis of SERS-Active Particles

Polymer-coated AuNPs described above have a typical particle size of approximately 10-25 nm. However, previous work by our group has shown that SERS activity for red and near infrared excitations is greater for larger particles, with a nanoparticle size of 60-80 nm being optimum [188]. It was hypothesized that these sizes may not be possible using polymers due to the growth kinetics for the polymer synthesis method described above. Experiments were conducted to determine the feasibility of producing AuNPs in a size regime ideal for SERS activity. Based on earlier observations, it was discovered that polymer concentration plays a key role in the final size of the AuNPs. A series of synthesis reactions were performed, gradually decreasing the polymer concentration and observing the effects on nanoparticle size. As seen in Figure 5.7a, a significant difference is seen in the solutions as the polymer concentrations are decreased (left to right). AuNP solutions prepared in this manner have an iridescent orange color, indicative of larger gold nanoparticles. These nanoparticles precipitate under mild centrifugation, further supporting the conclusion that large AuNPs had been synthesized.

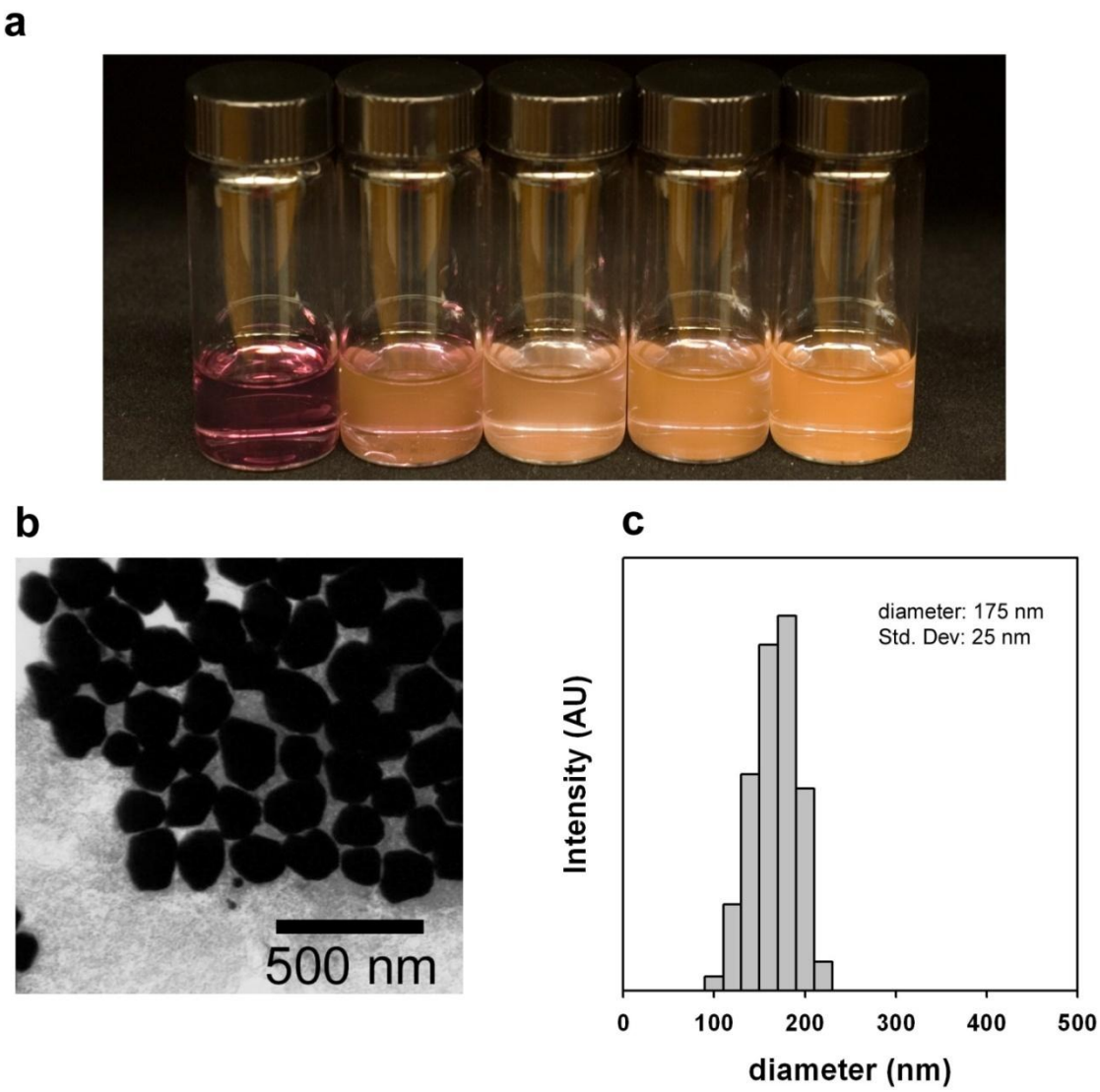

Figure 5.7. Synthesis of large gold nanoparticles. (a) Series of gold nanoparticles, showing a shift in color from red to an iridescent orange as polymer concentration is decreased (left to right), indicating the formation of larger particles. (b) Transmission electron micrograph (TEM) of large, polymer-coated gold nanoparticles in water. (c) Analysis of the TEM shows a relatively monodisperse sample with an average particle diameter of 175 nm with a standard deviation of 25 nm, as shown in the size histogram.

TEM of the prepared AuNPs was used to verify the particle size for these samples and determine if the nanoparticles were suitable for use as SERS tags. Examination of the TEM images showed uniform and monodispersed spherical particles, as seen in Figure 5.7b. Analysis of the images revealed AuNPs with a mean diameter of

175 nm and a standard deviation of 25 nm (Figure 5.7c), confirming the synthesis of large particles suitable for preliminary SERS studies. Additional studies have shown that the synthesis of large AuNPs can occur when the polymer concentration is reduced to the CMC or lower. At these lower concentrations, the polymer is no longer in large aggregates, limiting its ability to shield the forming nanoparticles and allowing for their increased size.

Although the polymer synthesis method was capable of producing particles in the appropriate size regime needed for SERS activity, an additional hurdle remained for the preparation of SERS active tags. Raman dyes must have access to the surface of the AuNP to produce a strong SERS signal. Because the polymer layer was shown to protect the nanoparticle very effectively, presence of the polymer could block access of the dye to the particle surface, preventing efficient SERS signal. It was hypothesized that the larger particles, synthesized using a lower concentration of polymer, would have pockets available for the dyes to access. To prepare SERS active particles, large polymer-coated AuNPs were synthesized as described above. A AuNP solution was then prepared and a dilute malachite green (MCG) solution was added dropwise, as described above.

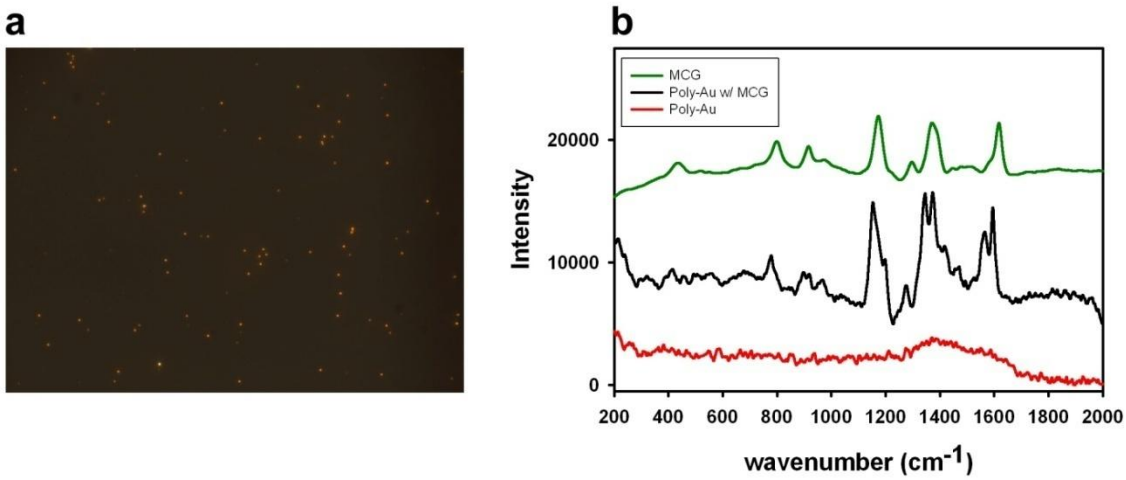

Figure 5.8. Polymer-coated SERS active gold nanoparticles for imaging applications. (a) Dark field microscopy shows uniform, monodispersed nanoparticles with no aggregation. (b) Raman spectra of gold particles (red), malachite green (green) and polymer-coated SERS active particles after incorporation of malachite green.

Samples were analyzed using dark field microscopy to determine the dispersity of the particles and verify the absence of large aggregates. These AuNPs were extremely bright and uniform under dark field microscopy, showing monodispersed particles with no aggregation, as seen in Figure 5.8a. Raman spectra of the particles were then recorded to determine if the AuNPs were SERS active. Polymer-coated AuNPs with no MCG showed no raman spectra (Figure 5.8b, red), as expected. In contrast, polymer-coated AuNPs labeled with dye showed a distinct raman signature for MCG (Figure 5.8b, black), nearly identical to the reference MCG spectrum (Figure 5.8b, green). These data show that a one-pot synthesis of polymer-coated, SERS active AuNPs is possible. These nanoparticles could have significant applications in the fields of *in vitro* and *in vivo* diagnostics, and the results presented here and in Chapter 4 open the possibility for new synthesis procedures for a number of other useful nanoparticles.

5.5 CONCLUSIONS

In conclusion, we have reported a new synthetic procedure for the preparation of AuNPs based on the use of amphiphilic multidentate ligands. The novel features associated with the use of polymeric stabilizers are controlled growth kinetics, increased nanoparticle stability and a wide range of possible nanoparticle sizes. This procedure also allows for the synthesis of large AuNPs suitable for use as SERS active tags. Indeed, upon the addition of a reporter dye, SERS active particles are spontaneously formed in a one-pot procedure, yielding AuNPs with high contrast under dark field microscopy and distinct Raman signatures.

CHAPTER 6

NOVEL NANOPARTICLE SURFACE CHEMISTRIES TO ELIMINATE NONSPECIFIC BINDING

6.1 ABSTRACT

Quantum dot (QD) nanocrystals are promising fluorescent probes for multiplexed staining assays in a number of biological applications. However, nonspecific QD binding to cellular membranes, organelles and biomolecules remains a limiting factor in detection sensitivity and specificity. In this chapter, we show a new class of hydroxyl (-OH) coated QDs for minimizing nonspecific cellular binding and for overcoming the bulky size problems encountered with current surface coatings. The hydroxylated QDs are prepared from carboxylated (-COOH) QDs via a hydroxylation and crosslinking process. With a compact hydrodynamic size of 13-14 nm (diameter), they are highly fluorescent (>60% quantum yields) and stable under both basic and acidic conditions. Using human cancer cells as well as biological staining buffers and human plasma, we have evaluated their superior nonspecific binding properties against that of carboxylated, protein-coated, and polyethylene glycol (PEG)-coated QDs. Quantitative cellular staining data indicate that the hydroxylated QDs result in a dramatic 140-fold reduction in nonspecific binding relative to that of carboxylated QDs, and a moderate 10-20 fold reduction relative to that of PEG- and protein-coated QDs in cells.

6.2 INTRODUCTION

With the development of novel coating strategies which can render nanoparticles soluble in water [80, 81, 83, 84, 108, 111, 115, 153, 198-202], QDs are quickly being designed as fluorescent labeling agents for a broad range of biological applications.[46,

48, 49, 53, 80, 81, 83-85, 87, 88] This broad interest is driven by their unique optical and electronic properties such as size-tunable light emission, superior signal brightness, resistance to photobleaching, and simultaneous excitation of multiple fluorescence colors [46, 48, 87, 88], which make them superior to traditional organic dyes for many applications. Recent advances in QD synthesis [103-105, 107, 124, 166, 167, 170-172] and coating strategies have led to highly bright and stable QD probes that are well suited for multiplexed molecular profiling of intact cells and clinical tissue specimens [54, 55, 90, 97-100]. In contrast to in-vivo clinical imaging, where the potential toxicity of cadmium-containing nanoparticles is still a major concern and will likely hinder clinical use in the near future, histological and cellular staining as well as solution assays are performed on in-vitro or ex-vivo clinical patient samples. Because potential toxicity is not a concern for these samples, the use of multicolor QDs as ultrasensitive probes for tissue, cell and fluid samples is likely one of the most important and clinically relevant applications in the near term [54, 55, 99, 100]. However, a major problem for this application is that QD probes tend to be "sticky" and often bind nonspecifically to cellular membranes, proteins, and extracellular matrix materials. In particular, nanoparticles with highly charged functional groups, such as carboxylic acids and amines, have been shown to exhibit strong nonspecific binding to various cells and tissues [110, 203-205] as well as proteins in serum and blood. This nonspecific binding problem causes a high level of background fluorescence that degrades the signal-to-noise ratio and limits tagging specificity and detection sensitivity.

A number of surface encapsulation methods have been used for QD solubilization and bioconjugation, including direct ligand-exchange reactions with small molecules, such as mercaptoacetic acid [81], dihydrolipoic acid [115] and polyethylenimine (PEI) [110], and indirect surface encapsulation using silica, lipids, and amphiphilic polymers [53, 80, 81, 83, 110-113]. One strategy commonly employed to

reduce the nonspecific binding of nanoparticles is the attachment of polyethylene glycol (PEG) [53, 57, 58, 203], a nontoxic and hydrophilic polymer that is commonly used to improve drug biocompatibility and systemic circulation [58, 206-208]. PEGylated QDs have nearly neutral surface charges and are able to maintain colloidal stability under various experimental conditions, such as acid and base as well as high concentrations of salt, through steric repulsion. Although recent work has shown the successful use of PEGylated QDs for both *in vitro* [53, 203] and *in vivo* [83-85, 209, 210] applications, nonspecific binding to biomolecules and complex intracellular and extracellular materials still exists and remains a bottleneck to increasing the signal-to-noise ratio and improving detection sensitivity and specificity [54]. In addition, PEG-coated nanoparticles have significantly larger hydrodynamic sizes than the uncoated nanoparticles, often more than doubling the particles' hydrodynamic size. This increased size could prevent the probes from accessing biological targets deep within complex tissue and cellular structures.

In contrast, small nanoparticles often rely on a highly negative or positive surface charge to maintain colloidal stability and prevent particle aggregation through electrostatic repulsion. This presents a problem for the use of these nanoparticles in complex biological environments, where biomolecules are highly charged or have charged regions necessary for their function. To address these problems, we have investigated the role of charge in QD-biomolecule interactions and have shown that the nonspecific binding of nanoparticles in cells, tissues and other complex biological samples can be minimized by reducing the surface charge of the nanoparticles. Moreover, through crosslinking and altering the surface chemistry of polymer coated QDs, we can increase the stability of the nanoparticles while maintaining a small hydrodynamic size. In this chapter, we show that nearly neutral hydroxyl (-OH) surface coatings can be used to minimize nonspecific cellular binding of QDs, and also to overcome the size problem associated with PEG coatings. These hydroxylated QDs are

prepared from traditional carboxylate-coated QDs via a hydroxylation and crosslinking process, which also serves to increase the integrity of the polymer coating. We have systematically studied the effects of hydroxylation on the physical and optical properties of QDs, including surface charge, hydrodynamic size, colloidal stability and fluorescence quantum yield.

Additionally, we have studied the effects of surface hydroxylation on the nonspecific binding of quantum dots in biological samples and optimized them for use in multiplexed imaging studies. Using human cervical cancer cells (cultured HeLa cells), we have evaluated their nonspecific binding properties in comparison with carboxylated QDs and protein-coated QDs (coated with streptavidin, PEG-antibodies, or PEG-peptides). This new class of QDs leads to a dramatic 140-fold reduction in nonspecific cellular binding relative to that of carboxylated QDs, a 20-fold reduction relative to streptavidin-QDs, a 16-fold reduction relative to PEG-Ab QDs, and a 13-fold reduction relative to PEG-peptide QDs (QTracker). We have also shown a significant reduction in binding to components in common biological staining buffers as well as human plasma.

6.3 METHODS

QD Synthesis, Encapsulation and Transfer to Water

CdSe/CdS/ZnS QDs were synthesized using methods described above. An aliquot of the crude QD solution was then purified using liquid-liquid extraction in hexane and MeOH and then precipitated and transferred to $CHCl_3$ using methods described above. Polymer coating, transfer to water and purification were performed as described previously.

Surface Hydroxylation and Crosslinking

Purified QDs (made in our lab or carboxyl-coated Qdots from Invitrogen) were diluted in deoinized water for surface modification/hydroxylation. Briefly, 100 pmol of QDs was diluted to a final concentration of 100 nM. Approximately 1 mg of *N*-hydroxysulfosuccinimide sodium salt (Sulfo-NHS) and 12 mg *N*-(3-Dimethylaminopropyl)-*N'*-ethylcarbodiimide hydrochloride (EDAC) were added to the QD solution and were mixed thoroughly. For hydroxylation and crosslinking, 11.5 mg of 1,3-amino-2-propanol (DAP) was dissolved in deionized water and added slowly to the QD solution under vigorous stirring. The reaction mixture was allowed to react for 24 hours and was then dialyzed against 50 mM borate buffer to remove excess reactants and byproducts. To vary the degree of hydroxylation, EDAC and DAP amounts were decreased appropriately. To perform the hydroxylation reaction without crosslinking, 3-amino-1,2-propanediol (APD) or a similar compound can be used.

Gel Electrophoresis

QDs were evaluated with a horizontal submerged gel electrophoresis apparatus (Mini-SubCell GT, BIO-RAD) using a 0.7% (w/v) agarose gel in tris-acetate-EDTA (TAE) buffer. Briefly, a 250 mL beaker was charged with 0.35g of agarose, to which 50 mL of 1X TAE buffer at pH 8.5 was added. The solution was then covered with a 50 mL beaker and heated in a microwave until completely melted, approximately 1 minute. The molten agarose was allowed to stand at room temperature for 10 minutes, at which point 50µL of Tween-20 was added for a final concentration of 0.01% (v/v). The solution, when at ~55ºC, was cast into a gel tray with a 1.0 mm 15 well comb and allowed to solidify. The gel was placed in the agarose electrophoresis tank and sufficient 1X TAE buffer was added to the tank to just cover the top of the gel. For each well, 20 µL of the QD samples at 50 nM were mixed with 5µL of 5X TAE loading buffer (5X TAE, 25% (v/v)

glycerol, 0.25% (w/v) Orange-G at pH 8.5) by pipetting before being loaded into the gel. The gel was resolved at 100 V for 30 minutes (PowerPak Basic, BIO-RAD) and then imaged with 2-second exposure using a UVP gel documentation system.

Hydroxylation Quenching

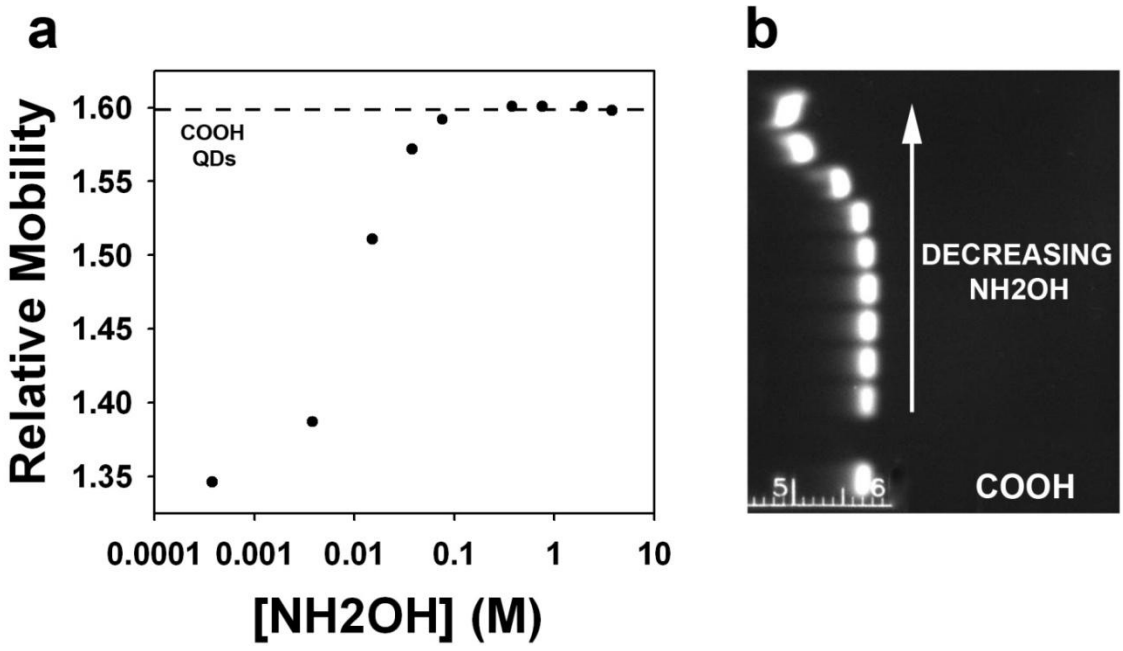

Figure 6.1. Quenching hydroxylation procedure using hydroxylamine. (a) Relative mobility of quantum dots in a gel shift assay as a function of hydroxylamine concentration. (b) High concentrations of hydroxylamine result in immediate quenching and gel shifts consistent with COOH-coated quantum dots. Decreasing the hydroxylamine concentration allowed the hydroxylation to progress, as evident by the decreased mobility of hydroxyl quantum dots.

A QD hydroxylation reaction was prepared, as described above, without EDAC. Separately, a stock solution of hydroxylamine in water was prepared and serial dilutions were made. 5 µL of the solutions were pipetted into 0.7 mL eppendorf tubes. EDAC was then added to the reaction solution as described in the hydroxylation method. 15 µL aliquots were taken immediately after the addition of EDAC and transferred to the eppendorf tubes containing the hydroxylamine solutions to quench the reaction. After 3

hours, the quenched reaction samples were analyzed using gel electrophoresis, as described above. Gel shifts were measured and compared to COOH coated QDs (Figure 6.1).

Reaction kinetics of hydroxylation reaction.

A stock solution of 4 M hydroxylamine in water was prepared to act as a reaction quencher. 5 µL of the quenching solution was pipetted into 0.7 mL eppendorf tubes. Separately, a QD hydroxylation reaction was prepared, as previously described. 15 µL aliquots of the reaction solution were taken at various time points and transferred to the quenching solution to halt the reaction progression. The quenched aliquots were then analyzed using gel electrophoresis and gel shifts were measured.

Quantum Yield

The Quantum Yield (QY) of QDs was determined experimentally by comparison to dyes with known QY. Briefly, a concentration series of dye with known QY that is close in emission to the QD being tested was prepared. Absorption at the planned excitation wavelength and emission spectra were recorded for each of the samples using a Uv-Vis absorption spectrometer and spectrofluorometer, respectively. The integrated fluorescence intensity (area under fluorescence spectrum) was calculated and plotted against the absorption to generate a line with slope, m_{ST}. The procedure was repeated for a concentration series of QDs and results plotted to give a slope, m_{QD}. QD quantum yield was calculated as:

$$QY_{QD} = QY_{ST} \times \left(\frac{m_{QD}}{m_{ST}}\right)$$ Equation 6.1

assuming identical solvents.

Cell Fixing and Staining

HeLa cells (ATCC number CCL-2) were cultured in RPMI media with 10% fetal bovine serum (FBS) at 37 ºC (5% CO_2) and grown in an 8-well chamber slide. After 24 hours for seeding, the cells were washed with 1X PBS and fixed with 3.7% formaldehyde and 0.1% triton X in 1X phosphate buffered saline (PBS) for 5 minutes. The fixative was then aspirated and the cells washed with 1X PBS 3 times for 5 min each. A 2% bovine serum albumin (BSA) blocking solution in 1X PBS was added to the wells for 20 min and then aspirated. QDs were diluted in the blocking solution to the desired concentration and incubated with the cells for 20 min. The QD staining solution was aspirated and the cells were washed with 1X PBS 3 times for 5 min each. A 1 µg/mL solution of 4',6-diamidino-2-phenylindole dihydrochloride (DAPI) in deionized water was added to the wells and incubated for 5 min for nuclear staining. The DAPI solution was then aspirated and the cells were washed for 5 min with deionized water. The slide was mounted and prepared for fluorescence microscopy.

QD Cell Binding Assays.

For quantitative analysis of nonspecific QD binding to cells, a fluorescent microplate reader (Synergy 2 Multi-detection Microplate Reader, Biotek Instruments) was used. Briefly, HeLa cells were cultured in a clear bottom 96 well plate for 24 hours, fixed, blocked and stained as described in the cell staining experiment protocol. DAPI nuclear staining was performed as described above to correct for variations in cell

densities. QD concentrations from 0 to 20 nM were used in replicates of six (n = 6). The fluorescence intensity from the QDs was measured, normalized using the DAPI fluorescence intensity, and background subtracted to determine the intensity of nonspecific staining.

QD-Biological fluid Binding Assays

QD solutions with various coatings (-COOH, -OH, Streptavidin (Strep) and PEG/antibody) were prepared at 100 nM. Separately, stock solutions of common biological fluids (5% goat serum/2% BSA, 6% BSA, human plasma) were prepared. QD solutions were diluted 1:5 into each of the biological fluids, vortexed to mix completely and allowed to incubate at room temperature for 2 hours. After incubation, aliquots of the samples were taken and used in gel electrophoresis. Relative migration rates for the samples were compared to QD samples that had been incubated in 1x PBS.

6.4 RESULTS AND DISCUSSION

A number of different techniques have been employed to protect the surface of semiconductor QDs and render them soluble in water for use in biological applications. These techniques generally fall into two categories: (a) exchanging the hydrophobic ligands on the QD surface with hydrophilic small molecule ligands, or (b) coating the nanoparticles with an amphiphilic polymer that can interact with both the hydrophobic ligands and the surrounding aqueous environment. While coating procedures that preserve the hydrophobic ligands have shown improved optical properties compared to QDs produced using ligand exchange procedures[116], the resulting nanoparticles are typically larger in size and may not perform well for complex samples such as cells and tissues. The size of these nanoparticles is further increased by surface treatments that are designed to reduce nonspecific binding. These treatments generally involve

attaching proteins (such as streptavidin) or large hydrophilic polymers such as polyethylene glycol (PEG) to the QD surface which have been shown to reduce, but not eliminate, nonspecific binding.

Surface Coating Chemistry

Nanoparticle surface charges are believed to play a critical role in the nonspecific binding process, because QDs with either highly negative or positive charges show significant nonspecific binding to cells and tissues [110, 203-205]. This is not unexpected, as many proteins and other molecules inside and outside the cell are charged or have charged regions which are important for a variety of biological processes [211]. Electrostatic interactions between proteins or other molecules play a significant role in molecular recognition, control of protein phosphorylation and the enhancement of catalytic rates [212]. These charged regions likely interact with nanoparticles electrostatically, leading to considerable nonspecific binding as observed for highly charged QDs. In this chapter, we have investigated nonspecific binding of QDs to biomolecules in cells and biological fluids and developed new coating methods to minimize nonspecific binding while maintaining the small size and stability of the QD probes.

Polymer-coated QDs produced using the methods described in Chapter 3 show excellent optical and colloidal properties when transferred to water. However, the nanoparticles have carboxylic acid functional groups covering their surface and are highly negatively charged. Initial staining of fixed cells using these QDs showed intense nonspecific binding, as expected. Because surface charge is believed to play a crucial role, a surface coating strategy was developed to reduce the charge of the nanoparticles while maintaining colloidal stability. As shown in Figure 6.2a, carboxylic acid functional groups of polymer coated QDs (as described in Chapter 3) were modified with a small

hydroxyl-containing molecule (1,3-diamino-2-propanol or DAP) to yield QDs with hydroxyl functional groups on the surface. Based on a geometric model of the polymer and the QD surface area, we have estimated that each QD is covered with about 150 amphiphilic polymer molecules, leading to approximately 2500 carboxylic acid functional groups (each polymer molecule has ~15 -COOH groups). These -COOH groups are converted to -OH groups by a hydroxylation and crosslinking process, creating a cage-like shell that locks the polymer coating in place. The hydroxylated QDs are stable for over 6 months in borate buffer solution at 4°C. They also show no aggregation in acidic environments, which has been a problem for traditional QDs with carboxylic acid functional groups (due to protonation at low pHs) [116] . Transmission electron microscopy (TEM) clearly shows polymer-encapsulated QDs with an average diameter of ~13 nm, as seen in Figure 6.2b. Fluorescence microscopic imaging further reveals a characteristic blinking behavior for immobilized QDs on a glass slide, indicating that the dots are primarily well dispersed single particles [160].

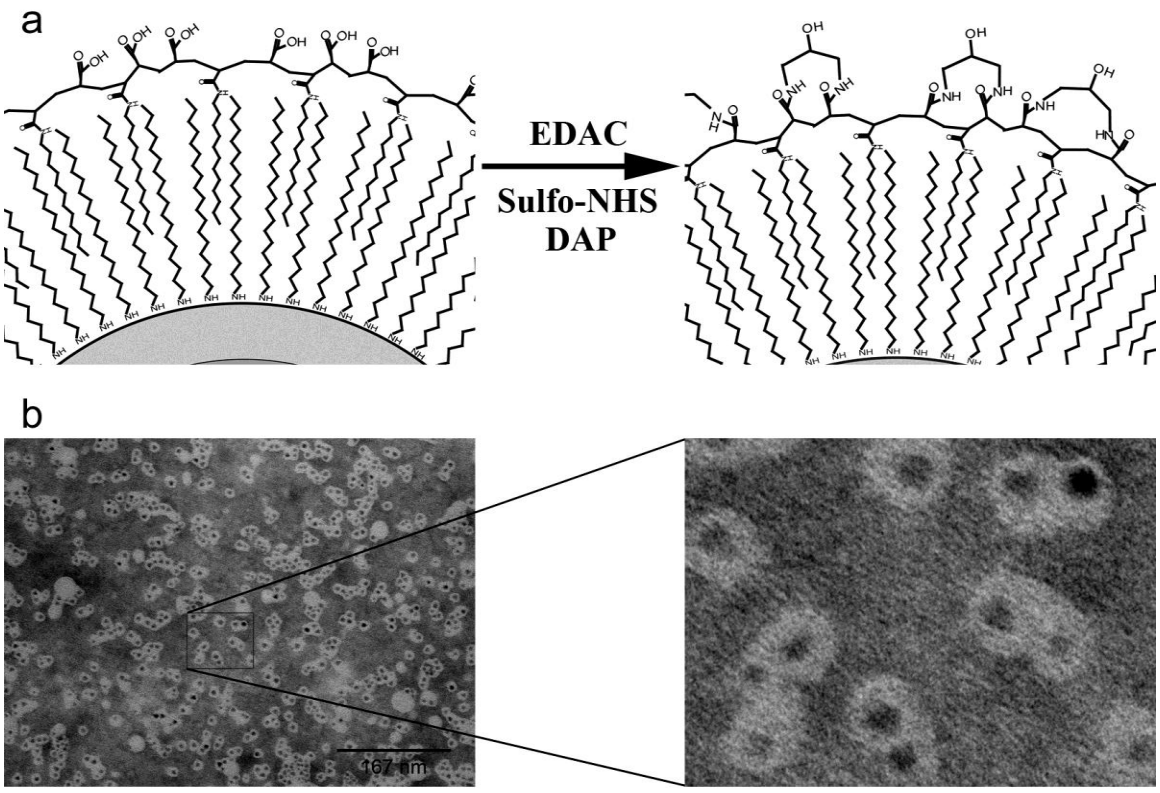

Figure 6.2. Surface coating chemistry and structure of polymer-encapsulated quantum dots (CdSe/CdS/ZnS). (A) Schematic diagram showing conversion of carboxylated quantum dots (coated with poly(acrylic acid)-octylamine) to hydroxylated and crosslinked quantum dots. The small-molecule agent for hydroxylation is 1,3-diamino-2-propanol. (B) Transmission electron micrograph (TEM) showing the structure of encapsulated quantum dots after surface hydroxylation and crosslinking.

Hydroxylation Kinetics

To confirm the success of the hydroxylation procedure and optimize the reaction parameters, the reaction kinetics of the process was analyzed. Sample aliquots were taken and the reaction was quenched to determine the progress of the reaction at various time points. These samples were analyzed using gel electrophoresis and the migration data was plotted as a function of time. Gel migration was expected to decrease as the reaction progressed, due to the replacement of carboxylic acid functional groups (which are highly negatively charged and run quickly towards the

positive electrode of the gel) with hydroxyl functional groups, which have a more neutral charge and thus run slower in the gel.

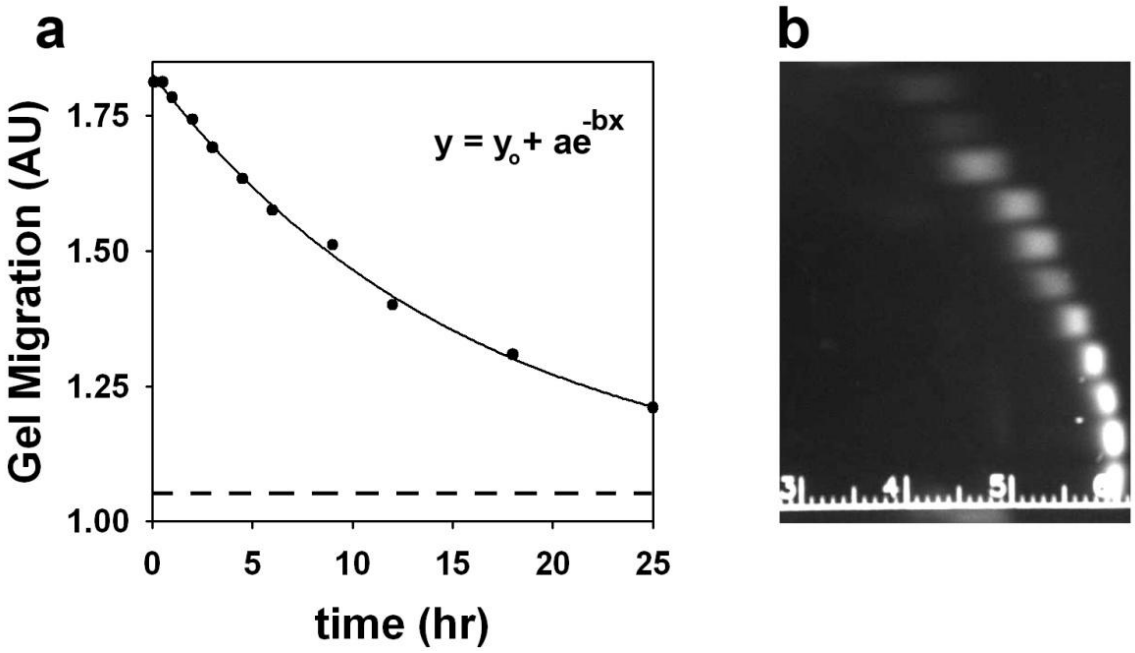

Figure 6.3. Quantum dot hydroxylation reaction kinetics. (a) Quantum dot gel migration as a function of time. Reaction kinetics follow simple exponential decay rate, with y_o=1.05, a=0.77 and b=0.063. These parameters give a "half-life" of approximately 11 hours. (b) Gel image showing decrease in gel migration and only slight band broadening as the hydroxylation progresses.

As expected, gel migration noticeably decreased as the hydroxylation reaction progressed, as seen in Figure 6.3b. Plotting the results as a function of time and fitting a curve to the data points (Figure 6.3a) showed the reaction kinetics follow a simple exponential decay model:

$$y = 1.05 + 0.77e^{-0.063t} \qquad \text{Equation 6.2}$$

Based on this equation, the reaction has a "half-life" (in this case, the time at which half of the carboxylic acid functional groups are converted to hydroxyl groups) of

approximately 11 hours. It is not surprising that the reaction kinetics resemble an exponential decay model, as steric hindrance may play a role in the process. Because of the polymer coating, some carboxylic acid functional group will be unobstructed on the surface of the particle, while others may be buried deeper within the polymer shell. As the reaction progresses, it is likely that the easily accessed functional groups are quickly converted, as shown in the sharp decrease in gel migration at shorter time points. Groups deeper within the polymer shell are not as easily accessed, resulting in a slowing of the reaction progress as it asymptotically approaches completion, as seen in the longer time points (Figure 6.3a). These results suggest that the hydroxylation procedure should be allowed to progress at least 11 hours to replace the majority of carboxylic acid groups with hydroxyl groups.

Quantum Dot Size, Charge and Optical Properties

To verify that the surface charge had been reduced and the optical and colloidal properties of the QDs were maintained, samples were taken and characterized using a variety of methods. As shown in Figure 6.4, polymer encapsulation and subsequent hydroxylation have no major effects on the QD's optical properties such as UV-Vis absorption and fluorescence emission. Polymer coating of the hydrophobic QDs and subsequent transfer to water resulted in a relatively small decrease in fluorescence quantum yield (from ~80% for hydrophobic QDs to ~60-65%). The hydroxylation procedure showed no noticeable decrease in fluorescence quantum yield compared to –COOH QDs. Importantly, both the coating process as well as hydroxylation procedure have no broadening effects on the spectral width of the QDs (Figure 6.4), with –OH QDs maintaining a narrow full width half max (FWHM) of 23 nm.

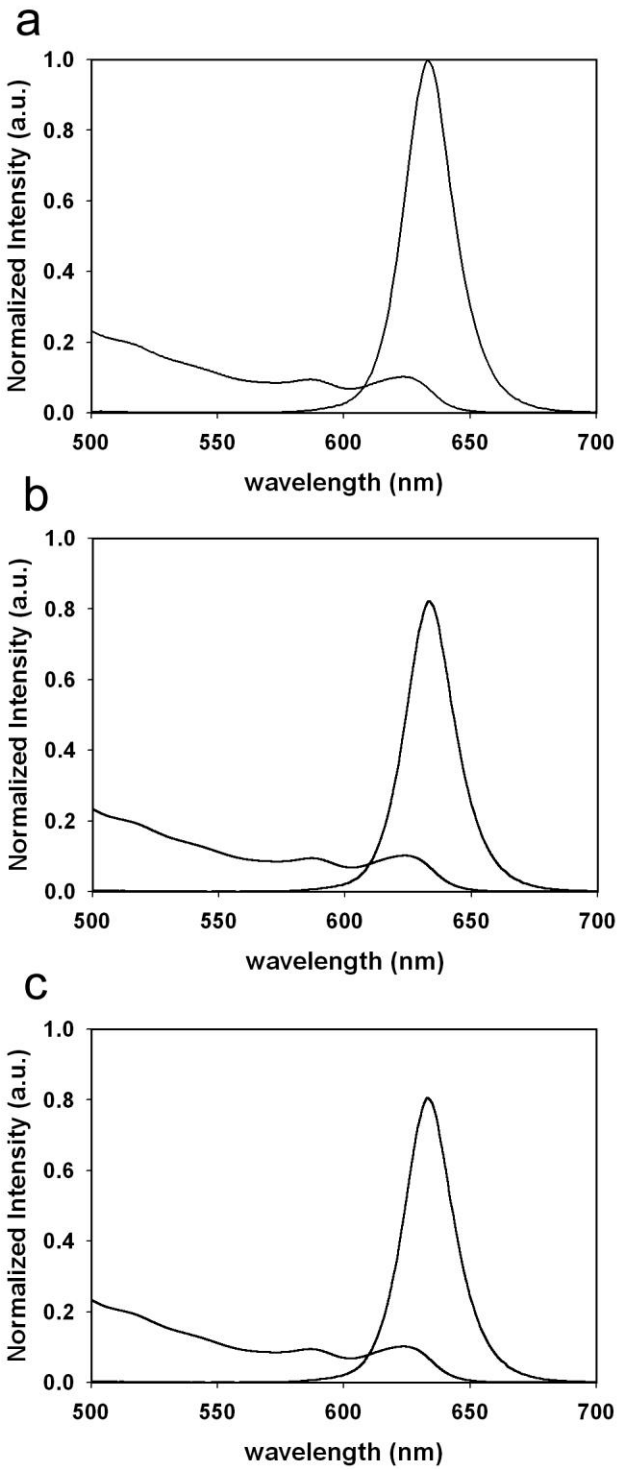

Figure 6.4. UV-Vis absorption (left sloping curves) and fluorescence emission spectra (symmetric peaks at 640 nm) of (a) hydrophobic quantum dots in chloroform, (b) solubilized quantum dots in buffer solution, and (c) hydroxylated quantum dots in buffer solution. Note that the water-solubilized quantum dots and the hydroxylated quantum dots have nearly identical fluorescence emission spectra with a quantum yield of 65% and a spectral width (full width at half maximum or FWHM) of 23 nm.

This surface treatment also has little or no effect on the overall particle size as measured by dynamic light scattering (DLS). In fact, the hydrodynamic sizes (13-15 nm in diameter) of the hydroxylated QDs are nearly the same or slightly smaller than that of the carboxylated QDs (14-16 nm). Although surface hydroxylation was expected to increase the physical size of the particles slightly, this result is not unexpected because the process also reduces the particle surface charge and the electrical double layer thickness (thus the hydrodynamic radius). In contrast, QDs coated with PEG and/or proteins often have hydrodynamic sizes of 25-30 nm, about twice the size of hydroxylated dots, as shown in Figure 6.5a.

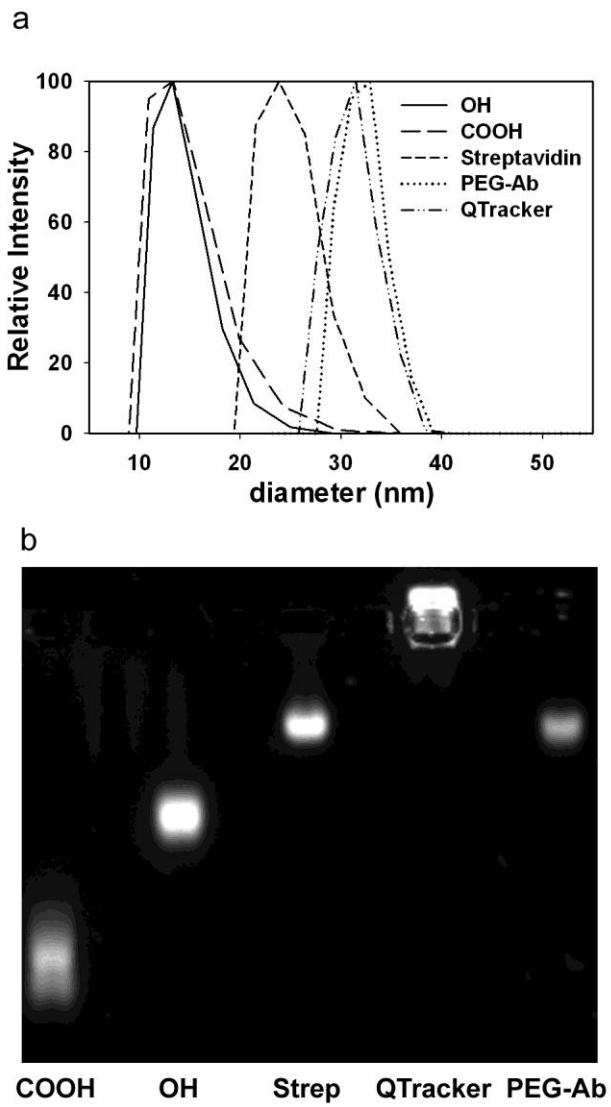

Figure 6.5. Size and charge comparison of quantum dots with varying surface coatings. (a) Hydrodynamic size data obtained from hydroxylated QDs, carboxylated QDs, streptavidin-coated QDs, QTracker QDs, and antibody-conjugated QDs by using dynamic light scattering measurement. (b) Gel electrophoresis migration data corresponding to the different types of QDs in (a).

The decrease in surface charge after hydroxyl modification was further confirmed by zeta potential and gel electrophoresis measurements. QDs with carboxylic acid surface groups have a measured zeta potential of -40 mV at pH 8.5, consistent with previously reported values [116], while the hydroxylated nanoparticles show a significant decrease in surface charge, with a zeta potential of -20 mV at pH 8.5. For gel

electrophoresis measurements, QDs coated with a PEG layer are expected to run very slowly due to their larger sizes and more neutral zeta potentials. Likewise, streptavidin-conjugated nanoparticles are expected to run slower because of their larger sizes and reduced charges from protein shielding. QDs with carboxylic acid surface groups are expected to run most rapidly towards the positive electrode because of their small sizes and high negative charges. In comparison, the hydroxylated QDs should run more slowly than the –COOH QDs due to their reduced surface charges, despite being identical in size. Indeed, gel electrophoresis studies (as seen in Figure 6.5b) reveal that carboxylated QDs migrate the farthest in distance, in agreement with their strongly negative zeta potential and small size. The hydroxylated QDs migrate less than the carboxylic acid QDs, but more than the protein or PEG-coated dots, most likely due to their smaller size. Streptavidin and secondary antibody conjugated QDs show a slow migration toward the positive electrode, suggesting a net negative surface charge. This negative charge suggests that that the antibody conjugate QDs are sparsely coated with PEG because heavy PEGylation would shield the surface of the QDs and produce nanoparticle with nearly neutral zeta potentials.[116]

Nonspecific Cellular Binding

To determine if hydroxylation can reduce the nonspecific binding of nanoparticles in cells, tissues and biological fluids, we have used human cancer cells to evaluate the nonspecific binding properties of QDs with different surface coatings. As shown in Figure 6.6, carboxylated QDs show very high nonspecific cellular binding when incubated at a concentration of 20 nM (Figure 6.6a,b); significant nonspecific binding is also observed at QD concentrations lower than 2 nM. In contrast, there is no detectable nonspecific binding for the hydroxylated QDs at similar concentrations (Figure 6.6c,d). Note that DAPI nuclear staining is used to ensure an equivalent cell density between the

samples. The QD concentration was then increased to 100 nM to determine if any nonspecific binding could be detected for the hydroxyl modified QDs. Even at this high concentration, there is minimal nonspecific binding relative to the negative control.

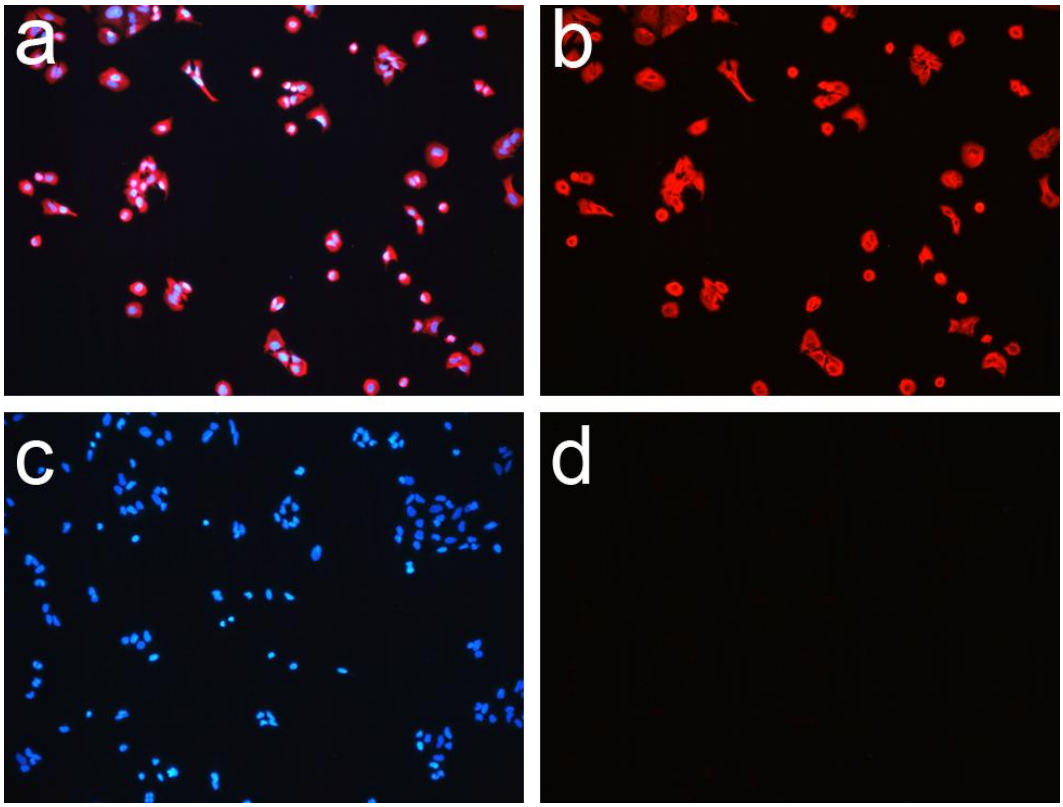

Figure 6.6. Fluorescence microscopy images of hydroxylated and carboxylated quantum dots nonspecifically bound to fixed human HeLa cells. (a, b): Carboxylated quantum dots with (a) and without (b) DAPI counter staining of cell nuclei, showing intense nonspecific cellular binding. (c. d): Hydroxylated quantum dots with (c) and without (d) DAPI counter staining of cell nuclei, showing the absence of nonspecific cellular binding.

For quantitative and statistical analysis of these results, we then used a fluorescence microplate assay to objectively measure a large population of QD-stained cells. As shown in Figure 6.7a, protein and PEG-coated QDs show a reduced level of nonspecific binding in comparison with carboxylated nanoparticles. Remarkably, our

hydroxylated QDs show virtually no nonspecific binding in the microplate assays, corroborating the fluorescence microscopy results shown in Figure 6.6. Another interesting result is that nonspecific QD binding has an approximately linear relationship with QD concentration, a behavior that is consistent with nonspecific interactions (Figure 6.7b).

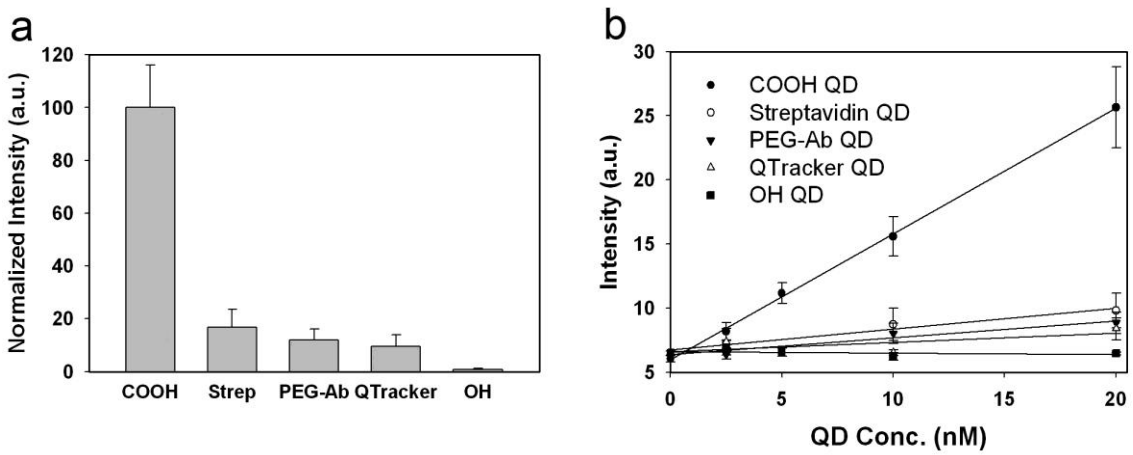

Figure 6.7. Quantitative evaluation and comparison of nonspecific cellular binding for various quantum dot surface coatings. (a) Normalized fluorescence staining at 20 nM quantum dot concentration as measured by microplate assays. (b) Plots of nonspecific cellular binding signal intensities as a function of quantum dot concentration.

Surface Charge Variations

To investigate how the degree of hydroxylation would affect cellular nonspecific binding, we then prepared a series of QD samples with increasing hydroxyl densities. As shown in Figure 6.8a, the degree of hydroxylation was measured by zeta potential and gel electrophoresis, and its effect on nonspecific QD binding was analyzed using fluorescence microplate assays. Fully carboxylated QDs have the highest negative charge, and migrate the farthest on a gel. As the degree of hydroxylation is increased, the net surface charge is reduced, hindering QD migration in the gel. An interesting finding is that the migration distance plateaus as the degree of hydroxylation approaches

100%. This plateauing effect is likely due to the increasing difficulty to hydroxylate the carboxylic acid groups due to steric hindrance, as described above. As expected, nonspecific binding is dependent on the degree of surface hydroxylation, with fully hydroxylated QDs showing virtually no nonspecific binding. These results are consistent with previous reports for highly charged nanoparticles and the hypothesis that charge plays a critical role in the nonspecific binding of QDs to cells and tissues.

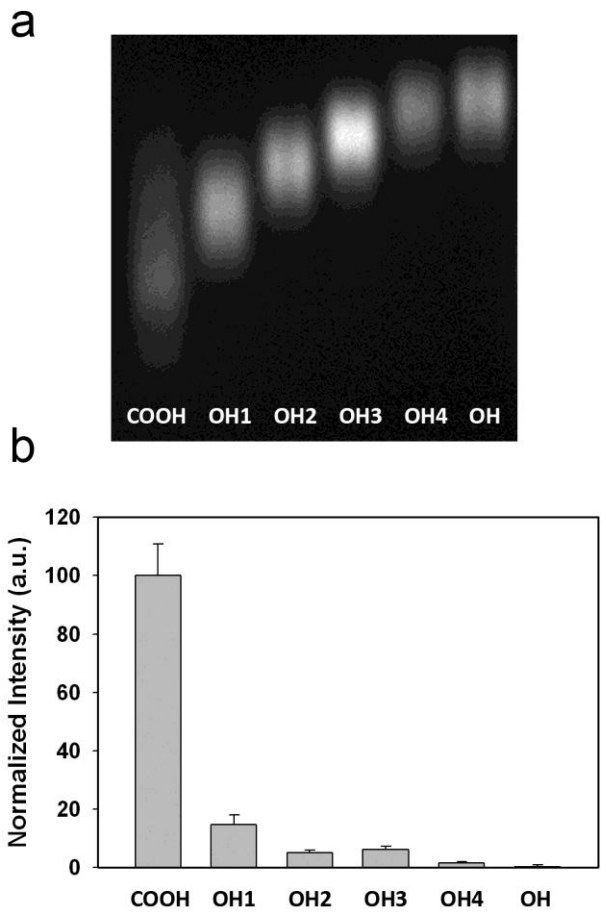

Figure 6.8. (a) Gel electrophoresis data for quantum dots with increasing degrees of hydroxylation, from 100% -COOH (left) to 100% -OH (right). (b) Nonspecific cellular binding data for quantum dots with corresponding degrees of hydroxylation in (a).

Nonspecific Binding in Biological Fluids

Nonspecific binding has also been observed in a number of biological environments (such as blood, serum and plasma) as well as in tissue staining buffers, presenting a problem for assays in which QDs or other nanoparticles encounter these fluids. Similar trends in binding are seen as with the cellular studies discussed above, with highly charged particles exhibiting strong nonspecific binding. To determine if the hydroxyl coated QDs were able to reduce this binding, studies were conducted in common tissue staining blocking buffers as well as human plasma, comparing the hydroxyl QDs with COOH QDs and other commercially available nanoparticles. After incubation in the fluids, samples of the nanoparticles were taken and analyzed using gel electrophoresis, measuring any change in migration as compared to particles incubated in 1x PBS. As seen in Figure 6.9, hydroxyl QDs performed exceptionally well in 6% BSA and 5% goat serum with 2% BSA, showing virtually no change in gel migrations.

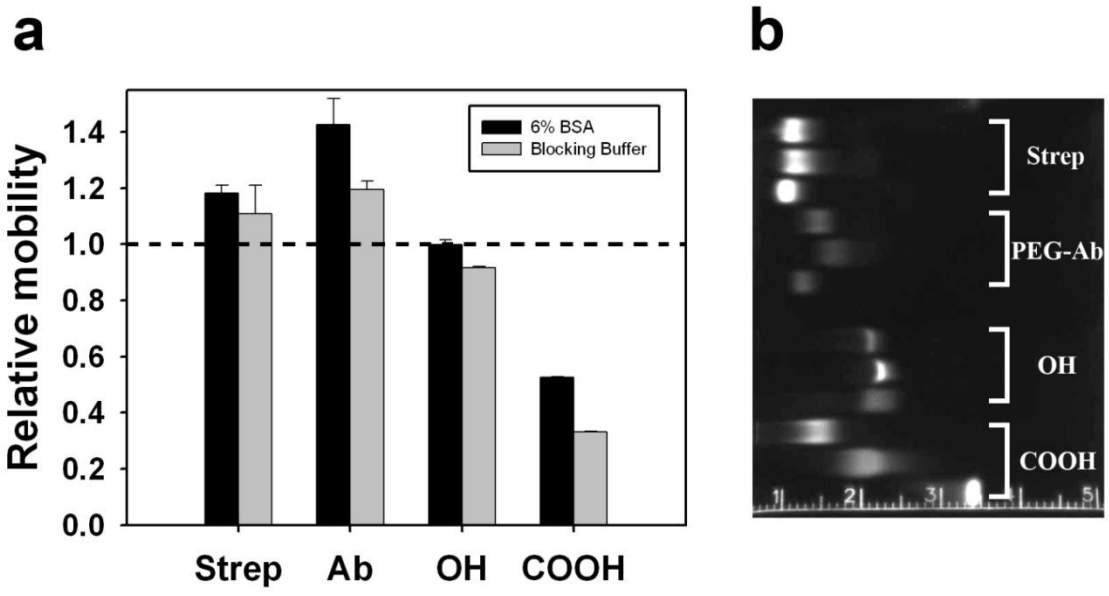

Figure 6.9. Nonspecific binding of quantum dots in staining buffers. (a) Relative migration and (b) gel image of quantum dots with different surface coatings when incubated in 6% BSA (black) and tissue staining blocking buffer (grey) as compared to gel migration of particles in PBS. Hydroxyl-coated quantum dots showed virtually no change in mobility, indicating little to no nonspecific binding to proteins present in the solutions.

Commercially available QD products (with streptavidin coatings and PEG) showed a moderate increase in gel migration (10-40% change), indicating the binding of proteins to the QDs. This change in migration is likely due to both a change in the overall surface charge of the nanoparticles as well as the size. Carboxyl coated QDs performed very poorly, as expected, with decreases in migration of over 50% in the presence of the staining buffers. This is likely due to both an increase in size as well as charge shielding as a result of the adsorption of biomolecules to the QD surface.

Similar results were seen when exposing the nanoparticles to human plasma (Figure 6.10). Hydroxyl coated QDs showed very little nonspecific adsorption of biomolecules, with gel migration changes of less than 10%. Commercially available nanoparticles performed moderately well (Figure 6.10a), with a 15-30% change in gel migration. The carboxyl-coated QDs performed even worse in plasma, with a change in migration of over 80% and a significant portion of the particles aggregated and stuck in the gel well (Figure 6.10b).

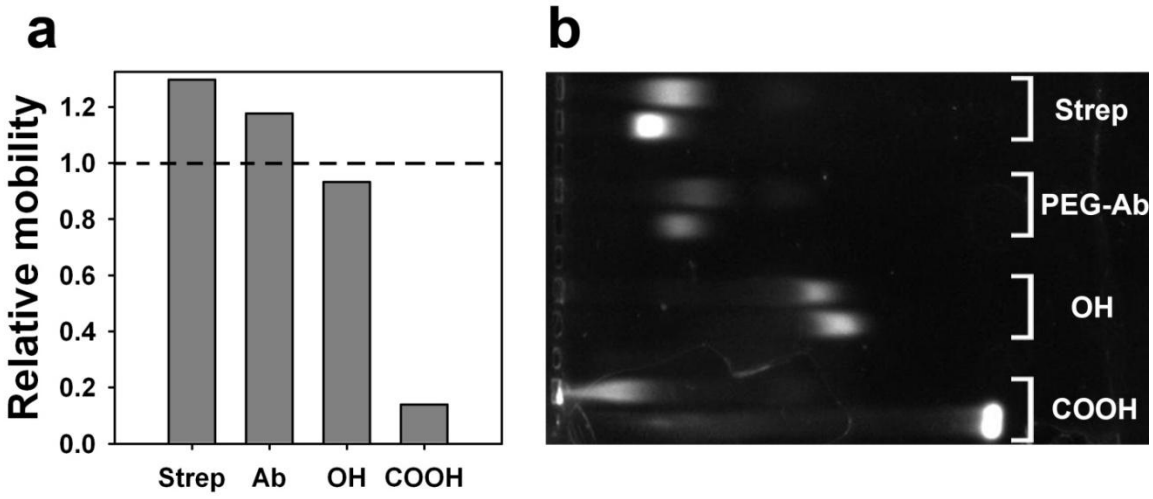

Figure 6.10. Nonspecific binding of quantum dots in biological fluids. (a) Relative migration and (b) gel image of quantum dots with different surface coatings when incubated in human plasma as compared to gel migration of particles in PBS. Hydroxyl-coated quantum dots showed virtually no change in mobility, indicating little to no nonspecific binding to biomolecules present in the plasma.

6.5 CONCLUSIONS

In this chapter, we have described the development of a new class of hydroxylated QDs to minimize nonspecific cellular binding and to maintain the small size of QD probes. These particles were prepared from carboxylated (-COOH) dots via a hydroxylation and crosslinking step. The hydroxyl-coated QDs have compact sizes (13-14 nm hydrodynamic diameter), and are bright (65% quantum yields) and very stable under both basic and acidic conditions. Quantitative data from human cancer cells indicate that the use of hydroxylated QDs results in a dramatic 140-fold reduction in nonspecific binding relative to that of carboxylated QDs, and a moderate 10-20 fold reduction relative to protein and PEG-coated QDs. Our results also indicate that surface charge plays a significant role in the nonspecific binding of these nanoparticles to cellular components. We expect these new nanoparticles to be useful in a range of biological applications where nonspecific binding is a major problem, such as staining in

cells and tissues, sensitive detection in body fluid samples (blood, urine, etc.), as well as live cell imaging. In particular, significant opportunities exist in using these hydroxylated QD probes for multiplexed disease diagnostics. In particular, QD probes can be used to measure a panel of biomarkers in intact cancer cells and tissue specimens, allowing a correlation of traditional histopathology and molecular signatures. With minimized nonspecific binding and background interference, QD probes are especially well suited for analyzing cancer biomarkers that are present at low concentrations or in small numbers of cells. Recent work by Xing et al. has shown the simultaneous staining of 4 different biomarkers for intact cancer cells [54, 99]. Work is also on going to develop sensitive assays for blood and serum analysis.

CHAPTER 7

LOW BINDING, HYDROXYL QUANTUM DOTS FOR STAINING APPLICATIONS

7.1 ABSTRACT

Histopathology is a powerful diagnostic method that allows pathologists to accurately diagnosis a number of diseases by microscopically observing diseased tissue samples. Significant progress has been made in the development of new instruments and technologies to aid in the analysis of the samples. However, significant hurdles remain in the rapid and quantitative analysis of multiple disease biomarkers. Because of their unique optical and colloidal properties, QDs present an exciting opportunity to develop the next generation of histopathology tools and could enable rapid and quantitative detection of multiple disease markers. In this chapter, we explore the use of a cyanogen bromide (CNBr) bioconjugation technique for the coupling of antibodies or other targeting molecules to the surface of hydroxyl-coated QDs. Preliminary results are promising and this technique could lead to a new class of targeted nanoparticles for use in clinical pathology.

7.2 INTRODUCTION

Histology has been performed for more than 100 years for the examination of tissue samples. With advances in the field of microscopy and the availability of new instruments and materials, microscopists have developed a number of ingenious techniques and procedures for enhancing the contrast of important tissue structures and imaging components of interest within the tissue sample. These technologies have allowed the field of histopathology (the microscopic examination of tissues in order to study or diagnose disease) to develop at a rapid pace, with the histological examination

of patient samples being common place in the clinic today. Tissue samples can be obtained from patients in a number of ways, particularly using surgical biopsy, and the sample is preserved for later study using a variety of techniques. The most commonly used fixative in histopathology is 10% formalin, which preserves the tissue structure by crosslinking proteins. After the tissue is fixed, it is then dehydrated and embedded with wax, which provides structural support for the soft tissue to allow thin sectioning and increases the shelf-life of the sample indefinitely. Rapid freezing is another technique used to preserve and prepare samples for imaging. While the shelf life of frozen sections, as well as the structural quality of the tissue, is not comparable to formalin-fixed, paraffin-embedded (FFPE) tissues, frozen sectioning can be done very rapidly, allowing the technique to be used during a surgical procedure. More recent sample acquisition techniques, such as imaged-guided fine needle aspiration (FNA), have allowed the collection of small samples without the need for surgery, allowing clinicians to diagnose patients in an inexpensive and rapid fashion.

In addition to advances in tissue sample acquisition techniques, the early development of staining procedures significantly contributed to the use of histology in the clinic. The most notable of these is the use of hematoxylin and eosin (H&E) stains for providing contrast in tissues [213-215]. H&E staining is probably the most widely used stain in diagnostic medicine and is routinely used for the examination of cancer biopsies as well as many other diseased tissue samples. The H&E procedure involves staining with a basic dye (hematoxylin), which stains basophilic components a bluish purple color, and an acidic dye (eosin), which stains eosinophilic components a pink color. Because it is a basic molecule, hematoxylin generally stains acidic structures within the cells and tissue, such as the nucleus and ribosomes, because of the large prevalence of nucleic acids. Likewise, eosin preferentially stains basic structures or regions, such the cell cytoplasm, due to the presence of protein. These stains provide pathologists with a

high degree of contrast for examining tissue structure (as seen in Figure 7.1a) and enable them to perform diagnostics for many diseases.

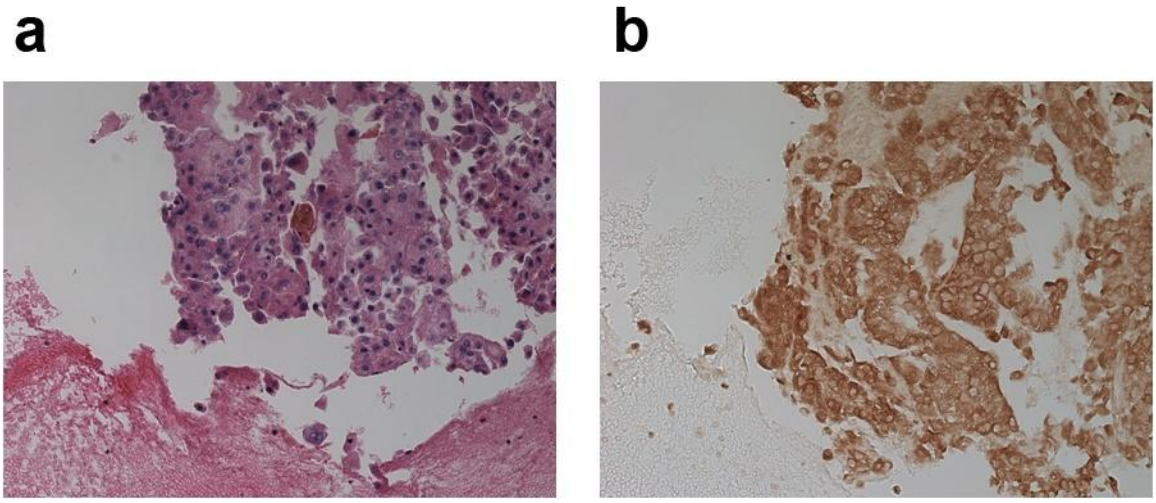

Figure 7.1. Standard staining procedures, shown on liver cancer tissue sections. (a) Hematoxylin and eosin (H&E) staining, which colors basophilic components bluish-purple (from hematoxylin) and eosinophilic components pink. (b) Immunohistochemistry (IHC) staining of a liver cancer biomarker using antibodies (for targeting) and horseradish peroxidase, which oxidizes a substrate to yield a brown stain.

Further progress in the diagnosis of disease using histopathology was seen 60 years ago with the introduction of immunohistochemistry (IHC) [216, 217]. This technique originally involved the use of fluorescently tagged antibodies to target and image proteins of interest within tissue samples. However, early versions of this technique were plagued with many problems, including high autofluorescence that significantly masked the signal, low photostability of the dyes which eventually render the sample unmeasurable and the difficulty and expense of using the necessary instruments to analyze the samples. In an effort to alleviate these problems, a new labeling technique was developed that allowed the visualization of the targeted molecules using standard light microscopes [218-221]. This technique uses enzyme-

linked antibodies (horseradish peroxidase, HRP, is the most commonly used today) to produce a signal visible under microscopy. After binding of the antibodies to the targeted molecules in the sample, a substrate is applied which can be oxidized by HRP to yield a visible stain. As shown in Figure7.1b, this leads to a stable, dark product that is easily visible using a standard microscope. This technique is now a standard procedure used in both research labs as well as the clinic for identifying proteins of interest.

The adoption of this technique by clinicians has revolutionized the field of histopathology, allowing pathologists to probe diseased tissue samples on the molecular level and more accurately diagnose diseases. This procedure has been particularly useful in oncology, where a number of important biomarkers have been identified for many cancer types. One such example is Her2, a surface receptor protein overexpressed in 25 to 30 percent of breast cancers, which can be targeted very effectively with humanized monoclonal antibodies, resulting in a significantly increased survival rate [222]. To determine which patients can benefit from this therapy, a diagnostic test (Herceptest) was developed to enable pathologists to estimate the level of Her2 expression based on analysis of the biopsy sample [223, 224]. In addition, other biomarkers, such as the estrogen receptor (ER) and progesterone receptor (PR) have been shown to indicate the aggressiveness of a particular cancer and the survival rate of the patient for various therapeutic strategies. These important proteins form a 3 biomarker panel that is now routinely used in the diagnosis of breast cancer patients and in the selection of treatment options [225-227].

However, preparation and analysis of these samples is time consuming and must be performed on separate sections, requiring a large amount of sample and increasing variability in the results. Additionally, analysis of the samples requires the eye of a trained and experienced pathologist and is subjective or semi-quantitative at best. QDs

have many properties that make them ideal as an optical imaging agent for use in clinical diagnostics. Of particular note, multiple QD colors can be excited using a single excitation source, allowing for the simultaneous measurement of multiple colors. The QDs also have very narrow and uniform emission profiles which can be tuned, providing a number of colors to be used in the multiplexed assays. Because of these unique properties, QDs present an exciting opportunity to develop the next generation of immunohistochemistry techniques. The ability to image multiple colors simultaneously allows the use of QDs in multiplexed assays, where multiple biomarkers can be analyzed on a single tissue section, dramatically reducing the amount of tissue needed for a pathological analysis. Newly developed instrumentation, such as CRI's Nuance multispectral imaging system, can also allow pathologists to measure and separate QD signals in an objective and quantitative way, significantly increasing consistency and repeatability in diagnoses.

Preliminary work by our group and others has shown the utility of these fluorescent nanoparticles in ultrasensitive imaging of biomarkers in cells as well as tissues [53, 54, 99, 100]. These techniques provide dramatic multicolored images for the analysis of biomarker expression and localization, as seen in Figure 7.2. Despite the early success of this technology, significant hurdles must be overcome before pathologists adopt this technology for use in clinical diagnostics. As described in Chapters 2 and 6, nonspecific binding of QDs and other nanoparticles to components in blood, cells and tissues presents a considerable challenge to the use of these nanoparticles for ultrasensitive detection in complex biological samples. This can significantly increase the background fluorescence and lead to false positive signals. This background also leads to degradation of the signal-to-noise ratio and limits tagging specificity and detection sensitivity.

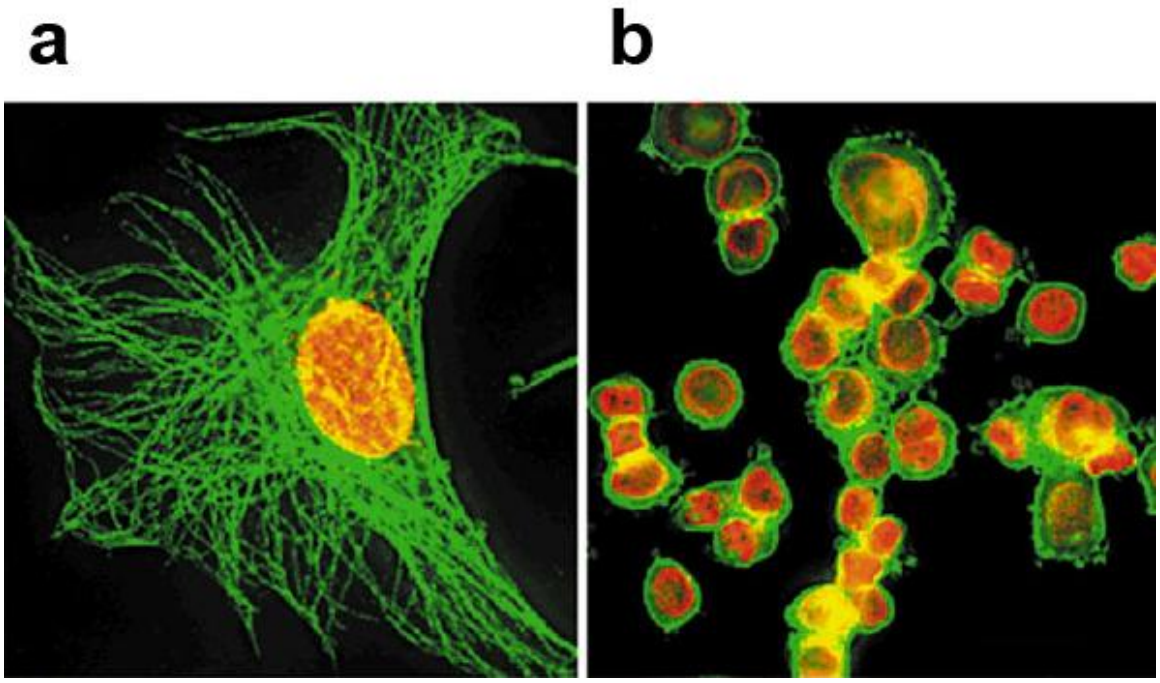

Figure 7.2. Multicolor staining of cells using quantum dots. (a) Nuclear (red) and microtubule (green) staining with streptavidin-coated quantum dots in NIH/3T3 cells. (b) Staining of SK-BR-3 breast cancer cells with streptavidin-coated quantum dots targeted against the nucleus (red) and Her2 surface receptors (green). From Wu et al [53].

It is hypothesized that the use of nonstick hydroxyl-QDs described in chapter 6 can eliminate these problems and improve the utility of QDs in these samples. In this chapter, we investigate bioconjugation techniques for the coupling of antibodies or other targeting molecules to the surface of OH-QDs.

7.3 METHODS

Quantum Dot Stability in Acetonitrile

50 nM solutions of OH-QDs and COOH-QDs were prepared in water. The samples were vortexed and sonicated for 15 minutes to disperse any aggregates and filtered using a 0.2 µm filter to remove contaminants. Separately, acetonitrile (ACN) was

diluted to different concentrations (from 0% to 75% ACN by volume) in water and transferred to glass vials. Aliquots of the QD samples were pipetted into the ACN containing vials and were vortexed to completely mix the samples. The fluorescence intensity of the samples was then measured and plotted as a function of ACN concentration.

Effect of Cyanogen Bromide on Hydroxyl-Coated Quantum Dots

Purified OH-QDs and COOH-QDs were mixed with DI water, 15% ACN and 0.5 M Cyanogen Bromide (CNBr) in 15% ACN. Aliquots were then taken and analyzed using gel electrophoresis to determine differences in gel migration. Separately, a concentration series of CNBr in 15 % ACN (1 M to 0.0001 M CNBr) was prepared in glass vials. Aliquots of the OH-QD sample were pipetted into the vials and were vortexed to mix thoroughly. The samples were then analyzed using gel electrophoresis and the migration shifts were measured and plotted as a function of CNBr concentration.

Antibody Coupling to Hydroxyl Quantum Dots

Purified OH-QDs were diluted into a buffer containing 15% ACN. The solution was cooled in an ice water bath and stirred vigorously to ensure the sample was well mixed. Separately, a stock 0.5 M CNBr solution was prepared by diluting CNBr into ACN. This solution was added dropwise to the QD solution under vigorous stirring to a final concentration of 0.0005 M CNBr and was allowed to react for approximately 2 min. A primary amine-containing targeting molecule (such as an antibody) was then added to the solution at a ratio of 25:1 targeting molecule : QD. This solution was mixed and allowed to react at 4°C for 24 hours. The sample was then purified using dialysis and transferred to a 50 mM borate buffer for storage.

Cell Labeling with Hydroxyl Quantum Dots

MDA MB 231 cells were cultured in RPMI media with 10% fetal bovine serum (FBS) at 37 ºC (5% CO_2) and grown in an 8-well chamber slide. After 24 hours for seeding, the cells were washed with 1X phosphate buffered saline (PBS) and fixed with 3.7% formaldehyde in 1X PBS for 5 minutes. The fixative was then aspirated and the cells were washed with 1X PBS 3 times for 5 min each. A 0.1% Triton X solution in 1X PBS was then used to permeabilize the cells for 5 min, followed by 3 washes of 1X PBS. A 2% bovine serum albumin (BSA) blocking solution in 1X PBS was added to the wells for 1 hour and then aspirated. A primary antibody solution was diluted into the blocking buffer to a final concentration of approximately 5 µg/mL and then applied to the cells for 30 min. Cells were then washed with 1X PBS 3 times for 5 min each. Secondary antibody-conjugated QDs were diluted in the blocking solution to a concentration of approximately 10 nM and incubated with the cells for 30 min. The QD staining solution was aspirated and the cells were washed with 1X PBS 3 times for 5 min each and prepared for imaging with a fluorescence microscope.

7.4 RESULTS AND DISCUSSION

Bioconjugation Strategies

Many bioconjugation strategies have been used to couple targeting molecules, such as proteins, antibodies, nucleic acids and small molecules, to nanoparticle labeling agents. These coupling strategies generally involve the covalent linkage of functional groups of the targeting molecule and groups on the surface of the nanoparticle. Typical functional groups include thiols (which can be coupled to reactive maleimide groups), amines (which can be coupled to reactive succinimidyl esters such as NHS) and carboxylic acids, which are routinely coupled to amines though a reactive carbodiimide intermediate [228]. The most widely used bioconjugation procedure involves the use of EDAC, a water soluble carbodiimide compound that activates carboxylic acids to form amide bonds with free amine groups. This technique has been used in a wide array of applications, including the crosslinking of molecules and the coupling of small molecule dyes to antibodies or other proteins. It has also been extensively used in the coupling of targeting molecules to nanoparticles such as quantum dots [229].

Other strategies for attaching targeting molecules to the surface of a nanoparticle include noncovalent methods, such as the use of streptavidin and biotin. This strategy typically involves coupling streptavidin (a 52.8 kDa protein) to the surface of the nanoparticle. Subsequently, a targeting molecule attached to biotin (vitamin H, a small molecule which binds strongly to streptavidin) is added and is spontaneously coupled to the nanoparticle surface. This bond is considered one of the strongest noncovalent bonds in nature, with a K_d on the order of 10^{-15} M.

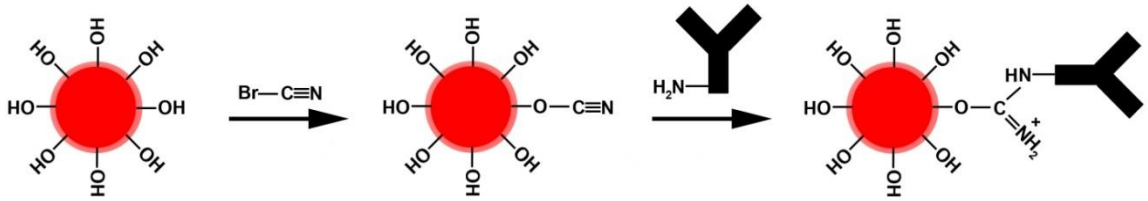

Figure 7.3. Reaction scheme for coupling targeting molecules, such as antibodies, to hydroxyl-coated quantum dots using cyanogen bromide (CNBr). The CNBr forms a cyanate ester which can react with primary amines to form an isourea derivative.

For the coupling of targeting molecules to the surface of nonstick, hydroxyl-modified QDs, a strategy was needed that could couple the hydroxyl functional groups on the surface of the nanoparticle to free amines, which are prevalent on antibodies and other proteins as well as modified nucleic acids and many small molecules. Cyanogen bromide (CNBr) was identified as a possible activating compound to aid in the bioconjugation of targeting molecules [230]. As shown in Figure 7.3, CNBr reacts with free hydroxyl groups to form a highly reactive cyanate ester which can react with free amines to yield an isourea linkage. Because this procedure is typically carried out in acetonitrile (ACN), it was necessary to ensure the optical and colloidal stability of OH-QDs is maintained in buffers containing this solvent.

Quantum Dot Stability in Coupling Buffer

To verify the optical and colloidal stability of polymer-coated QDs in ACN, a sample was prepared in water and filtered to remove any aggregates or contaminants. Aliquots were then taken and diluted into buffers containing increasing percentages of ACN to determine if this resulted in the precipitation of the nanoparticles. Little to no precipitation was seen in the samples (both OH-QDs and COOH-QDs) for ACN concentrations as high as 75% by volume. The samples were then analyzed using a

spectrofluorometer to determine if the nanoparticles' bright fluorescence was maintained. As shown in Figure 7.4a, the fluorescence properties of the QDs were unaffected in solutions with ACN concentrations of 40% or less. Increasing the concentration of ACN above 40 % resulted in a steady decline in the fluorescence intensity, with over 80% of the intensity lost in solutions containing 75% ACN.

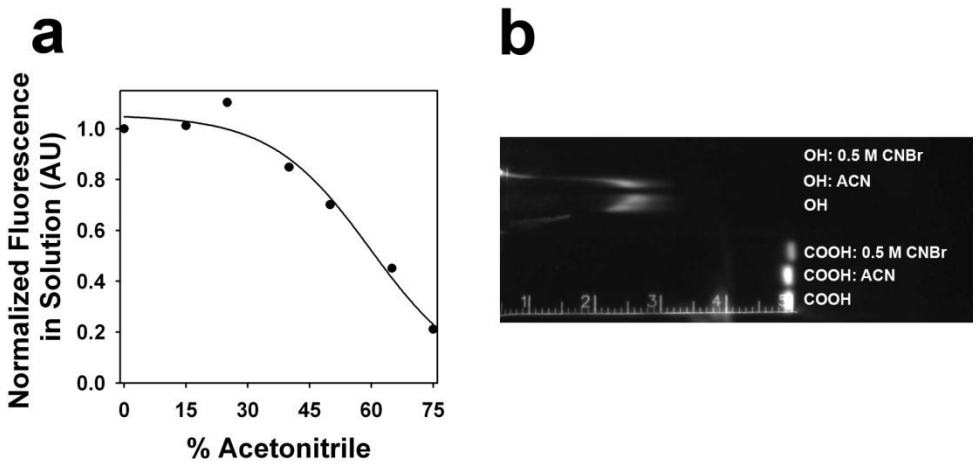

Figure 7.4. Polymer coated quantum dots in acetonitrile. (a) Normalized quantum dot fluorescence as a function of the percentage of acetonitrille. Quantum dots were stable in solutions containing up to ~40% acetonitrile. (b) Gel migration of COOH and OH coated quantum dots. Acetonitrile and 0.5 M cyanogen bromide (CNBr) had no effect on the migration of COOH quantum dots. However, high concentrations of CNBr caused aggregation of OH quantum dots as a result of the reaction.

Based on these results, a separate experiment was conducted to further examine the colloidal stability of QDs in the presence of ACN. Samples of OH-QDs and COOH-QDs were prepared and diluted into buffers for a final ACN concentration of 15%. The samples were then vortexed to ensure sufficient mixing and analyzed using gel electrophoresis. Samples containing CNBr were also analyzed to determine if this affected the stability of the nanoparticles. As seen in Figure 7.4b, the presence of ACN had no affect on the stability of the QDs. Both COOH-QDs (bottom) and OH-QDs (top) showed no shift in gel migration when compared to controls without ACN. In contrast,

the presence of CNBr has a significant effect on the gel migration of QDs. OH-QDs exposed to a solution containing 0.5M CNBr showed some aggregation and were unable to migrate in the gel. However, no effect was seen for COOH-QDs exposed to CNBr (Figure 7.4b, bottom), which showed no difference in migration rates when compared to samples containing ACN and the control. This difference is likely due to the reactivity of the CNBr, which is able to form cyanate ester intermediates with hydroxyl functional groups but is unreactive towards carboxylic acid groups, resulting in no change to their surface.

Reactivity of Quantum Dots with Cyanogen Bromide

After verifying the optical and colloidal stability of QDs in the ACN reaction buffers, a study was performed to determine the effective concentration range for the reaction of CNBr with the surface hydroxyl groups of the QDs. Dilutions of CNBr were made in ACN to prepare a concentration series from approximately 0.5 M to 0.0001 M CNBr. Aliquots of OH-QDs were then added to the samples and mixed, as described above. These samples were then analyzed using gel electrophoresis, as shown in Figure 7.5.

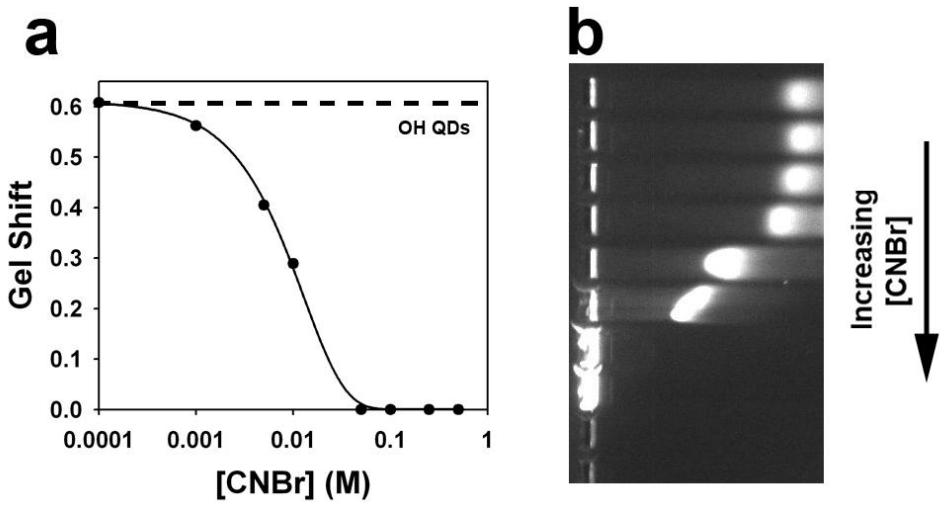

Figure 7.5. Reactivity of Cyanogen Bromide (CNBr) with hydroxyl-coated quantum dots. (a) Gel shift of hydroxyl quantum dots as a function of CNBr concentration and (b) gel image. Increasing CNBr concentrations results in a significant reduction in the gel migration of the nanoparticles as the CNBr reacts with the hydroxyl groups on the nanoparticle surface.

Gel analysis revealed a steady decline in gel migration as the concentration of CNBr increased, as expected from the results of the previous study. Significant migration shifts were seen with CNBr concentrations from 0.05 M to 0.001 M, with concentrations higher than these values showing signs of aggregation and no gel migration. Likewise, concentrations lower than 0.001 M showed no effect on the samples' colloidal stability or gel migration in comparison to the control. It is hypothesized that these lower concentration values result in the reaction of CNBr with the hydroxyl functional groups on the surface of the nanoparticles but do not alter the surface substantially or affect the overall surface charge of the QDs. From previous studies (Chapter 3), we have estimated the total number of functional groups on the surface of the QDs to be approximately 2500 per particle. This study suggests that a slight excess of CNBr, in comparison to surface functional groups, is needed to see effects on the overall surface charge. Based on these results, we have used a final

concentration of 0.0005 M CNBr for coupling to antibodies to avoid significant changes the surface of the nanoparticles.

Targeted Cell Staining using Quantum Dots

After determining the experimental parameters for reacting the hydroxyl functional groups of the OH-QDs with CNBr, coupling experiments were performed to attach secondary antibodies to the surface of the nanoparticles, as described in the methods section above. Secondary antibodies are commonly used in current IHC staining procedures and were used in this study for future comparisons to standard staining protocols. They also allow the production of a very versatile probe which can be used in conjunction with a wide variety of primary antibodies targeted against many markers of interest. In addition, multiple secondary antibodies are able to bind to a single primary antibody, resulting in an amplification of the signal intensity for bound probes.

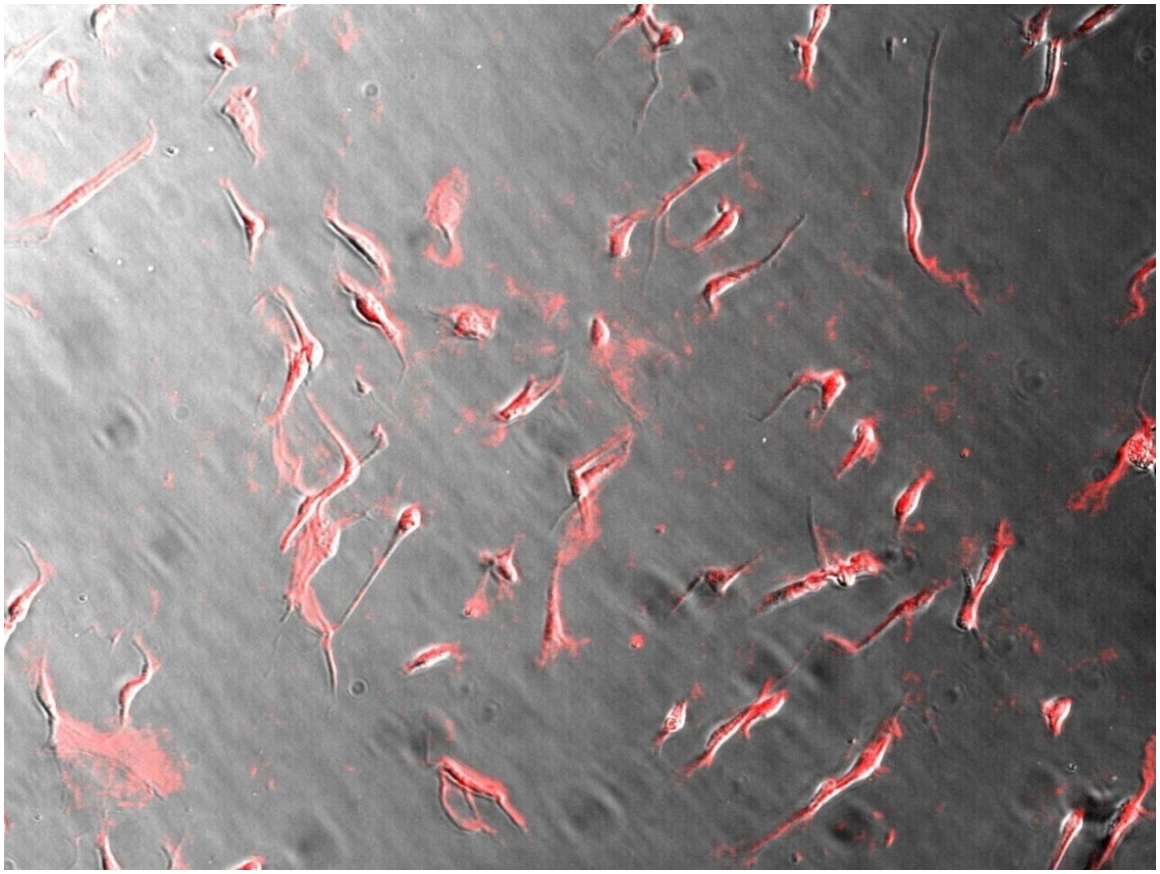

Figure 7.6. Labeling of MDA MB 231 breast cancer cells using antibody-conjugated, hydroxyl quantum dots. Fluorescence microscopy (registered with the cells by overlaying onto a bright field image) shows strong quantum dot staining of cells (red fluorescence).

The antibody-targeted QDs were then used to stain MDA MB 231 breast cancer cells, as shown in Figure 7.6. Whereas untargeted hydroxyl QDs show no detectable binding (Chapter 6), the targeted probes show moderate staining of the breast cancer cells. These data show that the synthesis of a targeted QD with reduced nonspecific binding is possible. These nanoparticles could have a significant impact on clinical *in vitro* diagnostics and open new possibilities for the future of personalized medicine.

7.5 CONCLUSIONS

In this chapter, we have reported the development of a bioconjugation procedure for the coupling of antibodies or other targeting molecules to the surface of OH-QDs with significantly reduced nonspecific binding (Chapter6). Data analysis shows that OH-QDs are optically and colloidally stable in buffers containing a moderate percentage of ACN and no gel migration shifts are seen. Further studies have shown that CNBr reacts preferentially with nanoparticles containing hydroxyl functional groups on their surface (in comparison to carboxylic acid groups). After performing antibody coupling experiments, preliminary staining results show a moderate staining in breast cancer cells, indicating the utility of these particles for targeted cell and tissues staining.

CHAPTER 8

FUTURE DIRECTIONS

8.1 ABSTRACT

In this chapter, we summarize the work presented in the previous chapters and its implications for future nanotechnology applications in the medical field. We also discuss future directions for continuing this work, specifically in ultrasensitive detection for diagnostic applications.

8.2 SUMMARY

This dissertation has focused on the design and development of polymer-coated nanoparticle imaging agents useful in biological environments, specifically diagnostic applications in cells, blood and tissue. In particular, the challenges of early stage detection and diagnosis of cancer present opportunities for cancer nanotechnology to make a significant impact on the practice of medicine and in the lives of patients. The ultrasensitive and multiplexed detection capabilities of semiconductor and metal nanoparticles could enable advanced diagnostic platforms for probing samples on the molecular level and detecting disease in its earliest stages, when treatment is most successful. In the first chapter, we briefly described the field of nanotechnology and its implications for therapeutic and diagnostic applications. We also discussed the complex and heterogeneous nature of cancer biology and the complications this presents to early stage diagnostics. With recent advances in nanotechnology, diagnostic techniques and our understanding of new disease biomarkers, “personalized medicine” is now within the realm of possibility.

In the second chapter of this dissertation, we further explored one class of nanoparticle, semiconductor nanocrystals (QDs), and the unique optical and physical

properties which make them promising for use in fundamental biology studies and other biomedical applications where ultrasensitive detection is needed. In addition, we describe the considerable progress made in the synthesis of high quality nanoparticles as well as the coating and surface chemistry strategies that have been used for transfer to aqueous solutions. These typically rely on the exchange of hydrophobic surface ligands for ones containing functional groups suitable for solubility in water or coating of the hydrophobic particles with an amphiphilic polymer or complex molecule. Using these strategies, a number of preliminary biological studies have been performed, both *in vitro* and *in vivo*, although hurdles remain for their adoption in the clinic.

The third chapter presented the design and development of low molecular weight amphiphilic polymers for use in nanoparticle coating applications. We discussed optimization of the polymer synthetic procedure as well as the nanoparticle coating and purification process. The coated nanoparticles were then extensively analyzed using a variety of techniques to determine their optical and colloidal properties and ensure they were suitable for use in biological applications.

In the fourth chapter, we explored the use of these amphiphilic polymers as multidentate ligands for the synthesis of QDs. It was shown that the polymers are capable of acting as cadmium precursor ligands and their use resulted in unique effects in the synthesis of the nanoparticles, including better control of the reaction kinetics, resistance to Ostwald ripening and the ability to produce ultrasmall particles. The polymer also allowed for the *in situ* growth of an inorganic passivating shell to protect the nanocrystal surface and bandgap engineering of the particles. Finally, we showed that the use of an amphiphilic noncoordinating solvent, such as PEG, and an excess of polymer enables a true one-pot synthesis technique for the synthesis of water soluble core-shell QDs.

The fifth chapter presented further exploration of the use of polymers in nanoparticle synthesis. Here, we reported a new synthetic procedure for the preparation of AuNPs using the multidentate polymers. There were many novel features associated with this procedure, including significantly reduced growth kinetics, increased nanoparticle stability and the ability to produce a very wide range of particle sizes. Upon the addition of reporter dyes to large AuNPs produced using this method, SERS-active particles were spontaneously formed in a on-pot method.

In the sixth chapter of this dissertation, we described the development of a new class of polymer-coated, hydroxylated QDs for use in clinical applications. These nanoparticles had compact sizes and were shown to significantly reduce the nonspecific binding of QDs in cells. Further studies revealed that surface charge plays a critical role in the nonspecific binding of nanoparticles to cellular structures as well as proteins and other components in biological fluids. This technology could enable highly sensitive detection of markers in clinical applications.

Finally, the seventh chapter described the development of a bioconjugation procedure coupling targeting molecules such as antibodies, nucleic acids or small molecules to the surface of nonstick OH-QDs. Upon coupling secondary antibodies to the QD surface, preliminary studies show staining in breast cancer cells, indicating the utility of these nanoparticles in a number of staining applications.

In summary, this dissertation has describe several improvements in the development of nanoparticles for use in biomedical applications, particularly *in vitro* diagnostics, and the results may further advance the understanding of nanoparticle interactions with biological samples.

8.3 FUTURE DIRECTIONS FOR DISSERTATION TECHNOLOGY

As described above, the work discussed in this dissertation mainly focuses on nanoparticle development and the interactions of nanoparticles with biological samples. While the results here conclusively demonstrate the utility of these particles, further development is needed for the adoption of these novel technologies in clinical diagnostic applications. Here, we discuss the future directions for this research and a number of studies that should be undertaken to progress the technologies.

Optimization of SERS-active Gold Nanoparticles for Biological Studies

In chapter 5, we presented several proof-of-concept studies demonstrating a one-pot synthesis procedure for the preparation of water soluble, SERS-active AuNPs. As described earlier, SERS-active nanoparticles have shown considerable promise for use in diagnostic assays. Because of the multi-peak nature of a SERS spectrum and the narrowness of the individual peaks, the multiplexing potential of SERS particles is significantly greater than the current generation of QDs. In addition, AuNPs do not contain toxic elements and are more likely to be approved for use in *in vivo* diagnostic applications. This work presents an opportunity to further develop highly sensitive probes using polymer-coated AuNPs. In particular, the adsorption of the reporter dye and the effects of the polymer coating have not been completely understood in this system and additional research could lead to better synthetic procedures. It is hypothesized that the thick polymer-coating on nanoparticles prevents a majority of the dye molecules from accessing the surface and producing a strong SERS signal. The covalent linkage of reporter dyes to the polymer backbone could circumvent this limitation and result in significantly brighter signal. Covalent linkage also offers the possibility of incorporating more than one dye on a single AuNP, in varying ratios, to

produce a SERS barcode technology to dramatically increase the multiplexing potential of these particles.

Multiplexed Tissue Staining using Nonstick Quantum Dots

Significant developments were presented in this work showing the preparation of QDs that eliminate the nonspecific binding problems seen with other nanoparticles. Preliminary work was also presented that described the development of a bioconjugation strategy for these hydroxyl-coated nanoparticles and targeted cell staining. Further studies should be conducted to optimize the staining protocols for imaging cells and tissue using these nonstick QDs. Additional studies are needed to determine the multiplexing capability of the OH-QDs. It is hypothesized that the reduction of nonspecific binding of QDs to tissue will dramatically increase the sensitivity and specificity of the targeted staining. A direct comparison should be performed against commercially available QDs to determine if there is any increase in multiplexing ability using OH-QDs and determine the lower limit of detection for these novel nanoparticles. Direct comparison studies should also be conducted using the nonstick QDs and standard IHC staining procedures to show this technology is as good or superior to the clinical gold standard for histopathology.

Ultrasensitive Detection of Rare Cells in Fluid Samples

One application not discussed in this dissertation is the detection of rare cells in fluid samples such as blood, serum or pleural fluid. The study of circulating tumor cells (CTCs) and developments of technology to detect them in clinical patients has been an area of intense research over the past few years. The detection of these cells could allow for the detection of cancer before metastasis has occurred, dramatically increasing the chances of successful treatment. Early attempts to detect these cells have involved

the use of magnetic particles to trap and magnetically isolate the CTCs from normal cells in the sample. These separation procedures take time and add additional steps to the process, which could decrease the recovery rate of the cells. For rare cells such as CTCs, even small losses could dramatically reduce the detection sensitivity, reducing the effectiveness of the assay. With the development of ultrasensitive QDs with bright fluorescence and reduced background staining described in this dissertation, a detection method that bypasses these additional separation steps may be possible, improving sensitivity. Studies should be conducted to determine the nonspecific binding of OH-QDs in these samples and the lower detection limit for indentifying CTCs using nonstick QDs targeted the cells.

8.4 CONCLUSIONS

In conclusion, we have summarized the work discussed in this dissertation and described several future directions for the continuation of this research and the further development of these technologies. This work has made a number of contributions in the design and development of polymer-coated nanoparticles for use in biological systems as well as furthered the understanding of nanoparticle interactions with components in cells, tissues and biological fluids. The developments presented here will prove significant in the translation of these and other technologies to the clinic and the further advancement of diagnostic technologies.

REFERENCES

1. *American Cancer Society, Inc. Cancer Facts and Figures.* 2009.

2. Sherr, C.J., *Cancer cell cycles.* Science, 1996. **274**(5293): p. 1672-7.

3. Hanahan, D. and R.A. Weinberg, *The hallmarks of cancer.* Cell, 2000. **100**(1): p. 57-70.

4. Jemal, A., et al., *Cancer statistics, 2008.* CA: a cancer journal for clinicians, 2008. **58**(2): p. 71.

5. Bishop, J.M. and R.A. Weinberg, *Molecular Oncology. New York: Scientific American*. 1996, Inc.

6. Renan, M.J., *How many mutations are required for tumorigenesis? Implications from human cancer data.* Molecular carcinogenesis, 1993. **7**(3): p. 139.

7. Foulds, L., *The experimental study of tumor progression: a review.* Cancer research, 1954. **14**(5): p. 327.

8. Nowell, P.C., *The clonal evolution of tumor cell populations.* Science, 1976. **194**(4260): p. 23-28.

9. Aplin, A.E., et al., *Signal transduction and signal modulation by cell adhesion receptors: the role of integrins, cadherins, immunoglobulin-cell adhesion molecules, and selectins.* Pharmacological reviews, 1998. **50**(2): p. 197-264.

10. Di Fiore, P.P., et al., *erbB-2 is a potent oncogene when overexpressed in NIH/3T3 cells.* Science, 1987. **237**(4811): p. 178-182.

11. Giancotti, F.G. and E. Ruoslahti, *Integrin signaling.* Science, 1999. **285**(5430): p. 1028.

12. Lukashev, M.E. and Z. Werb, *ECM signalling: orchestrating cell behaviour and misbehaviour.* Trends in cell biology, 1998. **8**(11): p. 437-441.

13. Bos, J.L., *Ras oncogenes in human cancer: a review.* Cancer Research, 1989. **49**(17): p. 4682.

14. Bos, J.L., et al., *Prevalence of ras gene mutations in human colorectal cancers.* 1987.

15. Medema, R.H. and J.L. Bos, *The role of p21ras in receptor tyrosine kinase signaling.* Critical reviews in oncogenesis, 1993. **4**(6): p. 615.

16. Medema, R.H., et al., *AFX-like Forkhead transcription factors mediate cell-cycle regulation by Ras and PKB through p27kip1.* Nature, 2000. **404**(6779): p. 782-787.

17. Vogelstein, B., et al., *Genetic alterations during colorectal-tumor development*. 1988. p. 525-532.

18. Fedi, P., S.R. Tronick, and S.A. Aaronson, *Growth factors.* Cancer medicine, 1997: p. 41-64.

19. Weinberg, R.A., *The retinoblastoma protein and cell cycle control.* Cell, 1995. **81**(3): p. 323.

20. Fynan, T.M. and M. Reiss, *Resistance to inhibition of cell growth by transforming growth factor-beta and its role in oncogenesis.* Critical reviews in oncogenesis, 1993. **4**(5): p. 493.

21. Markowitz, S., et al., *Inactivation of the type II TGF-beta receptor in colon cancer cells with microsatellite instability.* Science, 1995. **268**(5215): p. 1336-1338.

22. Moses, H.L., E.Y. Yang, and J.A. Pietenpol, *TGF-beta stimulation and inhibition of cell proliferation: new mechanistic insights.* Cell, 1990. **63**(2): p. 245.

23. Hueber, A.O., et al., *Requirement for the CD95 receptor-ligand pathway in c-Myc-induced apoptosis.* Science, 1997. **278**(5341): p. 1305.

24. Vaux, D.L., S. Cory, and J.M. Adams, *Bcl-2 gene promotes haemopoietic cell survival and cooperates with c-myc to immortalize pre-B cells.* 1988.

25. Ashkenazi, A. and V.M. Dixit, *Death receptors: signaling and modulation.* Science, 1998. **281**(5381): p. 1305.

26. Ashkenazi, A. and V.M. Dixit, *Apoptosis control by death and decoy receptors.* Current opinion in cell biology, 1999. **11**(2): p. 255-260.

27. Chao, D.T. and S.J. Korsmeyer, *BCL-2 family: regulators of cell death.* Annual review of immunology, 1998. **16**(1): p. 395-419.

28. Hollstein, M., et al., *p53 mutations in human cancers.* Science, 1991. **253**(5015): p. 49-53.

29. Hayflick, L., *Mortality and immortality at the cellular level. A review.* Biochemistry (Mosc), 1997. **62**(11): p. 1180-1190.

30. Wright, W.E., O.M. Pereira-Smith, and J.W. Shay, *Reversible cellular senescence: implications for immortalization of normal human diploid fibroblasts.* Molecular and cellular biology, 1989. **9**(7): p. 3088-3092.

31. Counter, C.M., et al., *Telomere shortening associated with chromosome instability is arrested in immortal cells, which express telomerase activity.* The EMBO journal, 1992. **11**(5): p. 1921-1929.

32. Folkman, J., *Angiogenesis in cancer, vascular, rheumatoid and other disease.* Nature medicine, 1995. **1**(1): p. 27-30.

33. Sporn, M.B., *The war on cancer.* Lancet, 1996. **347**(9012): p. 1377.

34. Ferrari, M., *Cancer nanotechnology: opportunities and challenges.* Nat Rev Cancer, 2005. **5**(3): p. 161-71.

35. Whitesides, G.M., *The'right'size in nanobiotechnology.* Nature biotechnology, 2003. **21**(10): p. 1161-1165.

36. Office of Basic Energy Sciences, U.S.D.o.E., http://www.science.doe.gov/bes/scale_of_things.html (June 2009).

37. Neuwelt, E.A., et al., *Imaging of iron oxide nanoparticles by MR and light microscopy in patients with malignant brain tumours.* Neuropathology & Applied Neurobiology, 2004. **30**(5): p. 456.

38. Harisinghani, M.G., et al., *Noninvasive detection of clinically occult lymph-node metastases in prostate cancer*. 2003. p. 2491-2499.

39. Kircher, M.F., et al., *A multimodal nanoparticle for preoperative magnetic resonance imaging and intraoperative optical brain tumor delineation*. 2003, AACR. p. 8122-8125.

40. Weissleder, R., et al., *Ultrasmall superparamagnetic iron oxide: characterization of a new class of contrast agents for MR imaging.* Radiology, 1990. **175**(2): p. 489-493.

41. Qian, X., et al., *In vivo tumor targeting and spectroscopic detection with surface-enhanced Raman nanoparticle tags.* Nat Biotechnol, 2008. **26**(1): p. 83-90.

42. Agrawal, A., et al., *Nanometer-scale mapping and single-molecule detection with color-coded nanoparticle probes.* Proc Natl Acad Sci U S A, 2008. **105**(9): p. 3298-303.

43. Agrawal, A., T. Sathe, and S. Nie, *Single-bead immunoassays using magnetic microparticles and spectral-shifting quantum dots.* J Agric Food Chem, 2007. **55**(10): p. 3778-82.

44. Agrawal, A., et al., *Real-time detection of virus particles and viral protein expression with two-color nanoparticle probes.* J Virol, 2005. **79**(13): p. 8625-8.

45. Agrawal, A., et al., *Counting single native biomolecules and intact viruses with color-coded nanoparticles.* Anal Chem, 2006. **78**(4): p. 1061-70.

46. Chattopadhyay, P.K., et al., *Quantum dot semiconductor nanocrystals for immunophenotyping by polychromatic flow cytometry.* Nat Med, 2006. **12**(8): p. 972-7.

47. Han, M., et al., *Quantum-dot-tagged microbeads for multiplexed optical coding of biomolecules.* Nat Biotechnol, 2001. **19**(7): p. 631-5.

48. Medintz, I.L., et al., *Quantum dot bioconjugates for imaging, labelling and sensing.* Nat. Mater, 2005. **4**(6): p. 435-446.

49. Michalet, X., et al., *Quantum dots for live cells, in vivo imaging, and diagnostics.* Science, 2005. **307**(5709): p. 538-44.

50. Qian, X., J. Li, and S. Nie, *Stimuli-responsive SERS nanoparticles: conformational control of plasmonic coupling and surface Raman enhancement.* J Am Chem Soc, 2009. **131**(22): p. 7540-1.

51. Qian, X., X. Zhou, and S. Nie, *Surface-enhanced Raman nanoparticle beacons based on bioconjugated gold nanocrystals and long range plasmonic coupling.* J Am Chem Soc, 2008. **130**(45): p. 14934-5.

52. Qian, X.M. and S.M. Nie, *Single-molecule and single-nanoparticle SERS: from fundamental mechanisms to biomedical applications.* Chem Soc Rev, 2008. **37**(5): p. 912-20.

53. Wu, X., et al., *Immunofluorescent labeling of cancer marker Her2 and other cellular targets with semiconductor quantum dots.* Nat Biotechnol, 2003. **21**(1): p. 41-6.

54. Xing, Y., et al., *Bioconjugated quantum dots for multiplexed and quantitative immunohistochemistry.* Nat Protoc, 2007. **2**(5): p. 1152-65.

55. Yezhelyev, M.V., et al., *Emerging use of nanoparticles in diagnosis and treatment of breast cancer.* Lancet Oncol, 2006. **7**(8): p. 657-67.

56. Langer, R., *Drug delivery and targeting.* Nature(London), 1998. **392**(6679): p. 5-10.

57. Duncan, R., *The dawning era of polymer therapeutics.* Nature Reviews Drug Discovery, 2003. **2**(5): p. 347-360.

58. Duncan, R., *Polymer conjugates as anticancer nanomedicines.* Nat Rev Cancer, 2006. **6**(9): p. 688-701.

59. Chen, H., V. Torchilin, and R. Langer, *Lectin-bearing polymerized liposomes as potential oral vaccine carriers.* Pharmaceutical research, 1996. **13**(9): p. 1378-1383.

60. Jain, R.K., *The next frontier of molecular medicine: delivery of therapeutics.* Nature medicine, 1998. **4**(6): p. 655-657.

61. Jain, R.K., *Delivery of molecular and cellular medicine to solid tumors.* Journal of controlled release, 1998. **53**(1-3): p. 49-67.

62. Quintana, A., et al., *Design and function of a dendrimer-based therapeutic nanodevice targeted to tumor cells through the folate receptor.* Pharmaceutical research, 2002. **19**(9): p. 1310-1316.

63. Potineni, A., et al., *Poly (ethylene oxide)-modified poly (-amino ester) nanoparticles as a pH-sensitive biodegradable system for paclitaxel delivery.* Journal of Controlled Release, 2003. **86**(2-3): p. 223-234.

64. Hirsch, L.R., et al., *Nanoshell-mediated near-infrared thermal therapy of tumors under magnetic resonance guidance.* Proceedings of the National Academy of Sciences, 2003. **100**(23): p. 13549-13554.

65. O'Neal, D.P., et al., *Photo-thermal tumor ablation in mice using near infrared-absorbing nanoparticles.* Cancer letters, 2004. **209**(2): p. 171-176.

66. Matsumura, Y. and H. Maeda, *A new concept for macromolecular therapeutics in cancer chemotherapy: mechanism of tumoritropic accumulation of proteins and the antitumor agent smancs.* Cancer research, 1986. **46**(12): p. 6387-6392.

67. Maeda, H., et al., *Tumor vascular permeability and the EPR effect in macromolecular therapeutics: a review.* Journal of Controlled Release, 2000. **65**(1-2): p. 271-284.

68. Finley, K.R., A.E. Davidson, and S.C. Ekker, *Three-color imaging using fluorescent proteins in living zebrafish embryos.* Biotechniques, 2001. **31**(1): p. 66.

69. Giepmans, B.N.G., et al., *The fluorescent toolbox for assessing protein location and function*. 2006, American Association for the Advancement of Science. p. 217-224.

70. Giuliano, K.A. and D.L. Taylor, *Fluorescent-protein biosensors: new tools for drug discovery.* Trends in Biotechnology, 1998. **16**(3): p. 135-140.

71. Jaiswal, J.K., et al., *Long-term multiple color imaging of live cells using quantum dot bioconjugates.* Nature biotechnology, 2002. **21**(1): p. 47-51.

72. Johnson, I., *Review: Fluorescent probes for living cells.* The Histochemical Journal, 1998. **30**(3): p. 123-140.

73. Derfus, A.M., W.C.W. Chan, and S.N. Bhatia, *Intracellular delivery of quantum dots for live cell labeling and organelle tracking.* Advanced materials(Weinheim), 2004. **16**(12): p. 961-966.

74. Cole, N.B., et al., *Diffusional mobility of Golgi proteins in membranes of living cells.* Science, 1996. **273**(5276): p. 797.

75. Presley, J.F., et al., *ER-to-Golgi transport visualized in living cells.* Nature, 1997. **389**(6646): p. 81-84.

76. Lippincott-Schwartz, J., E. Snapp, and A. Kenworthy, *Studying protein dynamics in living cells.* Nature Reviews Molecular Cell Biology, 2001. **2**(6): p. 444-456.

77. Schaller, R.D., V.M. Agranovich, and V.I. Klimov, *High-efficiency carrier multiplication through direct photogeneration of multi-excitons via virtual single-exciton states.* Nature Physics, 2005. **1**(3): p. 189-194.

78. Schaller, R.D. and V.I. Klimov, *High efficiency carrier multiplication in PbSe nanocrystals: Implications for solar energy conversion.* Physical Review Letters, 2004. **92**(18): p. 186601.

79. Bowers, M.J., 2nd, J.R. McBride, and S.J. Rosenthal, *White-light emission from magic-sized cadmium selenide nanocrystals.* J Am Chem Soc, 2005. **127**(44): p. 15378-9.

80. Bruchez, M.P., et al., *Semiconductor Nanocrystals as Fluorescent Biological Labels.* Science, 1998. **281**(5385): p. 2013-2016.

81. Chan, W.C.W. and S.M. Nie, *Quantum Dot Bioconjugates for Ultrasensitive Nonisotopic Detection.* Science, 1998. **281**(5385): p. 2016.

82. Choi, H.S., et al., *Renal clearance of quantum dots.* Nat Biotechnol, 2007. **25**(10): p. 1165-70.

83. Dubertret, B., et al., *In vivo imaging of quantum dots encapsulated in phospholipid micelles.* Science, 2002. **298**(5599): p. 1759-62.

84. Gao, X., et al., *In vivo cancer targeting and imaging with semiconductor quantum dots.* Nat Biotechnol, 2004. **22**(8): p. 969-76.

85. Kim, S., et al., *Near-infrared fluorescent type II quantum dots for sentinel lymph node mapping.* Nature Biotechnology, 2004. **22**(1): p. 93-97.

86. Sathe, T.R., A. Agrawal, and S. Nie, *Mesoporous silica beads embedded with semiconductor quantum dots and iron oxide nanocrystals: dual-function microcarriers for optical encoding and magnetic separation.* Anal Chem, 2006. **78**(16): p. 5627-32.

87. Alivisatos, P., *The use of nanocrystals in biological detection.* Nat Biotechnol, 2004. **22**(1): p. 47-52.

88. Smith, A.M., X. Gao, and S. Nie, *Quantum dot nanocrystals for in vivo molecular and cellular imaging.* Photochem Photobiol, 2004. **80**(3): p. 377-85.

89. Smith, A.M. and S. Nie, *Chemical analysis and cellular imaging with quantum dots.* Analyst, 2004. **129**(8): p. 672-7.

90. Gao, X., et al., *In vivo molecular and cellular imaging with quantum dots.* Curr Opin Biotechnol, 2005. **16**(1): p. 63-72.

91. Qu, L. and X. Peng, *Control of photoluminescence properties of CdSe nanocrystals in growth.* J Am Chem Soc, 2002. **124**(9): p. 2049-55.

92. Talapin, D.V., et al., *CdSe/CdS/ZnS and CdSe/ZnSe/ZnS Core Shell Shell Nanocrystals.* J. Phys. Chem. B, 2004. **108**(49): p. 18826-18831.

93. Talapin, D.V., et al., *Highly luminescent monodisperse CdSe and CdSe/ZnS nanocrystals synthesized in a hexadecylamine-trioctylphosphine oxide-trioctylphospine mixture.* Nano Lett, 2001. **1**(4): p. 207-211.

94. Xie, R., et al., *Synthesis and Characterization of Highly Luminescent CdSe Core CdS/Zn0. 5Cd0. 5S/ZnS Multishell Nanocrystals.* J. Am. Chem. Soc, 2005. **127**(20): p. 7480-7488.

95. Chan, W.C.W., et al., *Luminescent quantum dots for multiplexed biological detection and imaging.* Current Opinion in Biotechnology, 2002. **13**(1): p. 40-46.

96. Eggeling, C., et al., *Photobleaching of fluorescent dyes under conditions used for single-molecule detection: evidence of two-step photolysis.* Anal. Chem, 1998. **70**(13): p. 2651-2659.

97. Matsuno, A., et al., *Three-dimensional imaging of the intracellular localization of growth hormone and prolactin and their mRNA using nanocrystal (Quantum dot) and confocal laser scanning microscopy techniques.* J Histochem Cytochem, 2005. **53**(7): p. 833-8.

98. Ness, J.M., et al., *Combined tyramide signal amplification and quantum dots for sensitive and photostable immunofluorescence detection.* J Histochem Cytochem, 2003. **51**(8): p. 981-7.

99. Xing, Y., et al., *Molecular profiling of single cancer cells and clinical tissue specimens with semiconductor quantum dots.* Int J Nanomedicine, 2006. **1**(4): p. 473-81.

100. Yezhelyev, M.V., et al., *In Situ Molecular Profiling of Breast Cancer Biomarkers with Multicolor Quantum Dots.* Adv. Mater, 2007. **19**: p. 3146-3151.

101. Murray, C.B., et al., *Colloidal synthesis of nanocrystals and nanocrystal superlattices.* IBM Journal of Research and Development, 2001. **45**(1): p. 47-56.

102. Yu, W.W., et al., *Experimental determination of the extinction coefficient of CdTe, CdSe, and CdS nanocrystals.* Science, 1998. **281**: p. 2013.

103. Murray, C.B., D.J. Norris, and M.G. Bawendi, *Synthesis and Characterization of Nearly Monodisperse Cde (E = S, Se, Te) Semiconductor Nanocrystallites.* Journal of the American Chemical Society, 1993. **115**(19): p. 8706-8715.

104. Peng, Z.A. and X. Peng, *Formation of high-quality CdTe, CdSe, and CdS nanocrystals using CdO as precursor.* J Am Chem Soc, 2001. **123**(1): p. 183-4.

105. Yu, W.W. and X.G. Peng, *Formation of high-quality CdS and other II-VI semiconductor nanocrystals in noncoordinating solvents: Tunable reactivity of monomers.* Angewandte Chemie-International Edition, 2002. **41**(13): p. 2368-2371.

106. Dabbousi, B.O., et al., *(CdSe)ZnS core-shell quantum dots: Synthesis and characterization of a size series of highly luminescent nanocrystallites.* Journal of Physical Chemistry B, 1997. **101**(46): p. 9463-9475.

107. Hines, M.A. and P. Guyot-Sionnest, *Synthesis and characterization of strongly luminescing ZnS-Capped CdSe nanocrystals.* Journal of Physical Chemistry, 1996. **100**(2): p. 468-471.

108. Pellegrino, T., et al., *Hydrophobic nanocrystals coated with an amphiphilic polymer shell: a general route to water soluble nanocrystals.* Nano Lett, 2004. **4**(4): p. 703-707.

109. Yu, W.W., et al., *Forming biocompatible and nonaggregated nanocrystals in water using amphiphilic polymers.* J Am Chem Soc, 2007. **129**(10): p. 2871-9.

110. Duan, H. and S. Nie, *Cell-penetrating quantum dots based on multivalent and endosome-disrupting surface coatings.* J Am Chem Soc, 2007. **129**(11): p. 3333-8.

111. Uyeda, H.T., et al., *Synthesis of compact multidentate ligands to prepare stable hydrophilic quantum dot fluorophores.* J Am Chem Soc, 2005. **127**(11): p. 3870-8.

112. Wang, Y.A., et al., *Stabilization of inorganic nanocrystals by organic dendrons.* J Am Chem Soc, 2002. **124**(10): p. 2293-8.

113. Zhelev, Z., H. Ohba, and R. Bakalova, *Single quantum dot-micelles coated with silica shell as potentially non-cytotoxic fluorescent cell tracers.* J Am Chem Soc, 2006. **128**(19): p. 6324-5.

114. Smith, A.M. and S. Nie, *Minimizing the Hydrodynamic Size of Quantum Dots with Multifunctional Multidentate Polymer Ligands.* Journal of the American Chemical Society, 2008. **130**(34): p. 11278-11279.

115. Mattoussi, H., et al., *Self-Assembly of CdS-ZnS Quantum Dot Bioconjugates Using an Engineered Recombinant Protein.* Journal of the American Chemical Society, 2000. **122**(49): p. 12142-12150.

116. Smith, A.M., et al., *A systematic examination of surface coatings on the optical and chemical properties of semiconductor quantum dots.* Phys. Chem. Chem. Phys, 2006. **8**: p. 3895-3903.

117. Moffitt, M. and A. Eisenberg, *Size control of nanoparticles in semiconductor-polymer composites. 1. Control via multiplet aggregation numbers in styrene-based random ionomers.* Chemistry of Materials, 1995. **7**(6): p. 1178-1184.

118. Rhyner, M.N., *Development of Cancer Diagnostics Using Nanoparticles and Amphiphilic Polymers.* PhD Thesis, Georgia Institute of Technology, 2008.

119. Parak, W.J., et al., *Cell motility and metastatic potential studies based on quantum dot imaging of phagokinetic tracks.* Advanced Materials, 2002. **14**(12).

120. Voura, E.B., et al., *Tracking metastatic tumor cell extravasation with quantum dot nanocrystals and fluorescence emission-scanning microscopy.* Nature medicine, 2004. **10**(9): p. 993-998.

121. Ruan, G., et al., *Imaging and tracking of tat peptide-conjugated quantum dots in living cells: new insights into nanoparticle uptake, intracellular transport, and vesicle shedding.* J. Am. Chem. Soc, 2007. **129**(47): p. 14759-14766.

122. Dahan, M., et al., *Diffusion dynamics of glycine receptors revealed by single-quantum dot tracking*. 2003, Science. p. 442-445.

123. Courty, S., et al., *Tracking individual kinesin motors in living cells using single quantum-dot imaging.* Nano letters, 2006. **6**(7): p. 1491-1495.

124. Smith, A.M., A.M. Mohs, and S. Nie, *Tuning the optical and electronic properties of colloidal nanocrystals by lattice strain.* Nat Nanotechnol, 2009. **4**(1): p. 56-63.

125. Hardman, R., *A toxicologic review of quantum dots: toxicity depends on physicochemical and environmental factors.* Environmental health perspectives, 2006. **114**(2): p. 165.

126. Derfus, A.M., W.C.W. Chan, and S.N. Bhatia, *Probing the cytotoxicity of semiconductor quantum dots.* Nano Letters, 2004. **4**(1): p. 11-18.

127. Duncan, R., et al., *Preclinical evaluation of polymer-bound doxorubicin.* Journal of controlled release, 1992. **19**(1-3): p. 331-346.

128. Tomalia, D.A., et al., *A new class of polymers: starburst-dendritic macromolecules.* Polymer Journal, 1985. **17**(1): p. 117-132.

129. Heffernan, M.J. and N. Murthy, *Polyketal nanoparticles: a new pH-sensitive biodegradable drug delivery vehicle.* Bioconjugate Chem, 2005. **16**(6): p. 1340-1342.

130. Gros, L., H. Ringsdorf, and H. Schupp, *Polymeric antitumor agents on a molecular and on a cellular level?* Angewandte Chemie International Edition in English, 1981. **20**(4): p. 305-325.

131. Duncan, R., J.K. Coatsworth, and S. Burtles, *Preclinical toxicology of a novel polymeric antitumour agent: HPMA copolymerdoxorubicin (PK1).* Human & experimental toxicology, 1998. **17**(2): p. 93.

132. Alakhov, V., et al., *Block copolymer-based formulation of doxorubicin. From cell screen to clinical trials.* Colloids and Surfaces B: Biointerfaces, 1999. **16**(1-4): p. 113-134.

133. Torchilin, V.P., *Polymeric micelles in diagnostic imaging.* Colloids and Surfaces B: Biointerfaces, 1999. **16**(1-4): p. 305-319.

134. Moghimi, S.M., et al., *Surface engineered nanospheres with enhanced drainage into lymphatics and uptake by macrophages of the regional lymph nodes.* FEBS letters, 1994. **344**(1): p. 25.

135. Lee, D., et al., *In vivo imaging of hydrogen peroxide with chemiluminescent nanoparticles.* Nature Materials, 2007. **6**(10): p. 765-769.

136. Anelli, P.L., et al., *Mixed micelles containing lipophilic gadolinium complexes as MRA contrast agents.* Magnetic Resonance Materials in Physics, Biology and Medicine, 2001. **12**(2): p. 114-120.

137. Trubetskoy, V.S., et al., *Stable polymeric micelles: lymphangiographic contrast media for gamma scintigraphy and magnetic resonance imaging.* Academic radiology, 1996. **3**(3): p. 232.

138. Trubetskoy, V.S. and V.P. Torchilin, *New approaches in the chemical design of Gd-containing liposomes for use in magnetic resonance imaging of lymph nodes.* Journal of Liposome Research, 1994. **4**(2): p. 961-980.

139. Slinkin, M.A., A.L. Klibanov, and V.P. Torchilin, *Terminal-modified polylysine-based chelating polymers: highly efficient coupling to antibody with minimal loss in immunoreactivity.* Bioconjugate Chemistry, 1991. **2**(5): p. 342-348.

140. Burroughes, J.H., et al., *Light-emitting diodes based on conjugated polymers.* Nature, 1990. **347**(6293): p. 539-541.

141. Sirringhaus, H., N. Tessler, and R.H. Friend, *Integrated optoelectronic devices based on conjugated polymers.* Science, 1998. **280**(5370): p. 1741.

142. Colombo, A., et al., *Randomized study to assess the effectiveness of slow-and moderate-release polymer-based paclitaxel-eluting stents for coronary artery lesions*. 2003, Am Heart Assoc. p. 788-794.

143. Stone, G.W., et al., *A polymer-based, paclitaxel-eluting stent in patients with coronary artery disease*. 2004. p. 221-231.

144. Jones, M.C. and J.C. Leroux, *Polymeric micelles–a new generation of colloidal drug carriers.* European journal of pharmaceutics and biopharmaceutics, 1999. **48**(2): p. 101-111.

145. Matsen, M.W., *The standard Gaussian model for block copolymer melts.* Journal of Physics-Condensed Matter, 2002. **14**(2): p. R21-R47.

146. Bates, F.S., et al., *Fluctuations, Conformational Asymmetry and Block-Copolymer Phase-Behavior.* Faraday Discussions, 1994(98): p. 7-18.

147. Forster, S., et al., *Complex Phase-Behavior of Polyisoprene-Polystyrene Diblock Copolymers near the Order-Disorder Transition.* Macromolecules, 1994. **27**(23): p. 6922-6935.

148. Khandpur, A.K., et al., *Polyisoprene-polystyrene diblock copolymer phase diagram near the order-disorder transition.* Macromolecules, 1995. **28**(26): p. 8796-8806.

149. Matsen, M.W. and F.S. Bates, *Unifying weak- and strong-segregation block copolymer theories.* Macromolecules, 1996. **29**(4): p. 1091-1098.

150. Duxin, N., et al., *Cadmium sulphide quantum dots in morphologically tunable triblock copolymer aggregates.* J. Am. Chem. Soc, 2005. **127**(28): p. 10063-10069.

151. Sakuma, S., M. Hayashi, and M. Akashi, *Design of nanoparticles composed of graft copolymers for oral peptide delivery.* Adv Drug Deliv Rev, 2001. **47**(1): p. 21-37.

152. Sakuma, S., et al., *Stabilization of salmon calcitonin by polystyrene nanoparticles having surface hydrophilic polymeric chains, against enzymatic degradation.* International Journal of Pharmaceutics, 1997. **159**(2): p. 181-189.

153. Guo, W., et al., *Conjugation chemistry and bioapplications of semiconductor box nanocrystals prepared via dendrimer bridging.* Chem. Mater, 2003. **15**(16): p. 3125-3133.

154. Herdt, A.R., B.S. Kim, and T.A. Taton, *Encapsulated magnetic nanoparticles as supports for proteins and recyclable biocatalysts.* Bioconjug Chem, 2007. **18**(1): p. 183-9.

155. Kang, Y. and T.A. Taton, *Micelle-encapsulated carbon nanotubes: a route to nanotube composites.* J Am Chem Soc, 2003. **125**(19): p. 5650-1.

156. Kang, Y. and T.A. Taton, *Core/Shell gold nanoparticles by self-assembly and crosslinking of micellar, block-copolymer shells.* Angew Chem Int Ed Engl, 2005. **44**(3): p. 409-12.

157. Kim, B.S., et al., *Magnetomicelles: composite nanostructures from magnetic nanoparticles and cross-linked amphiphilic block copolymers.* Nano Lett, 2005. **5**(10): p. 1987-91.

158. Kim, B.S. and T.A. Taton, *Multicomponent nanoparticles via self-assembly with cross-linked block copolymer surfactants.* Langmuir, 2007. **23**(4): p. 2198-202.

159. Mandal, S.K., et al., *Encapsulation of magnetic and fluorescent nanoparticles in emulsion droplets.* Langmuir, 2005. **21**(9): p. 4175-4179.

160. Nirmal, M., et al., *Fluorescence intermittency in single cadmium selenide nanocrystals.* Nature, 1996. **383**(6603): p. 802-804.

161. Lodish, H.F., *Molecular cell biology*. 2003: WH Freeman.

162. Mohs, A.M., et al., *Proton-resistant quantum dots: Stability in gastrointestinal fluids and implications for oral delivery of nanoparticle agents.* Nano Research, 2009. **2**(6): p. 500-508.

163. Mancini, M.C., et al., *Oxidative quenching and degradation of polymer-encapsulated quantum dots: new insights into the long-term fate and toxicity of nanocrystals in vivo.* J Am Chem Soc, 2008. **130**(33): p. 10836-7.

164. Celebi, S., et al., *Synthesis and characterization of poly(acrylic acid) stabilized cadmium sulfide quantum dots.* Journal of Physical Chemistry B, 2007. **111**(44): p. 12668-12675.

165. Gaponik, N., et al., *Thiol-capping of CdTe nanocrystals: An alternative to organometallic synthetic routes.* Journal of Physical Chemistry B, 2002. **106**(29): p. 7177-7185.

166. He, Y., et al., *Synthesis of CdTe nanocrystals through program process of microwave irradiation.* Journal of Physical Chemistry B, 2006. **110**(27): p. 13352-13356.

167. He, Y., et al., *Microwave-assisted growth and characterization of water-dispersed CdTe/CdS core-shell nanocrystals with high photoluminescence.* Journal of Physical Chemistry B, 2006. **110**(27): p. 13370-13374.

168. Li, L., H.F. Qian, and J.C. Ren, *Rapid synthesis of highly luminescent CdTe nanocrystals in the aqueous phase by microwave irradiation with controllable temperature.* Chemical Communications, 2005(4): p. 528-530.

169. Qian, H.F., et al., *Microwave-assisted aqueous synthesis: A rapid approach to prepare highly luminescent ZnSe(S) alloyed quantum dots.* Journal of Physical Chemistry B, 2006. **110**(18): p. 9034-9040.

170. Zhang, H., et al., *Hydrothermal synthesis for high-quality CdTe nanocrystals.* Advanced Materials, 2003. **15**(20): p. 1712-15.

171. Kairdolf, B.A., A.M. Smith, and S. Nie, *One-pot synthesis, encapsulation, and solubilization of size-tuned quantum dots with amphiphilic multidentate ligands.* J Am Chem Soc, 2008. **130**(39): p. 12866-7.

172. Kim, S., et al., *Type-II quantum dots: CdTe/CdSe(core/shell) and CdSe/ZinTe(core/shell) heterostructures.* Journal of the American Chemical Society, 2003. **125**(38): p. 11466-11467.

173. Daniel, M.C. and D. Astruc, *Gold nanoparticles: assembly, supramolecular chemistry, quantum-size-related properties, and applications toward biology, catalysis, and nanotechnology.* Chem. Rev, 2004. **104**(1): p. 293-346.

174. Faraday, M., *Experimental Relations of Gold (and other Metals) to Light.* Philos. Trans., 1857. **147**: p. 145-181.

175. Turkevich, J., P.C. Stevenson, and J. Hillier, *A study of the nucleation and growth processes in the synthesis of colloidal gold.* Discussions of the Faraday Society, 1951. **11**: p. 55-75.

176. Frens, G., *Controlled nucleation for the regulation of the particle size in monodisperse gold suspensions.* Nature Phys Sci, 1973. **241**(105): p. 20-12.

177. El-Sayed, M.A., *Some interesting properties of metals confined in time and nanometer space of different shapes.* Accounts of Chemical Research, 2001. **34**(4): p. 257-264.

178. Link, S. and M.A. El-Sayed, *Size and temperature dependence of the plasmon absorption of colloidal gold nanoparticles.* Journal of Physical Chemistry B, 1999. **103**: p. 4212-4217.

179. Burda, C., et al., *Chemistry and properties of nanocrystals of different shapes.* Chem. Rev, 2005. **105**(4): p. 1025-1102.

180. Eustis, S. and M.A. El-Sayed, *Why gold nanoparticles are more precious than pretty gold: Noble metal surface plasmon resonance and its enhancement of the radiative and nonradiative properties of nanocrystals of different shapes.* Chemical Society Reviews, 2006. **35**(3): p. 209-217.

181. Storhoff, J.J., et al., *What controls the optical properties of DNA-linked gold nanoparticle assemblies?* Journal of the American Chemical Society, 2000. **122**(19): p. 4640-4650.

182. Elghanian, R., et al., *Selective colorimetric detection of polynucleotides based on the distance-dependent optical properties of gold nanoparticles.* Science, 1997. **277**(5329): p. 1078.

183. Storhoff, J.J., et al., *One-pot colorimetric differentiation of polynucleotides with single base imperfections using gold nanoparticle probes.* Journal of the American Chemical Society, 1998. **120**(9): p. 1959-1964.

184. Jin, R., et al., *What controls the melting properties of DNA-linked gold nanoparticle assemblies?* J. Am. Chem. Soc, 2003. **125**(6): p. 1643-1654.

185. Ehrenkranz, J.R.L., *Home and point-of-care pregnancy tests: a review of the technology.* Epidemiology, 2002: p. 15-18.

186. Kneipp, K., et al., *Single molecule detection using surface-enhanced Raman scattering (SERS).* Physical Review Letters, 1997. **78**(9): p. 1667-1670.

187. Emory, S.R. and S. Nie, *Probing single molecules and single nanoparticles by surface-enhanced Raman scattering.* Science, 1997. **275**(5303): p. 1102.

188. Krug, J.T., et al., *Efficient Raman enhancement and intermittent light emission observed in single gold nanocrystals.* J. Am. Chem. Soc, 1999. **121**(39): p. 9208-9214.

189. Emory, S.R., W.E. Haskins, and S. Nie, *Direct observation of size-dependent optical enhancement in single metal nanoparticles.* J. Am. Chem. Soc, 1998. **120**(31): p. 8009-8010.

190. Emory, S.R. and S. Nie, *Screening and enrichment of metal nanoparticles with novel optical properties.* J. Phys. Chem. B, 1998. **102**(3): p. 493-497.

191. Doering, W.E. and S. Nie, *Single-molecule and single-nanoparticle SERS: examining the roles of surface active sites and chemical enhancement.* J. Phys. Chem. B, 2002. **106**(2): p. 311-317.

192. McCabe, A.F., et al., *SERRS labelled beads for multiplex detection.* Faraday Discussions, 2006. **132**: p. 303-308.

193. Doering, W.E. and S. Nie, *Spectroscopic tags using dye-embedded nanoparticles and surface-enhanced Raman scattering.* Anal. Chem, 2003. **75**(22): p. 6171-6176.

194. Sau, T.K. and C.J. Murphy, *Room temperature, high-yield synthesis of multiple shapes of gold nanoparticles in aqueous solution.* Journal of the American Chemical Society, 2004. **126**(28): p. 8648-8649.

195. Shankar, S.S., et al., *Biological synthesis of triangular gold nanoprisms.* Nature materials, 2004. **3**(7): p. 482-488.

196. Sun, Y. and Y. Xia, *Shape-controlled synthesis of gold and silver nanoparticles*. 2002. p. 2176-2179.

197. Pong, B.K., et al., *New Insights on the Nanoparticle Growth Mechanism in the Citrate Reduction of Gold (III) Salt: Formation of the Au Nanowire Intermediate and Its Nonlinear Optical Properties.* 2007.

198. Gerion, D., et al., *Synthesis and Properties of Biocompatible Water-Soluble Silica-Coated CdSe/ZnS Semiconductor Quantum Dots†.* J. Phys. Chem. B, 2001. **105**(37): p. 8861-8871.

199. Kim, S. and M.G. Bawendi, *Oligomeric ligands for luminescent and stable nanocrystal quantum dots.* Journal of the American Chemical Society, 2003. **125**(48): p. 14652-14653.

200. Mitchell, G.P., C.A. Mirkin, and R.L. Letsinger, *Programmed assembly of DNA functionalized quantum dots.* Journal of the American Chemical Society, 1999. **121**(35): p. 8122-8123.

201. Osaki, F., et al., *A quantum dot conjugated sugar ball and its cellular uptake. On the size effects of endocytosis in the subviral region.* J. Am. Chem. Soc, 2004. **126**(21): p. 6520-6521.

202. Slocik, J.M., J.T. Moore, and D.W. Wright, *Monoclonal antibody recognition of histidine-rich peptide encapsulated nanoclusters.* Nano Letters, 2002. **2**(3): p. 169-173.

203. Bentzen, E.L., et al., *Surface Modification To Reduce Nonspecific Binding of Quantum Dots in Live Cell Assays.* Bioconjugate chemistry, 2005. **16**(6): p. 1488-1494.

204. Gerion, D., et al., *Sorting fluorescent nanocrystals with DNA.* Journal of American Chemical Society, 2001. **124**: p. 24.

205. Pathak, S., et al., *Hydroxylated quantum dots as luminescent probes for in situ hybridization.* J Am Chem Soc, 2001. **123**(17): p. 4103-4.

206. Couvreur, P. and C. Vauthier, *Nanotechnology: intelligent design to treat complex disease.* Pharm Res, 2006. **23**(7): p. 1417-50.

207. Torchilin, V.P., *Micellar nanocarriers: pharmaceutical perspectives.* Pharm Res, 2007. **24**(1): p. 1-16.

208. Moghimi, S.M., A.C. Hunter, and J.C. Murray, *Long-circulating and target-specific nanoparticles: theory to practice.* Pharmacol Rev, 2001. **53**(2): p. 283-318.

209. Ballou, B., et al., *Sentinel Lymph Node Imaging Using Quantum Dots in Mouse Tumor Models.* Bioconjug Chem, 2007.

210. Ballou, B., et al., *Noninvasive imaging of quantum dots in mice.* Bioconjugate Chem, 2004. **15**(1): p. 79–86.

211. Sheinerman, F.B., R. Norel, and B. Honig, *Electrostatic aspects of protein-protein interactions.* Curr Opin Struct Biol, 2000. **10**(2): p. 153-9.

212. Honig, B. and A. Nicholls, *Classical electrostatics in biology and chemistry.* Science, 1995. **268**(5214): p. 1144-9.

213. Titford, M., *Progress in the Development of Microscopical Techniques for Diagnostic Pathology.* The Journal of Histotechnology, 2009. **32**(1): p. 9-19.

214. Sheehan, D.C. and B.B. Hrapchak, *Theory and practice of histotechnology.* 1980.

215. Titford, M., *The long history of hematoxylin.* Biotechnic and Histochemistry, 2005. **80**(2): p. 73-78.

216. Coons, A.H., et al., *The demonstration of pneumococcal antigen in tissues by the use of fluorescent antibody.* The Journal of Immunology, 1942. **45**(3): p. 159.

217. Coons, A.H. and M.H. Kaplan, *Localization of antigen in tissue cells II. Improvements in a method for the detection of antigen by means of fluorescent antibody.* Journal of Experimental Medicine, 1950. **91**(1): p. 1-13.

218. Nakane, P.K. and A. Kawaoi, *Peroxidase-labeled antibody a new method of conjugation.* Journal of Histochemistry and Cytochemistry, 1974. **22**(12): p. 1084-1091.

219. Nakane, P.K. and G.B. Pierce, *Enzyme-labeled antibodies: preparation and application for the localization of antigens.* Journal of Histochemistry and Cytochemistry, 1966. **14**(12): p. 929-931.

220. Nakane, P.K. and G.B. Pierce, *Enzyme-labeled antibodies for the light and electron microscopic localization of tissue antigens.* Journal of Cell Biology, 1967. **33**(2): p. 307-318.

221. Graham, R.C. and M.J. Karnovsky, *THF EARLY STAGES OF ABSORPTION OF INJECTED HORSERADISH PEROXIDASE IN THE PROXIMAL TUBULES OF MOUSE KIDNEY: ULTRASTRUCTURAL CYTOCHEMISTRY BY A NEW TECHNIQUE.* Journal of Histochemistry and Cytochemistry, 1966. **14**(4): p. 291-302.

222. Slamon, D.J., et al., *Use of chemotherapy plus a monoclonal antibody against HER2 for metastatic breast cancer that overexpresses HER2*. 2001. p. 783-792.

223. Jacobs, T.W., et al., *Specificity of HercepTest in determining HER-2/neu status of breast cancers using the United States Food and Drug Administration-approved scoring system.* Journal of Clinical Oncology, 1999. **17**(7): p. 1983.

224. Masood, S. and M.M. Bui, *Assessment of Her-2/neu overexpression in primary breast cancers and their metastatic lesions: an immunohistochemical study.* Annals of Clinical & Laboratory Science, 2000. **30**(3): p. 259-265.

225. Carey, L.A., et al., *The triple negative paradox: primary tumor chemosensitivity of breast cancer subtypes.* Clinical Cancer Research, 2007. **13**(8): p. 2329.

226. Cleator, S., W. Heller, and R.C. Coombes, *Triple-negative breast cancer: therapeutic options.* Lancet Oncology, 2007. **8**(3): p. 235-244.

227. Rakha, E.A., et al., *Prognostic markers in triple-negative breast cancer.* Cancer, 2007. **109**(1).

228. Hermanson, G.T., *Bioconjugate techniques*. 2008: Academic Press.

229. Bruchez, M.P. and C.Z. Hotz, *Quantum dots: applications in biology*. 2007: Humana Pr Inc.

230. Hermanson, G.T., A.K. Mallia, and P.K. Smith, *Immobilized affinity ligand techniques*. 1992: Academic Press New York.

CURRICULUM VITAE

BRAD ANTHONY KAIRDOLF

Education

Georgia Institute of Technology and Emory University Dec 2009
Doctorate of Philosophy, Biomedical Engineering **GPA: 4.0/4.0**
Thesis: Development of Polymer-Coated Nanoparticle Imaging Agents For Diagnostic Applications
Advisor: Shuming Nie, PhD
Minor: Business

Dupree College of Management, Georgia Institute of Technology *Dec 2009*
Technology Innovation: Generating Economic Results (TI:GER) Program

Louisiana State University (LSU) May 2003
Bachelor of Science, Biological Engineering (Summa Cum Laude) **GPA: 4.0/4.0**
Minors: Chemistry, Biology

Publications and Presentations

AM Mohs, H Duan, **BA Kairdolf**, AM Smith and SM Nie, "Proton-Resistant Quantum Dots: Stability in Gastrointestinal Fluids and Implications for Oral Delivery of Nanoparticle Agents," *Nano Research, **2009**, 2 (6), 500-508.*

BA Kairdolf, AM Smith and SM Nie, "One-Pot Synthesis, Encapsulation and Solubilization of Size-Tuned Quantum Dots with Amphiphilic Multidentate Ligands," *J. Am. Chem. Soc.,* **2008**, 130 (39), 12866-12867.

BA Kairdolf, M Mancini, AM Smith and SM Nie, "Minimizing nonspecific cellular binding of quantum dots with hydroxyl-derivatized surface coatings," *Anal. Chem.*, **2008**, 80, 3029-3034.

BA Kairdolf and SM Nie, "A Hydroxyl Quantum Dot Surface Coating for Minimizing Nonspecific Cellular Binding," *Emory-Georgia Tech Frontiers of Cancer Nanotechnology Symposium*: March 31, **2008**.

MC Mancini, **BA Kairdolf**, AM Smith and SM Nie, "Oxidative Quenching and Degradation of Polymer-Encapsulated Quantum Dots: New Insights into the Long-Term Fate and Toxicity of Nanocrystals in Vivo," *J. Am. Chem. Soc.*, **2008**, 130 (33), 10836-10837.

BA Kairdolf and SM Nie, "A New Quantum Dot Surface Coating for Overcoming the Nonspecific Binding Problem," *Joint Molecular Imaging Conference*: P03.0387, **2007.**

G Kim, **BA Kairdolf**, J Li and SM Nie, "Cancer Nanotechnology—Designing Multifunctional Nanostructures for Targeting Tumor Cells and Vasculatures," *ACS Meeting*: March 26, **2006**.

G Kim, **BA Kairdolf**, J Li, C Chen, L Chu and SM Nie, "Targeted Cancer Nanotherapeutics," *Emory-Georgia Tech Frontiers of Cancer Nanotechnology Symposium*: March 27, **2006**.

M Rhyner, **BA Kairdolf**, H Duan and SM Nie, "Development of Diagnostics and Therapeutic Nanoparticle Agents Using Amphiphilic Polymers," *Emory-Georgia Tech Frontiers of Cancer Nanotechnology Symposium*: March 27, **2006**.

BA Kairdolf and WT Monroe, "Molecular Beacon Sequence Design Algorithm," *Proceedings of the 2003 Annual Fall Meeting of the Biomedical Engineering Society*: 9.P2.85, **2003**.

BA Kairdolf, J Whately, J Maier and WT Monroe, "Design proposal for an automated sterile external mixer," *BEST Fellows Day*, Louisiana State University Ag Center: May 28, **2003**.

Professional Experience

Founder and CEO. DiagNano. Atlanta, GA 2009 — Present

- Founded in vitro diagnostics company based on technology developed at Emory University
- Secured $50,000 startup funding from Georgia Research Alliance grant
- Featured in Fortune Small Business/CNNMoney.com article and asked to present at a number of conferences, including the 2008 Georgia Life Sciences Summit and 2009 SEMDA conference

Research Assistant. Bao Lab, Georgia Tech. Atlanta, GA Summer 2004

- Analyzed transfection methods for efficient delivery of nanostructures into live cells including Streptolysin-O, Lipofectamine™, polyamidoamine dendrimers and translocation peptides

Research Assistant. Murthy Lab, Georgia Tech. Atlanta, GA Spring 2004

- Synthesized block copolymers using ATRP for delivery of DNA/RNA or peptides, characterized polymers using NMR and analyzed DNA encapsulation of nanoparticles using gel electrophoresis

Research Associate. Monroe Lab, LSU. Baton Rouge, LA Summer 2003

- Designed and tested protocols and devices for cellular engineering research
- Optimized and performed molecular biology assays, general chemical reagent preparation, and instrumentation setup and maintenance
- Designed algorithms and computer programs, installed software and hardware, and reported results through text and graphical documentation

Student Researcher. Monroe Lab, LSU. Baton Rouge, LA 2002 — 2003

- Composed grants to LSU Biotechnology Education for Students and Teachers program (received $7000) for developing automated microfluidic delivery system and LSU AgCenter (received $1500) for developing Java program to analyze DNA molecular beacon structures
- Created Java program to optimally design DNA molecular beacon probes

- Analyzed probe design using fluorescence spectroscopy
- Designed, fabricated and tested computer automated microfluidic delivery system for bioengineering applications
- Developed and constructed mammalian cell culture lab

Student Researcher. Ecological Infrastructure Engineering Laboratory (EIEL). Baton Rouge, LA 1999 — 2002

- Analyzed water quality of recirculating aquaculture system during spawning cycle
- Designed, fabricated and tested foam fractionation system for removal of organic waste

Patents

BA Kairdolf and S Nie, "Coated Quantum Dots and Methods of Making and Using Thereof", PCT/US09/33196

BA Kairdolf and S Nie, "One-Pot Synthesis, Encapsulation, and Solubilization of Size-Tuned Quantum Dots with Amphiphilic Multidentate Ligands", Filed in 2008, United States and International Patents Pending

Fellowships, Grants and Honors

Felowships:

NSF IGERT Fellowship	2006—2008
NSF Honorable Mention	2004, 2005
Center for Drug Design, Development and Delivery Fellowship	2004—2005
LSU BEST Biotechnology Fellowship	2002—2003

Honors:
Dean's Medal for Excellence (LSU)
University Medalist (LSU)
Delivered Valedictory for LSU College of Engineering graduation ceremony (2003)

Affiliations:
Tau Beta Pi Engineering Honor Society
Golden Key International Honor Society